CONTENTS

SYMBOLS

a	Speed of sound, m/sec
b	Airfoil or strut span, m
c	Airfoil, strut, or splitter ring chord, m
f	Frequency, Hz
M	Free stream Mach number, U/a
M_1	Nozzle exit Mach number
$\overline{p^2}$	Mean square acoustic pressure $(N/m^2)^2$
p_{ref}	Reference acoustic pressure, 2×10^{-5} N/m^2
P	Acoustic power, W
r	Far field radius, m
r_{le}	Airfoil leading edge radius
R	Acoustic pressure reflection coefficient
S_F	Sears function for lift force
U	Streamwise mean velocity, m/sec
$\overline{v^2}$	Mean square velocity fluctuation normal to airfoil $(m/sec)^2$
α'	Acoustic pressure transmission coefficient
ρ	Air density, kg/m^3
Λ	Turbulence streamwise integral scale length, m
ϕ_F	Spectral density of lift force fluctuation, N^2/Hz
ϕ_P	Spectral density of acoustic pressure, $(N/m^2)^2/Hz$
ϕ_T	Spectral density of turbulence-produced incidence fluctuation, rad^2/Hz
θ	Direction angle measured from nozzle upstream centerline, deg

NASA Contractor Report 2955

A Method for Calculating Strut and Splitter Plate Noise in Exit Ducts - Theory and Verification

Martin R. Fink

CONTRACT NAS3-17863
MARCH 1978

NASA

NASA Contractor Report 2955

A Method for Calculating Strut and Splitter Plate Noise in Exit Ducts - Theory and Verification

Martin R. Fink
United Technologies Research Center
East Hartford, Connecticut

Prepared for
Lewis Research Center
under Contract NAS3-17863

National Aeronautics
and Space Administration

**Scientific and Technical
Information Office**

1978

BLank Page

A METHOD FOR CALCULATING STRUT AND SPLITTER PLATE NOISE IN EXIT DUCTS - THEORY AND VERIFICATION

Martin R. Fink
United Technologies Research Center

SUMMARY

Portions of a four-year analytical and experimental investigation relative to noise radiation from engine internal components in turbulent flow are summarized. Spectra measured for such airfoils over a range of thickness ratio, flow velocity, and turbulence level are compared with predictions made by an available rigorous thin-airfoil analytical method. This analysis includes the effects of flow compressibility and source noncompactness. Generally good agreement is obtained.

This noise calculation method for isolated airfoils in turbulent flow is combined with a method for calculating transmission of sound through a subsonic exit duct and with an empirical far-field directivity shape. These three elements were checked separately and were individually shown to give close agreement with data. This combination provides a method for predicting engine internally generated aft-radiated noise from radial struts and stators, and annular splitter rings. A FORTRAN program listing and users guide is included for the resulting digital computer program. Calculated sound power spectra, directivity, and acoustic pressure spectra are compared with the best available data. These data were for noise caused by a fan exit duct annular splitter ring, large-chord stators blades, and turbine exit struts. However, the lack of turbulence intensity and scale length measurements for these flow ducts prevented an absolute validation of the prediction method.

INTRODUCTION

Noise generated by solid bodies in the presence of engine airflow can determine the inherent minimum noise of installed aircraft engines. For example, struts necessary for structural support of the engine and splitters are likely to be immersed in high-velocity turbulent engine airflows. Acoustically treated splitters within the engine inlet and exhaust ducts can attenuate turbomachinery noise but produce noise at their outer edges. Turbofan stator blades are subjected to fluctuating wakes produced by the fan rotor blades. In all these cases, a solid surface of finite extent is scrubbed by turbulent airflow.

Experimental evaluation of methods for predicting noise generated by these surfaces has been conducted during the past four years under Contract NAS3-17863. The portions of this investigation which apply to strut, stator, and splitter plate noise are summarized in this final report. Noise calculations are compared with NASA and UTRC data for isolated airfoil-shaped struts in turbulent flow. Extension of that calculation procedure to include sound transmission through a subsonic exhaust nozzle and radiation to the far field had not been given elsewhere and is developed herein. A digital computer program is presented for calculating noise generated by hard-wall struts, stator vanes, and splitter rings in fan exit ducts and radiated out the exhaust nozzle to the far field. Calculated results are compared with the best applicable acoustic data obtained by NASA Lewis Research Center for full-scale fan stator and duct splitter installations and by NGTE for cold-flow tests of noise produced by model turbine exit struts.

Work conducted under this Contract was reported in three annual technical reports (references 1 through 3). An additional final report (reference 4) contains the application of this study of noise components to prediction of externally blown flap noise. Some of the material contained in these reports has also been presented as papers at professional-society meetings and published in journals and books. A complete list of publications prepared under this Contract, and of publications based on direct outgrowths of work conducted under this Contract, is presented in APPENDIX A to this report.

Editorial review of this Contractor Report was performed at NASA Lewis Research Center and by colleagues within UTRC, to assure clarity of ideas expressed and correct evaluation of data.

EVALUATION OF NOISE PREDICTION METHOD FOR ISOLATED AIRFOILS

Development of Noise Prediction Method

When the work conducted under this Contract was begun, there were several analytical methods and empirical procedures available for predicting noise radiated by an airfoil in turbulent flow. It was recognized that turbulence would produce fluctuations of airfoil surface pressures and lift force. These force fluctuations would generate noise. A small, acoustically compact airfoil would generate lift dipole noise that could, in principle, be calculated from the force fluctuations predicted for incompressible flow. This appr ach had previously been shown in reference 5 to give reasonable predictions of measured noise radiation for a small airfoil at low frequencies. However, noise measured at high frequencies was significantly overpredicted. Some procedure to account for flow compressibility and acoustic noncompactness effectswould have to be included in the analysis.

Measurements were obtained under this Contract of surface pressure fluctuations on, and noise radiation from, a 46 cm (18 in.) chord airfoil in turbulent flow. The uniform turbulent flow, at five airspeeds and two turbulence levels, was produced by grids within the nozzle of the United Technologies Research Center (UTRC) acoustic wind tunnel (reference 6). Data and comparisons with predictions were published in references 1 and 7. It was found that of several theories then available for predicting the fluctuations of surface pressure on airfoils in three-dimensional turbulence, the analysis developed by Filotas in reference 8 gave closest agreement with data. As with the acoustic data given in reference 5, far-field noise was correctly predicted at low frequencies and overpredicted at high frequencies. A qualitative analysis of incidence fluctuation noise, including a term to account for acoustic noncompactness, had been developed by Hayden in reference 9. This analytical expression contained a physical length factor but gave no method for calculating this length from the airfoil chord or span. It was shown in references 1 and 7 that if this length was taken as half of the chord, the resulting predicted spectra agreed with the data given in references 1 and 5.

Acoustic tests were later conducted at NASA Lewis Research Center on thin airfoil models having a large range of chord. These data eventually were published in reference 10 but were available for evaluation of predictions at an earlier date. The analytical method developed by the above approach predicted the spectra measured with the smaller models but was in poor agreement with data for airfoils with larger chord. It was recognized that an improved, more rigorous analytical method was needed.

The analytical method developed by Amiet in references 11 and 12 was not developed under this Contract. However, the impetus for that analysis was to some extent an outgrowth of the above evaluation of noise prediction methods. This new method includes a highly rigorous solution for the induced pressure fluctuation on a thin airfoil in compressible subsonic flow with known three-dimensional turbulence. Acoustic noncompactness, in the sense of phase cancellation of sound waves arriving at the same far-field point from different chordwise and spanwise positions, is calculated in detail. There are no empirical constants in the analysis. It was shown in reference 11 that the data of reference 1 for a 46 cm chord airfoil in turbulent flow were closely predicted by this method. Good agreement was also obtained (reference 12) with data for a 23 cm (9 in.) chord NACA 0012 airfoil tested with the same equipment. However, the high frequency, low Mach number portion of the data generally was overestimated.

A similar analysis was developed by Goldstein in reference 13 and evaluated in comparisons shown in reference 10 with data for a range of airfoil chords. The two methods use different normalized turbulence spectra, and the method of reference 13 applies only for acoustically compact sources. Amiet's method was used for the predictions shown herein because its computer program was readily available.

For large Strouhal numbers, corresponding to high frequencies and small flow velocities, most of the noise radiation is predicted by Amiet's analysis to arise from the portion of the airfoil very near the leading edge. This calculated result has two important effects. Noise radiation from airfoils which have large chords relative to the turbulence integral scale length is predicted to resemble that for a thin plate having a sharp leading edge but infinite downstream extent. Such noise is trailing-edge noise with its directivity shape reversed in direction (reference 7). Its amplitude varies not with velocity to the sixth power but with velocity to the fifth power, and its directivity shape is given by the cartiod $\cos^2((\theta-\pi)/2)$ which has maximum amplitude downstream. This change of directivity shape with increased chord at constant turbulence properties had been observed in the data reported in reference 10. Also, the assumption that the airfoil was thin and sharp relative to all other length dimensions becomes questionable for large Strouhal numbers. Gust wavelengths into which the high-frequency three-dimensional turbulence could be decomposed are of the same order as the airfoil maximum thickness and leading edge radius. Thus it was reasonable that the predictions should not match data for these conditions.

Amiet's method of references 11 and 12 assumes that both the mean flow and the turbulence are homogeneous. An available computer program used in calculations presented herein had been developed using the additional

assumption that the turbulence is isotropic and is described by the von Karman turbulence spectrum. Resulting calculated spectra are oscillatory because of flow compressibility (phase cancellation of sound waves which leave different chordwise regions at difference times but reach the far-field point at the same time). Spectra plotted in this report are less oscillatory than those given in references 11 and 12. In those early uses of the method, 1/3 octave sound pressure levels had been calculated as the pressure-squared spectral density evaluated at each 1/3 octave band center frequency, increased by 10 times the logarithm of the bandwidth. This calculation procedure gave results in error by one or two dB when the center frequency nearly matched a phase cancellation frequency. The curves in this report were computed by subdividing each 1/3 octave band into four equal ratio bands (1/12 octave bands). Pressure-squared spectral densities were calculated at the five upper and lower frequencies of these bands. These were averaged and increased by the appropriate bandwidth to obtain the 1/12 octave band sound pressure levels, which were combined to get 1/3 octave levels.

These analytical and experimental studies were directed toward development of a method for predicting noise radiated by a rigid hard-wall strut in turbulent flow. Additional effort was conducted under this Contract for the application of such methods to prediction of engine strut and splitter noise. Measurements were obtained of turbulence intensity and scale length at different radial and angular positions downstream of the stators of a large-scale low-speed turbofan model. The resulting turbulence information was used in predicting the sound power spectrum of noise generated by a fan exit duct annular splitter tested at NASA Lewis Research Center. A noise prediction method developed from that approach is described herein.

In addition to these studies of noise generation, tests were conducted to investigate methods for reducing strut noise. A number of passive modifications (perforated leading and trailing edge regions, turbulence screens, and bluff trailing edges) and one active modification (trailing edge blowing) were applied to a 46 cm (18 in.) chord strut to attain noise reductions in turbulent flow. A perforated leading edge backed by a bulk acoustic absorber, over the forward 1.5% chord, was the most effective device. It achieved up to 6 dB noise reduction above 1.6 kHz center frequency at 125 and 172 m/sec (410 and 565 ft/sec) flow velocity, but was ineffective below 0.8 kHz frequency. These results were reported in reference 2.

General Discussion of Calculations and of Test Equipment

Calculation Method

The general approach used in this investigation was to regard noise radiated to a far-field point from a strut within an engine fan duct as a combination of three processes.

far field noise from strut in flow duct	=	isolated airfoil sound spectrum in turbulent flow	X	spectrum correction due to nozzle and duct with flow	X	far field radiation pattern	(1)

A method for predicting each of these processes was obtained from available literature. Each method had been developed by use of limited data taken for that specific purpose. Then the combined prediction of far-field spectra and directivity was examined by comparisons with the limited unambiguous available data.

Of these individual processes, the most important is the prediction of initial noise radiation from an isolated airfoil in uniform turbulent flow. Such noise can be expressed by use of Lighthill's acoustic analogy as an integral over the surface. Then the spectrum ϕ_p of far field acoustic pressure in the centerline plane normal to the airfoil surface caused by a spectrum ϕ_F of fluctuating lift dipole force is given by

$$\phi_p = (f \cos\theta / 2ra)^2 \, \phi_F \tag{2}$$

if the compressibility frequency parameter $(fc/a)(1-M^2)^{-1}$ is assumed small compared with one. The lift force spectrum can be related to the spectrum ϕ_T of incident turbulence by

$$\phi_F = (1/2 \, \rho U^2)^2 (cb)^2 (2\pi S_F)^2 \, \phi_T \tag{3}$$

where S_F is the Sears function (the ratio of lift coefficient slope at a given reduced frequency to 2π). Turbulence spectrum, normalized as $U\phi_T/\overline{u^2}\Lambda$, can be expressed as a function of Strouhal number fU/Λ based on turbulence integral scale length. Then, as with equation (5) of reference 10, sound pressure level in any 1/3 octave frequency band can be expressed in terms of a product of three factors.

$$SPL = 10 \log \left[F_1 \left((bc/r^2)(\overline{v^2}/U^2) U^6 \right) \times \sin^2\theta \times F_3 (fc/U, \Lambda/c, M) \right] \tag{4}$$

The quantity within square brackets in equation (4) can be regarded as the product of an amplitude factor F_1, a radiation pattern shape factor, and a spectrum shape factor F_3. The effect of Mach number M on the factor F_3 and the turbulence length scale Λ is small. Therefore the spectra can be approximately normalized at moderate subsonic Mach numbers by use of the Strouhal number fc/U.

For large-chord airfoils the radiation pattern shape factor, spectrum shape, and velocity dependence at a given measurement direction are affected by flow compressibility. Radiation shape is also changed because retarded time for different chordwise positions becomes a function of direction angle and reduced frequency. Chordwise variations of retarded time do not occur at 90° direction angle; measured and predicted normalized spectrum shapes should have least variation with airfoil chord and flow Mach number at this direction. Note that the functional dependence of spectrum amplitude and shape on Strouhal number, ratio of turbulence to chord, and Mach number can be examined in tests at 90° direction angle even if the flow is nonuniform in the spanwise direction.

Alternately, equations (2) and (3) can be combined and rearranged to yield equation (24) of reference 1.

$$SPL_{1/3} - 10\log(\overline{v^2}/U^2) - 10\log(0.232\,\Lambda/c) - 10\log\left(\frac{\pi}{2}\,\frac{\rho U^3}{ap_{ref}}\,\frac{\sqrt{bc}}{r}\sin\theta\right)^2 \qquad (5)$$

$$= 10\log S_F^{\,2} + 10\log(U\phi/\overline{v^2}\,\Lambda) + 30\log(fc/U)$$

Here the left side of the equation is the far-field spectrum minus three terms which are independent of frequency. One term is the adjustment for mean square turbulence level, another is the adjustment for ratio of turbulence integral length scale to airfoil chord, and the third expresses a dependence on velocity to the sixth power and sine squared of the measurement direction. Thus the measured 1/3 octave spectra can be plotted in the form of the left side of equation (5) by adjusting the amplitude and plotting against Strouhal number fc/U rather than frequency.

Test Equipment

Two different types of test equipment were used for measuring noise radiation from an isolated strut in subsonic turbulent flow. Neither is satisfactory for all purposes, but a combination of data from both types will allow evaluation of all predicted features of such noise. These two forms of test equipment are the conventional open-jet acoustic wind tunnel (reference 6) and the large subsonic exhaust jet (reference 10).

A conventional acoustic wind tunnel, such as that described in reference 6, provides a nearly uniform test flow field with nearly uniform turbulence. Turbulence generated by upstream grids can have arbitrary scale length but is limited to about 5% turbulence level if the grid is not too close to the nozzle exit. The range of measurement direction angle tends to be limited to about 45° on either side of a normal to the flow direction. Also, strut noise caused by these moderate turbulence levels must be measured against tunnel background noise. The usable spectrum range tends to be limited at low frequencies by edge noise generated at the nozzle exit lip and at high frequencies by tunnel shear-layer jet noise and/or collector noise. Thus the advantage of uniform flow, which permits experimental evaluation of predicted absolute spectrum level at mid-frequencies, is accompanied by inability to evaluate predicted levels at extremes of frequency or direction angle.

Data were reported in reference 10 for noise radiated from struts extending across the spatially nonuniform turbulent mixing region of an open jet. At its closest distance from the jet centerline, the strut was in the region of largest turbulence level. Compared with measurements in an acoustic wind tunnel, the strut-radiated noise stood further above background noise and the jet nozzle did not physically obstruct the line of sight to the strut. These differences permitted measurements to be made with the strut and jet over larger ranges of frequency and direction angle than could be obtained with an acoustic tunnel. However, mean velocity and turbulence level were not uniform along the strut span as assumed in the theory. The experimental results given in reference 10 show that shapes of the spectra and directivity pattern were not affected by this nonuniformity. Absolute levels were strongly affected, but these can be related to that for a strut of unknown span in a uniform flow having the local maximum mean velocity and turbulence level. In summary, tests in the high-turbulence region of an open jet permit experimental validation of normalized spectrum shapes and normalized directivity shapes. However, they cannot be used for validating predictions of absolute level.

Comparisons are given, in the following section of this report, between calculated and measured spectra for isolated struts in both types of turbulent flow. The absolute levels predicted for struts in an open jet were obtained by use of an arbitrary choice of span, mean velocity, and turbulence properties. Details of measured normalized spectra and directivity shapes have been previously discussed and compared with analytical predictions in reference 10. Agreement generally was excellent over a large range of frequency, polar angle, azimuth angle, velocity, and chord.

Comparisons With NASA Strut Noise Data

Test Configurations and General Comparison

An experimental study of noise radiation from a strut in a turbulent exhaust jet was described in reference 10. The experimental configuration consisted of an uncambered strut placed at zero incidence relative to the centerline of a 10 cm (4 in.) diameter nozzle. These struts had 0.95, 2.5, 10, and 61 cm (3/8, 1, 4, and 24 in.) chord and 0.32 cm (1/8 in.) maximum thickness, with identical hemicylindrical leading edges and 0.64 cm (1/4 in.) converging aft portions but different lengths of constant-thickness central portion. The strut leading edge was four nozzle diameters downstream of the nozzle exit and one radius away from the centerline.

Flow properties at the leading edge were described by the local mean velocity (0.62 times the nozzle exhaust velocity), rms velocity fluctuation (25% of that local mean velocity), and a turbulence length scale of 1.9 cm. Measured turbulence spectra in this exhaust jet were found to be best described by the exponential decay law (reference 15).

Spectra measured in the direction 100° from the strut chord, at 152 m/sec (500 ft/sec) nozzle exhaust velocity and therefore 94 m/sec (310 ft/sec) maximum impingement velocity at the leading edge, are plotted in the upper part of figure 1 for the four strut chord lengths. Measured background noise of the exhaust jet was subtracted from the raw data, and corrections for atmospheric absorption were applied. These NASA-supplied spectra are free-field and lossless; they contain only the noise caused by the strut. Spectra calculated for these cases by the method of reference 11 are plotted in the lower part of this figure. Because sound pressure levels (SPL) for the various lengths are intermixed at high frequencies, the measured and calculated spectra are plotted separately in this one figure to emphasize general trends. At less than 500 Hz center frequency, increased chord produced increased measured SPL. Maximum SPL occurred not for the largest (61 cm) chord but for the chord length equal to the 10 cm nozzle exit diameter. Maximum SPL's for the two smallest chord models occurred at a higher center frequency than for the larger ones. Above 5000 Hz center frequency the data for all chord lengths matched within 4 dB, and the models with smallest chord generally had the largest SPL. These four experimentally determined trends were reproduced by the calculated spectra.

These struts were tested extending across the nonuniform flow of an exhaust jet, tangent to the circle of maximum turbulence intensity. Spectrum shape, directivity shape, and variation of OASPL with velocity should not have been affected by the flow nonuniformity. Measured spanwise variations of mean velocity and turbulence could, in concept, be used for calculating

an effective span within uniform flow so that absolute levels could be predicted. Those data have not been published and were not supplied for this comparison. Comparisons with calculations made by the method of reference 11 for uniform flow were therefore obtained by (1) using a uniform flow which matched the measured maximum values of local impingement velocity, turbulence level, and turbulence length scale, (2) assuming an effective strut span that provided a close match between calculated and measured spectrum levels for the 2.5 cm chord airfoil at 94 m/sec impingement velocity, (3) assuming that these uniform quantities existed along the strut for all other impingement velocities and all four chord lengths, and (4) comparing spectrum levels calculated for the struts in this back-figured equivalent uniform flow with those measured in the actual flow. The purpose of the calculations shown here was to see whether this calculation method would predict the measured effect on 1/3 octave spectrum caused by increasing the chord by factors of 4 and 24.

Detailed Comparison

Calculated and measured spectra for each of the four chords are compared in the four parts of figure 2. Spectra are plotted for 92 and 152 m/sec (300 and 500 ft/sec) nozzle exhaust velocities, corresponding to 57 and 94 m/sec (186 and 310 ft/sec) maximum impingement velocities at the leading edge. The comparison is shown in figure 2(a) for the 0.95 cm (3/8 in.) chord. The spectrum measured at the higher velocity was closely matched (generally within 1 dB) up to 8 kHz center frequency. The spectrum calculated for the lower velocity was about 2 to 3 dB too low up to 5 kHz; it would have closely matched the data if the measured 15% turbulence level had been used. At higher frequencies, the data for both velocities decayed more rapidly than the calculated spectra. The frequency above which calculated and measured spectra differ in shape can be regarded as determined by a turbulence wavelength equal to the ratio of velocity to frequency. For both velocities this turbulence wavelength was approximately 1.1 cm which was about 1.2 chords, 3.6 maximum thicknesses, and 7 leading edge radii. At this point in the comparison, it has not been proven which is the pertinent length dimension. In fact, these data do not clearly contradict an assumption that both measured spectra differ in shape from the calculated spectra above 8 kHz frequency corresponding to about 4 cm acoustic wavelength. Then the upper limit of validity of this thin-airfoil theory might be the ratio of acoustic wavelength to chord, maximum thickness, or leading edge radius. Some portion of the difference may also have been caused by differences between the assumed and actual turbulence spectrum.

Calculated and measured spectra for 2.5 cm (1 in.) chord airfoils are compared in figure 2(b). Additional measured spectra are shown as square and diamond symbols. These additional spectra were obtained for an airfoil with 2.9 cm (9/8 in.) chord and 0.95 cm (3/8 in.) maximum thickness. That is, chord was only slightly increased but thickness and leading edge radius were tripled. The spectra measured with the standard-thickness airfoil generally werematched by the calculated curve within 2 dB at both velocities, with a tendency to underpredict at the higher velocity and overpredict at the lower. The spectrum calculated for the lower velocity was 3 to 4 dB above the data for larger than 3.15 kHz center frequency. However, major differences between calculated and measured spectrum shapes did not occur until 16 and 12.5 kHz center frequencies for the higher and lower velocities. The data exhibited the rapid decay predicted at the onset of compressibility effects. Spectra measured with the thicker airfoil matched these for the standard-thickness airfoil below 500 Hz. They fell about 3 dB lower at center frequencies to 3.15 kHz at the higher speed and 2.0 to 2.5 kHz at the lower speed. Spectra for the thicker airfoil decayed more rapidly at higher frequencies, and above 5.0 kHz the data for the two airfoils were parallel but about 8 dB apart. Increasing thickness at constant chord caused a decrease in the frequency above which the measured and calculated spectra changed shape. Taking this frequency as 3.15 and 2.0 kHz, the turbulence wavelength was 3 cm which is about 3.4 maximum thicknesses or 6.7 leading edge radii. These are about the same ratios found for the 0.95 cm chord standard-thickness airfoil of figure 2(a). Onset of the high-frequency differences for the standard-thickness airfoil at both velocities probably corresponds to an acoustic wavelength of about 2.4 cm or about one chord.

The comparison shown in figure 2(c) for the 10 cm (4 in.) chord airfoil is not as favorable as for the smaller airfoils. The ratio of assumed turbulence integral scale length to airfoil chord was 0.15 for this airfoil but 0.6 and 2.25 for the two smaller airfoils. Measured SPL's at low frequencies were underpredicted by about 4 dB at the higher velocity. Measured frequencies for peak amplitude were overpredicted. The high-frequency portion of the spectrum measured at the lower velocity was underpredicted above 3.15 kHz, the frequency at which the acoustic wavelength was equal to the chord. However, at the higher velocity the high-frequency portion of the spectrum generally was matched within 3 dB. The calculated phase-reinforcement peak did not occur in the measured spectrum. Generally similar results are shown in figure 2(d) for the 61 cm (24 in.) chord airfoil. Below 630 Hz center frequency calculated levels were about 5 dB below the data. At higher frequencies, good agreement was obtained up to 10 kHz for the higher and 5 kHz for the lower velocity. All four chord lengths had some discrepancies above these frequencies for these velocities. These results are consistent with an assumption that measured high-frequency noise is overpredicted when the

turbulence wavelength is less than about 3.5 maximum thickness or 7 leading edge radii. (Unlike most families of airfoils, these models had a constant ratio of maximum thickness to leading edge radius.) Measured noise seems to be well-predicted if the chord is not larger than twice the turbulence integral scale length. It is underpredicted at low frequencies if the chord is at least an order of magnitude larger than this scale length. It is not known whether this difference is caused by failure of the assumed von Karman spectrum shape to match the actual turbulence at low frequencies.

Comparisons With Additional Strut Noise Data

Acoustic Wind Tunnel and Airfoil Models

The UTRC acoustic wind tunnel, described in reference 6 and shown in figure 3, is an open-jet wind tunnel with the test section enclosed in an anechoic chamber. For these tests the cross-section of the open jet was 0.79 m (31 in.) by 0.53 m (21 in.). Horizontal sidewalls provided upper and lower boundaries for the jet. The open vertical shear layers permitted noise generated by models within the jet to be radiated laterally into the relatively quiescent anechoic chamber. The nozzle could be rotated 90 deg and the sidewall spacing adjusted to permit testing airfoils with either 0.79 m or 0.53 m span.

This test section inlet has a contraction ratio of 16.5, which provides less than 0.2% turbulence level. Grids can be installed within the nozzle to generate higher turbulence levels. The two grids used for these tests had also been used in the test program described in reference 1. As shown therein, they both provide approximately isotropic turbulence with 3.2 cm (1.27 in.) streamwise integral scale length and 1.9 cm (0.75 in.) transverse integral scale length. Streamwise and transverse turbulence intensities were approximately equal and were approximately uniform within the test region. The rms streamwise turbulence amplitude decreased slightly with increasing airspeed, being given approximately by a constant times velocity (m/sec) raised to the -0.2 power. This constant was 0.123 for the large grid, denoted L, and 0.081 for the medium grid, denoted M. Turbulence levels at 100 m/sec airspeed therefore were about 5% and 3%.

Two airfoil models were used for these tests. One had a 23 cm (9 in.) chord, 53 cm (21 in.) span, 18% thickness ratio, and NACA 0018 airfoil section. This model spanned the narrow dimension of the test section. The other model had an 11.4 cm (4.5 in.) chord, 0.79 m (31 in.) span, 12% thickness ratio, and NACA 0012 airfoil section. It spanned the wide dimension of the test section. These two airfoil models are cited as the thick airfoil

and the small thin airfoil, respectively. A photograph of the small thin airfoil installed between the sidewalls, but before acoustic absorbing material was placed on the airfoil support framework, is shown as figure 4.

Because these two uncambered airfoil sections were of the same airfoil family, the contours were affinely related. The leading edge radii varied as thickness ratio squared. Thus the thick airfoil had three times the maximum thickness of the small thin airfoil but 4.5 times its leading edge radius. It had been expected that observed differences between measured noise from an airfoil in turbulent flow and predictions by thin-airfoil compressible flow theory which includes acoustic noncompactness were caused by the thin-airfoil assumption. Deviations between predictions and data might occur at some turbulence wavelength proportional to airfoil maximum thickness or leading edge radius. Comparisons already were available in reference 12 for an NACA 0012 airfoil model with 23 cm (9 in.) chord and 12% thickness ratio. Tests of these two available airfoil models, and comparison with predictions, would indicate whether leading edge radius or maximum thickness ratio was the dominant factor in decreasing the measured noise below predictions. Once this was known, some reductions of engine strut annoyance-weighted noise might be achieved by use of blunter or thicker struts, if acceptably low losses can be achieved at the engine duct Mach numbers.

Test Conditions and Procedures

Far-field noise spectra were measured with three commercially available 0.635 cm (1/4 in.) condenser microphones. They were located at three positions on an arc of 3.04 m (10 ft) radius in a horizontal plane through the test section centerline. The center of this arc was at midchord of the airfoil. The microphones were at 60°, 90°, and 120° angular position relative to the test section centerline. Sound pressure levels were measured in decibels referenced to 2×10^{-5} newtons per square meter (2×10^{-4} microbar). All microphones were calibrated daily with a 250 Hz pistonphone.

Background noise measurements were obtained with each of the two turbulence grids at 31.5, 50, 80, 125, and 177 m/sec (103, 164, 262, 410, and 580 ft/sec) test section velocities. The four lower velocities differ by a factor of about 1.6, which facilitates comparison of 1/3 octave spectra. The highest velocity, which is larger by a factor of the square root of two, was nearly the maximum attainable with the turbulence grids installed. Acoustic data were obtained as 1/3 octave spectra for a useful range of center frequencies from 400 to about 4,000 Hz. Both airfoils were tested with the two turbulence grids at all five velocities at both zero and 10° geometric angle of attack. The effective angle of attack for a lifting airfoil in

a subsonic open jet is less than the geometric angle because the jet is distorted by airfoil lift. Previous tests in this wind tunnel have established that this required correction is predicted by available wind tunnel interference theory for open jets having a constraint on downstream position. Thus the 10° geometric angle of attack corresponds to about 8° and 9° effective angle of attack for the thick airfoil and the small airfoil, respectively.

The far-field spectrum of measured background noise was logarithmically subtracted from each spectrum measured with an airfoil in place. Resulting spectra, corrected for background noise, were not extended to frequencies at which less than 2.5 dB difference occurred between spectra measured with and without the airfoil. A correction to amplitude and direction of this airfoil-minus-background-noise measurement was then applied to account for refraction of sound waves at the open jet shear layer. These corrections were calculated by Amiet's method (reference 14).

Presentation of Experimental Results

As with the presentation used in reference 1 for noise from an airfoil in turbulent flow, the measured spectra are plotted in a normalized form. It was found that this type of plot facilitated evaluating the effects of various parameters. Measured spectrum levels were adjusted in amplitude by an amount which depended on flow velocity, turbulence grid, and measurement direction but was independent of frequency. These adjusted 1/3 octave sound pressure levels are given by the left side of equation (5). Frequency is plotted as Strouhal number referenced to airfoil chord.

Adjusted measured spectra are plotted in this manner in figures 5 and 6 for the small thin airfoil and the thick airfoil, respectively. Each figure contains five pages, each for a different velocity. Each page has two plots, the upper for zero and the lower for 10° geometric angle of attack. Four data symbols are shown on each plot, corresponding to the 60 and 90° microphone positions for the large and medium grids. The 120° microphone position (furthest downstream) was not used because background noise at high frequencies (most likely, jet mixing noise from the shear layer) was too large at this direction. Uncorrected spectra therefore disappeared into background noise at lower frequencies than those for other positions. The envelope of data measured at zero incidence is shown with the data for 10° geometric incidence.

Also shown on each plot is a predicted adjusted spectrum, determined from the right side of equation (5). Normalized turbulence spectrum was taken as equation (1-95) of reference 15. The spectrum for noise radiated

from the airfoil was calculated by Amiet's compressible flow solution (reference 11) for the test airspeed at 90° measurement position, where effects of acoustic noncompactness do not occur.

In each figure, the two data symbols corresponding to different rms turbulence levels at the same measurement position were in close agreement. This result shows that noise intensity varies with turbulence intensity squared, for the turbulence levels of these tests. Data for different measurement directions, including 120° (not shown), generally coalesced at low Strouhal numbers. Oscillatory differences occurred at higher Strouhal numbers, with decreased noise appearing first at 90° direction. Increasing the angle of attack, which increased the airfoil lift coefficient from zero to about one, had no clear effect on noise radiation. For most cases there was no effect. However, for the thick airfoil at the highest airspeed (figure 6(e)) the increased angle of attack seemed to produce about 3 dB average noise reduction at Strouhal numbers above 2. This result is contrary to the "small but measurable" 1 to 2 dB increase shown in figure 12 of reference 12 for a 12% thickness ratio, 23 cm (9 in.) chord airfoil tested with the same equipment.

The comparison between predicted and measured spectra is more readily seen in figures 7 through 9, which show the effect of velocity on adjusted spectra. The upper curve shows the predicted adjusted spectrum for an acoustically compact lift dipole with a fluctuating lift force calculated for incompressible flow. This curve was calculated using the right side of equation (5) with the Sears function given by low-frequency and high-frequency asymptotic solutions obtained by Filotas (reference 8). Because these asymptotic solutions do not join with continuous slope, the calculated spectra have discontinuous slope at a Strouhal number of $(2\ )^{-1}$ times the ratio of airfoil chord to turbulence integral scale length. Adjusted spectra calculated by the method of reference 11 for compressible flow generally showed no effect of velocity at low Strouhal numbers, with levels below those calculated from the simpler approximate solution.

Adjusted noise levels calculated by the compressible flow analysis decayed in an oscillating manner at high Strouhal numbers. The high-Strouhal number portions of the spectra measured for the small airfoil at the lowest velocities (figures 5(a) and (b)) were closely predicted up to a Strouhal number of 4 or 5 but were overpredicted at larger Strouhal numbers. Generally good agreement occurred at 80 m/sec (figure 5(c)) for data obtained with the medium grid, but levels above a Strouhal number of 4 were overpredicted for the large-grid data. Similarly, spectra calculated for the two highest velocities (figures 5(d) and (e)) generally were about 4 dB below data at Strouhal numbers from 1 to 4 but crossed into the data at larger Strouhal

numbers. This general result of a significant underprediction of data for Strouhal numbers larger than about 4 were also shown in figure 13 of reference 12 for an NACA 0012 airfoil. There, underprediction occurred above a Strouhal number of about 6 for 60 m/sec velocity and about 4 for 90 and 120 m/sec velocities. Generally good agreement was found at Strouhal numbers up to 6 (the upper limit shown) and 165 m/sec velocity. That airfoil had twice the chord of the small-chord NACA 0012 airfoil for which data are reported herein. It had twice the maximum thickness, and the same thickness ratio.

Evaluation of Noise Prediction Method

Spectra measured with the thin small airfoil, summarized in figures 7 and 8, generally matched the calculated spectra at the lower three velocities up to Strouhal numbers of 5 to 10. Amplitudes were underestimated at the two higher velocities, but general levels and shapes remained in agreement. In contrast, spectra measured for the thick airfoil decayed more rapidly than was predicted at Strouhal numbers larger than about 4. This Strouhal number corresponds to a turbulence wavelength of 1.4 times the maximum thickness and 7 times the leading edge radius. If the appropriate dimension was maximum thickness, data for the small thin airfoil would be expected to be overpredicted above a Strouhal number of 6. Scaled with leading edge radius, this upper limit of validity would be a Strouhal number of 9. Both of these predictions are in general agreement with the data, but the larger Strouhal number gives a better indication of the onset of major differences. For the two flat-plate airfoils tested by NASA which had the same chord but different thickness, overprediction at high frequencies developed above a turbulent wavelength of 3.6 times the maximum thickness and 7 times the leading edge radius. The condition of 7 times the leading edge radius (Strouhal number $fc/U = c/7r_{le}$) therefore is the upper limit of validity for noise calculated from a theory which uses the lift response of a flat-plate airfoil in a compressible subsonic turbulent flow. Wavyness of the calculated spectra developed when the acoustic wavelength became smaller than the chord (Strouhal number larger than the reciprocal of Mach number). However, this calculated wavyness often did not worsen the agreement between measured and calculated spectra.

As had been shown in figure 2(b) and can be seen from figures 6(a) through (c), measured noise radiation is overpredicted by about 8 dB at Strouhal numbers greater than twice the above critical Strouhal number. Strut noise radiation can therefore be significantly decreased at greater than some frequency f, in a flow with velocity U, if the leading edge radius r_{le} is larger than $0.3\ U/f$.

Strut Noise Radiation

Two methods for reduction of strut noise in turbulent flow were identified during this contract investigation. Noise radiated by struts in turbulent flow is predicted (reference 12) to be produced mainly near the leading edge, due to fluctuations of local lift force. Use of a large leading edge radius was shown in the preceding section to cause about 8 dB noise reductions at frequencies greater than about 0.3 times velocity divided by leading edge radius. Local radius of curvature for these airfoils was minimum at the leading edge and increased with increasing chordwise distance. The limit of such shapes, at constant allowable maximum thickness, is a constant-thickness flat plate with a cylindrical leading edge. Thus there is a limit to the minimum frequency above which substantial noise reduction can be achieved for a hard-wall strut in turbulent flow.

Tests conducted during the second year of this contract and reported in reference 2 showed that use of an acoustically soft leading edge region could achieve further reductions of strut noise. From the above results, noise of that strut with 1.27 cm (0.50 in.) leading edge radius would be expected to depart from the predicted sharp-leading-edge spectrum above 1.4 kHz and achieve considerable noise reduction beyond 3 kHz frequency at 125 m/sec (410 ft/sec) test airspeed. Major noise reduction therefore was achieved only at frequencies higher than those which have the largest effects on annoyance-weighted noise. Spectra for that hard-wall strut were compared with those for the strut with a perforated-plate leading edge region backed by a bulk acoustic absorber. Use of this acoustically treated leading edge achieved considerable noise reduction beyond 1.6 kHz for that test condition. Annoyance-weighted noise levels would be strongly affected by such reductions. Methods are not available for designing acoustically compliant leading edge regions to achieve noise reductions at specific frequencies.

Low-noise struts for the turbulent flow in engine ducts therefore should have the largest leading edge radius that provides acceptable strut maximum thickness based on duct flow blockage and losses. In the above example, use of 2.5 cm (1.0 in.) leading edge radius would have greatly reduced the annoyance-weighed noise by causing large noise reduction beyond 1.5 kHz frequency. It is not clear whether use of acoustically soft leading edges could achieve further noise reduction for those frequencies. However, a penalty in aerodynamic performance would be associated with the resulting 5.1 cm (2.0 in.) strut maximum thickness within a duct.

NOISE FROM FAN EXIT DUCT STRUTS AND SPLITTER RINGS

Calculation Method

Prediction of noise radiated from hard-wall struts, splitter plates, and splitter rings in fan exit ducts involves calculation of three acoustic processes: sound power generation by surfaces within the fan duct, noise transmission at the exit nozzle, and noise radiation outside the exit nozzle.

$$SPL(r,\theta,f)=PWL(f)+10\log\alpha'(f,M_1)+10\log\frac{\rho a}{2\pi r^2}F(\theta) \qquad (6)$$

The method used for calculating each of these three processes is discussed below. Implementation of this calculation method by a digital computer program is discussed in Appendix B and summarized by the flow chart given as figure 21.

Noise Generation From Isolated Airfoils

The first of these processes, noise generation, was done by the method developed by Amiet in reference 11. Turbulence within the fan duct was assumed to be described by the von Karman power spectrum. The mean velocity, rms normalized intensity, and integral scale length must be specified. Generally, the required turbulence information is not known within a fan duct.

For axial positions downstream of the stators, the dominant type of turbulence is likely to depend on radial position. Rotor tip vortexes chopped by the stators would be most important near the outer wall, and stator hub vortexes would dominate near the inner wall. Near midspan, the major turbulence encountered by a nonrotating surface generally would be the rotor wake after it has been chopped by the stators. Measurements of turbulence intensity and integral scale length at various positions downstream of the stator of a full scale (1.5 m diameter) low speed fan were reported in reference 2.

Acoustic intensity of struts and rings as determined for the turbulent flow within a fan exit duct was calculated by the computer program used in reference 12. Spectra computed for a fixed direction are relatively wavy. Calculated intensity was numerically integrated over direction angles from 90° to 180° from upstream to obtain aft-radiated sound power spectra within the fan duct. These calculated sound power spectra decayed smoothly at high frequencies. The computer program must be given as input the stagnation pressure ratio, speed of sound, and flow velocity within the duct. Additional

inputs are the number of radial struts, strut or ring chord, strut span or ring diameter, and the previously mentioned rms turbulence intensity and integral scale length. This provides the first term in equation (6).

Noise Transmission at Duct Exit

Acoustic power generated within a duct and radiated toward the downstream exit is partially reflected at the exit plane. A solution for the acoustic pressure reflection coefficient at an unflanged circular pipe with zero flow speed is available in reference 16. Approximate equations for reflection coefficient in the limits of large and small wavelength relative to duct radius are given as equations VII-1 and VII-2 of that reference. Complete reflection (reflection coefficient $R_{(M_1=0)}$ equal to unity), and therefore no transmission of sound, is predicted in the limit of very large wavelength and zero duct Mach number. An experimental study of transmission of acoustic waves at an unflanged circular exhaust with subsonic flow was given in reference 17. Increases of exit Mach number M_1 were found to increase the acoustic transmission coefficient toward unity (no reflection). Measured values of transmission coefficient $\alpha'(M_1)$ were adequately approximated by

$$\alpha'(f, M_1) = 1 - R^2_{(M_1=0)} \left[(1 - M_1)/(1 + M_1) \right]^2 \qquad (7)$$

Reflection coefficient R and therefore transmission coefficient α' are functions of frequency. This equation was utilized to predict the small decrease of sound power radiated from the duct exit, relative to that generated within the duct. Note that the refection coefficient at zero duct Mach number, and therefore the transmission coefficient at all subsonic Mach numbers, is a function of sound frequency, speed of sound at the exit, and exit diameter. The presence of a centerbody extending downstream of the nozzle exit plane was neglected in calculating reflection from the exit as a function of frequency. However, duct exit Mach number was calculated using the actual flow exit area.

Duct resonances, duct acoustic losses caused by sound-absorbing linings, and internal reflections have been completely neglected. All noise generated within the duct is assumed to approach the nozzle exit as plane waves moving parallel to the duct centerline. For the frequencies and duct Mach numbers of practical importance in predicting engine strut noise, the transmission coefficient given by equation (7) approaches one, and this term within equation (6) does not have a significant effect.

Far-Field Directivity

Analytical solutions were not available for the directivity of noise radiated from a duct exit having subsonic flow. From a brief review of limited available data, the measured directivity seemed to have little dependence on flow Mach number or measurement frequency. Noise amplitude clearly increased with increasing downstream direction angle, and then decreased abruptly as the exit centerline was approach. This behavior resembles that for jet exhaust noise. Therefore the directivity was arbitrarily modeled with the same functional dependence as jet noise. It was found that the factor $(1-.5\cos\theta)^3$ generally matched the measured variations from 70 to 140° direction. The refraction valley was approximated as an 0.5 dB/deg decrease from that factor at angles beyond 140° direction. Directivity at each polar angle θ was therefore represented by

$$SPL(\theta) = SPL(\theta = 90^\circ) + 30\log(1-0.5\cos\theta) + \Delta SPL \qquad (8)$$

where the quantity ΔSPL was zero for polar angles less than 140° and

$$\Delta SPL = -20\left[1-(180^\circ-\theta)/40^\circ\right] \qquad 140^\circ \le \theta \le 180^\circ \qquad (9)$$

Sound power P and far-field acoustic pressure are related by

$$\rho_a P = 2\pi r^2 \int_0^{2\pi} \overline{p^2} \sin\theta \, d\theta \qquad (10)$$

The integral in equation (10) was numerically integrated, using the directivity expressed by equations (8) and (9), to obtain a value of $2.0171\overline{p^2}(\theta = 90^\circ)$. Then the 1/3 octave sound pressure level at 90° direction can be expressed in terms of sound power level as

$$SPL(\theta = 90^\circ) = PWL + 10\log\frac{\rho_a}{2\pi r^2}\,\frac{10^{-13}}{(2\times10^{-5})^2}\,\frac{1}{2.0171} \qquad (11)$$

if far-field distance r and acoustic impedance ρ_a of the ambient air are expressed in metric-system units. For standard sea-level atmospheric properities, the argument of the logarithm is approximately $0.00823/r^2$. Sound pressure level SPL and sound power level PWL are referenced to 2×10^{-5} N/m^2 and 10^{-13} W, respectively. This directivity pattern is assumed to apply at all frequencies.

The assumed directivity pattern for noise radiated from a fan exit duct can be compared with data from reference 18 for orifice-generated noise introduced in the outer duct of a coaxial nozzle. Noise radiation patterns were measured for unheated jets with 183 m/sec (600 ft/sec) inner (core) duct velocity and three different outer (fan) duct velocities. Noise generated by the orifice and radiated out the nozzle exit clearly exceeded jet noise in the 1/3 octave band having 10 kHz center frequency. Measured directivity patterns for that frequency band are compared with the assumed pattern in figure 10(a). At direction angles to 120° from upstream, the data closely matched the assumed pattern and was unaffected by fan duct velocity. Measured levels at angles closer to the duct exit centerline decreased as the ratio of fan to core duct velocity increased. That is, fan duct flow produced refraction of the aft-radiated noise. In this region the assumed curve matched the general shape but not the relative levels of data.

Another check on approximate validity of the assumed directivity pattern is to compare with that for measured aft-radiated fan broadband noise. Noise data were given in reference 19 for three large single-stage fans having different design tip speeds. Tone and broadband noise was analyzed separately. Amplitude of aft-radiated broadband noise was found to depend on fan diffusion coefficient and therefore on wake momentum loss, in addition to the dependence on rotational speed. Normalized spectrum shape was reported to be independent of direction angle, as assumed in the method herein. Normalized broadband noise directivity patterns were given in figure 67 of reference 19 for these fans at subsonic and supersonic tip speeds. These data symbols are reproduced in figure 10(a) herein, along with the curve calculated from equations (8) and (9). The fan noise data increase somewhat more rapidly than the calculated curve between 90° and 120° directions, and start to decay beyond 120° or 130° rather than the assumed 140° angle. However, the general trend and level of this measured rotor-stator interaction noise is matched by the assumed behavior of noise radiated from fan exit ducts.

This assumed directivity can also be compared with that which was assumed in reference 20. In that NASA study, measured directivity of static engine noise was divided into jet mixing noise and internally generated noise. Forward flight effects on each type of noise were then calculated. The static directivity shape of internally generated engine noise was approximated in figure 2 of reference 20 by five straight line segments, each for a different range of direction angle. This shape, plotted in figure 11 as a dash line, is shown to match that from equations (8) and (9).

Comparisons With Engine Duct Noise Experiments

Turbine Exit Strut Noise

Test Configuration

Contributions of turbine exit struts to aft-radiated core engine noise were investigated in a (British) National Gas Turbine Establishment study reported in reference 21. The model tested was a 1/8 scale simulation of the Olympus 593 engine exhaust system downstream of the turbine exit plane. As sketched in figure 12(a), it had ten 45° cambered struts mounted on the converging aft portion of the centerbody exhaust cone. In an actual engine, these struts would remove swirl from the turbine exhaust flow. A constant-area jet pipe and convergent nozzle extended beyond the centerbody. Twelve adjustable nonrotating 30° camber swirl vanes, located far upstream of the struts in a region of low flow velocity, produced swirl in the flow approaching the struts.

Sound power spectra were given in figure 12 of reference 21 for various configurations. The struts caused about 10 dB increase of high-frequency sound power above that for the exhaust jet alone at low exhaust velocities. Addition of the swirl vanes, without the downstream struts, caused negligible increase of measured noise above that for the exhaust jet alone. Addition of the swirl vanes, at the incidence which produced zero swirl at the struts, caused negligible increase of measured noise above that for the jet and struts. This comparison proved that the presence of the struts, but not the swirl vanes, caused a major increase of noise at low exhaust velocities. To demonstrate that the increased noise was radiated by the struts and transmitted out the nozzle, tests were conducted with the hard-wall jet pipe replaced by an acoustic lining. Measured noise was reduced to the levels predicted for the known lined-duct attenuation at each frequency band, acting on the measured noise increment caused by the struts. The following acoustic comparisons utilize only data taken with the hard-wall jet pipe.

Noise data were measured for a 30° range of swirl vane incidence and constant strut incidence. At 139 m/sec (455 ft/sec) jet velocity, a 15° decrease of vane incidence above nominal zero swirl caused 3 to 4 dB decrease of sound power at greater than 2 kHz center frequency. A 5° increase caused 2 to 3 dB increase, and a further 10° increase caused about 6 dB additional increase of sound power with constant spectrum shape. Measured axial turbulence level at this flow velocity was shown in figure 5 of reference 21 to be approximately constant near 3.4% at the strut inlet for this range of swirl vane angles at 152 m/sec (500 ft/sec) jet velocity. Turbulence level at the strut exit was unchanged for the smaller angles but varied circumferentially

from 8 to 18% at the highest positive incidence. Measured strut wake profiles, plotted in figure 3 of reference 21, show that the strut passages at mid-annulus were stalled for this largest angle.

Strut chord was specified at 8.5 cm (1.27 in.), and span at the leading edge was scaled from figure 1 of reference 21 as 4.25 cm (1.67 in.). Turbulence integral length scale was taken equal to twice the calculated flat-plate turbulent boundary layer thickness at the trailing edge of the swirl vanes. This calculated length scale was 0.50 cm (0.19 in.) and 0.45 cm (0.17 in.) for 139 m/sec (455 ft/sec) and 287 m/sec (940 ft/sec) jet exhaust velocities. Local mean velocities at the strut leading edge were calculated from the area ratio and compressible flow equations as 103 m/sec (338 ft/sec) and 176 m/sec (576 ft/sec) for these exhaust velocities, with an unheated air supply.

Comparison With Data

Measured free-field directivity in three different octave frequency bands was plotted in figure 11 of reference 21 for 146 m/sec exhaust velocity. These data were given for the struts tested only with the largest swirl vane deflection. This angle had produced stalled flow at the struts, and had greatly increased the radiated sound power. Data for this condition therefore should not be used for evaluating calculated sound pressure levels at various direction angles. However, they can provide a test of the predicted normalized directivity shape. The data for 0.8 kHz center frequency, where measured SPL was not greatly increased by the struts, had the same directivity shape that was measured for the datum jet without struts or vanes. For 5 and 25 kHz, the presence of the struts caused more than 10 dB increase of SPL and produced greater variation with angular position than that measured with the moderate subsonic jet. These directivity shapes, normalized to their measured values at 90° from the centerline, are compared in figure 12(b) with the curve given by equations (8) and (9). The measured variation at 5 kHz center frequency was matched within 1.5 dB by that curve, except for the one data point in the refraction region near the exhaust direction. At the higher frequency, measured variations in the region of strongest noise (between 90° and 135° from the inlet) agreed with the lower-frequency variation and the predicted curve. However, measured values decreased more rapidly than was predicted as the upstream or downstream centerline was approached.

The logarithmic sums of power spectra calculated for aft-radiated strut noise, and reported for the datum jet noise, are compared in figure 13 with measured spectra. This comparison is given for 139 m/sec (455 ft/sec) and 287 m/sec (940 ft/sec) exhaust jet velocities, the two conditions for which

data are given in figure 10 of reference 21. Data symbols are shown for 40° swirl vane angle along with dash lines which indicate the data band for the range from 25° to 45° (unstalled flow). At the higher velocity, strut noise was calculated to be largest at 6.3 kHz and was nearly equal to the measured jet noise. The sum of calculated strut noise and measured jet noise, shown as the upper solid line, matched the data for greater than 2 kHz model frequency (250 Hz full scale frequency). Turbine exit struts would have caused about 3 dB increase of annoyance-weighted noise at full scale and this exhaust velocity.

Strut noise as calculated for the lower exhaust velocity was of the order of 10 dB above noise of the datum jet at greater than 2 kHz model frequency. Measured noise of the configuration with design swirl was overpredicted 2 to 4 dB between 1.25 and 4 kHz center frequencies but was closely matched at higher frequencies. Annoyance-weighted noise at full scale and this velocity, due to the struts, would be about 9 dB greater than that for the datum jet and would be closely predicted. The measured increases of sound power by several dB at low frequencies (below 630 Hz at the lower and 1.6 kHz at the higher speed) were not predicted by this method. However, the strut-generated noise at frequencies that would be most annoying at full scale was closely predicted for both exhaust velocities.

Splitter Ring Noise Comparison

Test Configuration

Acoustically lined splitter rings can be placed within turbofan exit ducts to absorb aft-radiated fan noise. As was shown in figure III-37 of reference 22, a hard-wall splitter ring in a fan exit duct increased the broadband sound power at 1/3 octave center frequencies from 400 Hz to blade passing frequency of 2.8 kHz at 90% speed. It was concluded that splitters could generate a noise floor that would limit attainable fan noise reductions.

Duct flow velocity was taken as the nominal design condition for the QCSEE engine, with duct flow area sized (reference 23) to give a Mach number of 0.50 downstream of the stator. Tabulated noise data for this configuration are available in reference 24 for 60, 70, and 80% of design speed. Aerodynamic performance data for this fan stage are presented in reference 25. For these noise calculations, required duct flow properties were calculated from measured stagnation pressure ratio and temperature ratio, nozzle discharge velocity, and the duct and discharge nozzle dimensions. There were no direct measurements of either duct flow velocity or turbulence level, but reasonable numbers could be estimated or assumed. Flow properties utilized in the noise calculations are tabulated on the following page.

Percent Speed	Pressure Ratio	Nozzle Exit Velocity, m/sec	Duct Speed of Sound, m/sec	Duct Flow Velocity, m/sec	Duct Flow Mach No.
60	1.14	148	349	116	0.34
70	1.20	171	353	132	0.38
80	1.26	197	356	150	0.43
90	1.36	223	360	166	0.47
100	1.40	244	365	178	0.50

The duct flow Mach number calculated in this manner for the design pressure ratio of 1.4 at 100% speed is 0.50 as specified in reference 23. The test configurations with and without the exhaust duct splitter ring included three taped splitter rings in the fan inlet.

Comparisons With Data

Typical 1/3 octave spectra of sound pressure levels in the far field at 110° measurement direction, taken from the tabulations in reference 24, are given in figure 14 for the three rotational speeds tested. This direction would yield near-maximum aft-radiated flyover or sideline noise. Measured spectra are shown for the configurations with and without the fan exit duct splitter ring. Noise radiation from the engine duct, caused by the presence of the splitter ring, was determined from the difference between these spectrum levels. The noise spectrum generated by this ring is plotted as solid square symbols. These symbols are omitted when the differences were less than 2 dB because the corresponding inferred noise increment would be unreliable relative to data scatter. This added noise exceeded that of the configuration without exit splitter rings in the range from 400 to about 1600 Hz frequency. Also plotted are calculated spectra for this noise increment. The calculations used a 6.5% turbulence level and 1.1 cm integral scale length. These curves matched the general shape of the inferred spectra. In the frequency range where splitter ring noise could be measured accurately, the spectra were closely predicted at the two lower speeds and underestimated at the highest speed. Measured spectra at higher frequencies are consistent with the predicted calculated splitter ring noise increment.

Directivity of noise from the splitter ring was evaluated for SPL at 1000 Hz center frequency, where this noise increment could be determined reliably. Measured and calculated directivities of this quantity are plotted in figure 15. Data for the aft hemisphere are closely predicted at the two lower speeds and underestimated 3 to 4 dB at the highest speed.

In addition to a broad region of aft-radiated sound, the splitter ring produced a relatively sharp peak of forward-radiated noise centered near 30° polar angle. This noise, not predicted by the calculation method given herein, probably was radiated upstream through the stator, rotor, and inlet. This unpredicted noise is weaker than the aft peak and is distributed at polar angles closer to the rotational axis, so its contribution to sound power was unimportant.

Measured and calculated sound power spectra from the fan exit duct splitter ring are plotted in figure 16. The measured spectra were determined from sound power spectra tabulated in reference 24 for numerical integration over all direction angles. That is, they are the sum of noise radiated in both the inlet and exhaust hemispheres. Sound power spectra at 80% speed had been plotted in figure III-37 of reference 22 and figure 18(b) of reference 24 for the exhaust hemisphere. Spectra for the inlet hemisphere were plotted in figure 18(a) of reference 23. In the frequency range where splitter ring sound power level caused a significant increase of noise, the contribution within the exhaust hemisphere was about 4 dB larger. Use of the available tabulated sound power levels evaluated for all directions therefore introduced less than 1.5 dB error as compared with numerical integration of tabulated SPL spectra to obtain the separate contributions from each hemisphere. These total sound power spectra were closely predicted for the two highest speeds and overestimated about 3 dB for the lowest speed. Thus the amplitude, spectrum, and directivity of noise generated by an annular splitter ring in a fan exit duct, and radiated from the exhaust nozzle, can be predicted for a range of fan rotational speeds by the method described herein and given in Appendix B. Unambiguous data were available only for the limited frequency range from about 250 to 2000 Hz, so the predicted spectra cannot be fully validated.

If these results are typical of noise radiation from a large turbofan engine, then additional noise from annular splitter rings in fan exit ducts will only be important in the mid-frequency range at low power settings, relative to fan and jet noise.

Long-Chord Stator Vane Noise Comparison

Test Configurations

Effects of fan stator length on tone and broadband noise were reported in references 26 and 27. These tests were conducted at NASA Lewis Research Center with a nominal full-scale, 1.83 m (6 ft) diameter fan. The original design had 53 rotor blades and 112 stator vanes. This blade-vane ratio had been chosen to prevent propagation of the tone at rotor blade passing frequency. However, this tone occurred and was attributed to the interaction

of inlet flow distortion or turbulence with the rotor blades. Long-chord stator vanes containing acoustic damping material were tested in place of the original stators. Comparisons discussed herein are for configurations where the sound-absorbing material was made inactive by being covered with metal tape. Only the additional noise caused by increased stator chord is examined.

To achieve a vane thickness equal to the acoustic liner depth, the number of stator vanes was decreased to 1/8 the original number (14 rather than 112). The shortest of three sets of long-chord stator vanes had a chord approximately nine times that of the original vanes. Thus the total stator vane area was nearly identical for the shortest long-chord vanes and the original vanes. As described in reference 26, unsteady lift force per unit area at blade passing frequency was predicted to be 1/3 as large as that for the original vanes. Thus the sound power at and above blade passing frequency was expected from that analysis to be reduced by a factor of 9, or about 9.5 dB decrease of sound power level and sound pressure level. The long-chord stator vanes could be extended in length by adding straight pieces behind the turning section. The longest set of long-chord vanes was 37 times the length of the original stator vanes. It extended beyond the pylon which supported the simulated engine centerbody. A third set was 3/4 that length. Note that the longest long-chord vanes had about four times the chord and four times the area of the shortest set of those vanes. From the analysis developed in reference 26, they would be expected to have about half the lift force fluctuation per unit area, twice the total lift force fluctuation, and about 6 dB more noise than the shortest long-chord vanes at constant frequency.

An analytical method for predicting the effect of stator chord on noise radiation can be applied as either an absolute or a relative calculation. As an absolute calculation, one would estimate the flow velocity approaching the stator at each test point and the turbulence properties of the rotor blade wake swept across the stator vanes, calculate the noise spectrum for each set of stator vanes, and compare directly with data. When this was done for the original stator, the general shape was correctly predicted but absolute levels of sound power were overpredicted. Uncertainty in estimating both the local velocity and local turbulence level contributed to this difference. For the purpose of this study, the error was arbitrarily attributed to inadequate prediction of turbulence amplitudes. A relative prediction was then obtained by (1) adjusting the input turbulence to obtain calculated sound power spectra which matched those for the original stator vanes, (2) changing the vane chord and vane number to those for each set of long-

chord vanes while retaining the adjusted input turbulence, and (3) comparing sound power spectra calculated in this manner with the data for long-chord stator vanes. Acoustic power spectra, which include both forward- and aft-radiated noise, are plotted in reference 26 for the various stator configurations tested with a hard-wall inlet without inlet splitter rings. Acoustic absorbing liners in the exhaust duct were taped. Tabulated 1/3 octave sound pressure levels for the three sets of long-chord splitters and this test configuration are given as configurations 70, 71, and 77 of reference 27.

Comparisons With Data

Measured 1/3 octave total sound power spectra for the fan with its original stator vanes are plotted in figure 17. At each rotational speed the 1/3 octave sound power was approximately constant between 100 and 500 Hz center frequencies, increased to a peak at blade passing frequency, and slowly decreased at higher frequencies. Calculated spectra of aft-radiated sound power levels, plotted as solid curves, match the data for moderate and high frequencies. They do not predict the constant levels at low frequencies. These curves were calculated for 1.1 cm turbulence length scale and 1.5% turbulence level. This length scale had been used in the previous calculation of noise from a fan exit duct splitter ring, but the turbulence level which had to be assumed in order to match these data is only about 1/4 as large.

Noise radiation from the long-chord stator vanes was calculated with these turbulence properties. Relative sizes of the original vanes and the shortest and longest long-chord vanes are shown in the sketch at the top of figure 18. Calculated and measured 1/3 octave acoustic power spectra for these three configurations are plotted in figure 16 for three rotational speeds. All of the long-chord stators were predicted by the method of Appendix B to have the same spectrum within 0.2 dB. This result is contrary to the 6 dB variation expected from use of the method used in reference 25. The shortest set of long-chord stator vanes produced up to 10 dB increase of sound power at low frequencies. This increased noise was attributed in reference 27 to aerodynamic flow separation at the pylon, caused by adverse interference with the stator flow field. At the lowest rotational speed, the longest long-chord stator vanes produced little increase of low-frequency noise over that for the original stator vanes. They achieved 5 to 6 dB noise reduction between there and blade passing frequency, and between blade passing frequency and twice that frequency. These levels approached the calculated reductions of 7 dB near 1000 Hz and 9 dB above 2500 Hz center frequencies. These noise reductions decreased somewhat at 70% speed. With further increase to 80 and (not shown) 90% speed, amplitude of the low-frequency part of the spectrum increased above that for the original stator vanes. Also,

noise reductions at higher frequencies became much smaller. It seems likely that these longest-chord stator vanes produced flow constriction and local flow separation near the pylon at high rotational speeds. The resulting increase of noise would not be predicted by the calculation method developed here. As shown by narrowband spectra (figure 27 of reference 26), amplitude of the tone at blade passing frequency was essentially independent of stator vane chord. This propagating tone was attributed to turbulence ingested through the inlet and convected through the rotor, rather than interaction between the rotor and stator. Turbulence convected through the fan rotor would also cause tone and broadband noise at higher frequencies; this additional noise would be unaffected by stator vane chord. Only limited portions of the frequency range were caused by noise generated by convection of rotor blade wakes past the stator vanes, the noise process represented herein.

The effect of long-chord stator vanes on directivity of sound pressure level in the 1/3 octave band having 3150 Hz center frequency had been shown in figure 29(a) of reference 26 for 80% speed. This frequency lies between blade passing frequency and its first overtone. Measured directivities are compared in figure 19 with those calculated for aft-radiated strut noise. Measured levels are taken from the tabulation in reference 27. Forward-radiated noise at angles up to 50° from the inlet was reduced about 9 dB, in agreement with the predicted increment. Noise reductions obtained with the longest long-chord stator were about 8 dB between 80 and 110° angles from the inlet but were only about 6 dB near peak amplitude. That is, measured noise reductions were less than was calculated. The shortest long-chord stator vanes produced more aft-radiated noise than the longest vanes.

The effect of long-chord stator vanes on directivity in the 1/3 octave band centered at 1250 Hz is shown in figure 20 for two rotational speeds. At 60% speed, calculated directivity curves generally matched all of the data. Amplitudes were overestimated about 2 dB for the original stator vanes and longest stator vanes, and were overestimated by that amount for the shortest long-chord vanes. Measured levels of aft-radiated noise for the longest long-chord stator vanes at 70% speed were about 2 dB higher than predicted. Those for the shortest long-chord stator vanes, which had additional noise caused by separated flow, had increased to the noise levels of the original configuration. Further increases of rotational speed (not shown) increased the aft-radiated noise levels for all long-chord stator vanes to more than those for the original stator vanes.

Results of this comparison are somewhat ambiguous because several noise mechanisms such as local separated flow and ingestion of atmospheric turbulence were present in addition to rotor-stator interaction, and local mean velocity and turbulence approaching the stators had not been measured. To the limited extent for which the comparison is valid, the method developed herein seems to predict the spectrum and directivity of aft-radiated noise caused by changes of stator vane number and chord. This prediction applies only for those portions of the spectrum dominated by noise caused by rotor blade wakes moving past the stator vanes. Vane geometry must be selected to prevent flow separation, and its additional noise, at the intended operating configuration.

CONCLUSIONS

1. Methods for calculating each of the steps required for predicting engine aft-radiated noise from fan exit duct struts (noise generated by isolated airfoils in uniform turbulence, noise transmission through a nozzle exit, and noise propagation through the fan discharge shear layer to the far field) have been separately validated.

2. Comparisons of predictions with far-field noise data for struts, vanes, and rings in complete turbofan engine ducts were not reliable because even the best available data did not give unambiguous measurement of noise increments, and local flow conditions were not adequately known.

REFERENCES

1. Fink, M. R.: Investigation of Scrubbing and Impingement Noise. NASA CR-134762, Feb. 1975.

2. Fink, M. R.: Prediction of Externally Blown Flap Noise and Turbomachinery Strut Noise. NASA CR-134883, Aug. 1975.

3. Fink, M. R.: Additional Studies of Externally Blown Flap Noise. NASA CR-135096, Aug. 1976.

4. Fink, M. R.: A method for Calculating Externally Blown Flap Noise. NASA CR-2954, 1978.

5. Dean, L. W.: Broadband Noise Generated by Airfoils in Turbulent Flow. Paper 71-587, AIAA, June 1971.

6. Paterson, R. W., Vogt, P. G., and Foley, W. M.: Design and Development of the United Aircraft Research Laboratories Acoustic Research Tunnel. J. Aircraft, Vol. 10, No. 7, July 1973, pp 427-433.

7. Fink, M. R.: Experimental Evaluation of Theories for Trailing Edge and Incidence Fluctuation Noise. AIAA Journal, Vol. 13, No. 11, Nov. 1975, pp 1472-1477.

8. Filotas, L. T.: Theory of Aircraft Response in a Gusty Atmosphere. Part II - Response to Discrete Gusts or Continuous Turbulence. Univ. of Toronto, Inst. for Aerospace Studies, UTIAS Rep. 141, AFOSR 69-3089TR, Nov. 1969.

9. Hayden, R. E.: Noise From Interaction of Flow With Rigid Surfaces: A Review of Current Status of Prediction Techniques. NASA CR-2126, Oct. 1972.

10. Olsen, W. A.: Noise Generated by Impingement of a Turbulent Jet on Isolated Airfoils of Varying Chord, Cylinders, and Other Flow Obstructions. Paper 76-504, AIAA, July 1976.

11. Amiet, R. K.: Acoustic Radiation from an Airfoil in a Turbulent Stream. J. Sound and Vib., Vol. 41, No. 4, 1975, pp 407-420.

12. Paterson, R. W. and Amiet, R. K.: Acoustic Radiation and Surface Pressure Characteristics of an Airfoil Due to Incident Turbulence. NASA CR-2733, Sept. 1976.

13. Goldstein, M. E.: Aeroacoustics. NASA SP-346, 1974, pp 218-219.

14. Amiet, R. K.: Correction of Open Jet Wind Tunnel Measurements for Shear Layer Refraction. Paper 75-532, AIAA, Mar. 1975.

15. Hinze, J. O.: Turbulence. McGraw-Hill Book Co., New York, 1959, p 60.

16. Levine, H. and Schwinger, J.: On the Radiation of Sound from an Unflanged Circular Pipe. Physical Review, Vol. 73, No. 4, Feb. 15, 1948, pp 383-406.

17. Schlinker, R. H.: Transmission of Acoustic Plane Waves at a Jet Exhaust. Paper 77-22, AIAA, Jan. 1977.

18. Olsen, W. A. and Friedman, R.: Jet Noise From Co-Axial Nozzles Over a Wide Range of Geometric Flow Parameters. Paper 74-43, AIAA, Jan. 1974.

19. Burdsall, E. A. and Urban, R. H.: Fan-Compressor Noise: Prediction, Research, and Reduction Studies. FAA-RD-71-73, Feb. 1973.

20. Stone, J. R.: Flight Effects on Exhaust Noise for Turbojet and Turbofan Engines - Comparison of Experimental Data With Prediction. NASA TM X-73552, Nov. 1976.

21. Bryce, W. D. and Stevens, R. C. K.: An Investigation of the Noise From a Scale Model of an Engine Exhaust System. Paper 75-459, AIAA, Mar. 1975.

22. Feiler, C. E., et al.: Fan Noise Suppression. Aircraft Engine Noise Reduction. NASA SP-311, May 1972, pp 63-102.

23. Cornell, W. G.: Experimental Quiet Engine Program - Summary Report. NASA CR-2519, Mar. 1975.

24. Dittmar, J. H. and Groeneweg, J. F.: Effect of Treated Length on Performance of Full-Scale Turbofan Inlet Noise Suppressors. NASA TN D-7826, Dec. 1974.

REFERENCES (Concluded)

25. Goldstein, A. W., Lucas, J. G., and Balombin, J. R.: Acoustic and Aerodynamic Performance of a 6-Foot-Diameter Fan for Turbofan Engines, II-Performance of QF-1 Fan in Nacelle Without Acoustic Suppression. NASA TN D-6080, Nov. 1970.

26. Dittmar, J. H., Scott, J. N., Leonard, B. R., and Stakolich, E. G.: Effects of Long-Chord Acoustically Treated Stator Vanes on Fan Noise. I-Effect of Long Chord (Taped Stator). NASA TN D-8062, Oct. 1975.

27. Dittmar, J. H., Scott, J. N., Leonard, B. R., and Stakolich, E. G.: Effects of Long-Chord Acoustically Treated Stator Vanes on Fan Noise. II-Effect of Acoustical Treatment. NASA TN D-8250, Oct. 1976.

28. Amiet, R. K.: Computer Programs for Calculation of the Forces on and Sound Produced by an Airfoil in a Turbulent Flow. Report R76-111204-1, United Technologies Research Center, June 1976.

APPENDIX A: LIST OF PUBLICATIONS PRODUCED

The following three annual reports and two final reports were prepared under this Contract and published as NASA Contractor Reports.

Fink, M. R.: Investigation of Scrubbing and Impingement Noise. NASA CR-134762, Feb. 1975.

Fink, M. R.: Prediction of Externally Blown Flap Noise and Turbomachinery Strut Noise. NASA CR-134883, Aug. 1975.

Fink, M. R.: Additional Studies of Externally Blown Flap Noise. NASA CR-135096, Aug. 1976.

Fink, M. R.: A Method for Calculating Strut and Splitter Plate Noise in Exit Ducts - Theory and Verification. NASA CR-2955, 1978.

Fink, M. R.: A Method for Calculating Externally Blown Flap Noise. NASA CR-2954, 1978.

The following AIAA papers, and subsequent publications of some of these papers, provided wider distribution of major results obtained under this Contract.

Fink, M. R.: Experimental Evaluation of Theories for Trailing Edge and Incidence Fluctuation Noise. AIAA J., Vol. 13, No. 11, Nov. 1975, pp 1472-1477. Also, Paper 75-206, AIAA, Jan. 1975.

Fink, M. R.: Scrubbing Noise of Externally Blown Flaps. Progress in Astronautics and Aeronautics, Vol. 45, Aeroacoustics: STOL Noise, Airframe and Airfoil Noise, M.I.T. Press, Cambridge, Ma., pp 3-25, 1976. Also, Paper 75-469, AIAA, Mar. 1975.

Fink, M. R. and Olsen, W. A.: Comparison of Predictions and Under-the-Wing EBF Noise Data. Paper 76-501, AIAA, July 1976.

Fink, M. R.: Forward Flight Effects on EBF Noise. Paper 77-1314, AIAA, Oct. 1977.

The following AIAA paper, prepared by NASA Lewis Research Center, compared NASA data with predictions calculated under this Contract.

Olsen, W. A., Burns, R., and Groesbeck, D.: Flap Noise and Aerodynamic Results for Model QCSEE Over-the-Wing Configurations. Paper 77-23, AIAA, Jan. 1977.

The following AIAA paper and publication, while not conducted under this Contract, described a direct extension of contract results to an additional practical application.

Fink, M. R.: Approximate Prediction of Airframe Noise. J. Aircraft, Vol. 13, No. 11, Nov. 1976, pp 833-834. Paper 76-526, AIAA, July 1976.

APPENDIX B: COMPUTER PROGRAM FOR CALCULATING STRUT OR SPLITTER NOISE

General Description

This digital computer program, written in FORTRAN IV, predicts noise radiated from struts, exit guide vanes, or annular splitter rings in fan exit ducts exhausting to sea-level standard ambient air. Noise is calculated as overall and 1/3 octave sound pressure levels in the free field at points on a sphere centered at the nozzle exit. These points are equally spaced in polar angle, with zero polar angle taken as forward along the nozzle centerline. The pressure field is assumed axisymmetric about this centerline. Atmospheric properties are those of the standard sea-level atmosphere. The only dimensional input quantities are lengths and velocities. All lengths except far-field distance R must be given in the same units, and velocities in length units per second (meters and meters per second, feet and feet per second). Far-field distance must be in meters. The program is relatively small, requiring less than 12K of computer memory.

A title card, prepared for each run, provides a printed title to identify each specific configuration. Data input uses standard NAMELIST format starting in column 2. The required 1/3 octave frequency range is defined by the lower frequency FL and upper frequency FU. The one integer input, TYPE, describes the type of noise-producing surface (1 for an annular ring and 2 for struts). Surface geometry is described by the chord C, ring diameter or strut span S, and number of struts N. Flow properties within the exit duct are given by local mean flow velocity V, speed of sound A, ratio P of duct static pressure to standard sea-level static pressure, turbulence integral scale length L, and normalized turbulence intensity U. Turbulence was assumed to be described by the von Karman power spectrum. Sound power spectrum radiated within the duct in the downstream direction is then calculated by the method of Amiet (reference 12) by numerically integrating over direction angles from 91° to 179° in 2° increments. This portion of the computer program was taken directly from a program developed by him and given in reference 28. The calculation flow chart is shown in figure 21.

Duct exit conditions are described by the nozzle exit diameter DEXIT and velocity VEXIT. Transmission of sound power at the subsonic exit is calculated as a function of reduced frequency and exit Mach number, using Schlinker's approximate solution for plane waves (reference 17). Far-field sound pressure levels are calculated at input radius R, for direction angles from lower angle THL to upper angle THU in increments DELTH. These three angles must be specified in degrees. If R is input as less than 0.1, this

far-field calculation is omitted and only the power spectrum is computed. Atmospheric attentuation is not represented.

Data input are given below for a simple test case of 3 struts, with 1.0 m chord and 0.5 m span, in a fan exit duct at two values of fan rotational speed. An 0.01 m turbulence scale length and 5% turbulence level were assumed. Each rotational speed produces a different input pressure ratio, speed of sound, duct velocity, and nozzle exit velocity. Far-field spectra are calculated at 30.5 m radius for three direction angles. The resulting print-out, which consists of a table of input parameters and a table of spectra and overall quantities for each rotational speed, follows the program listing.

```
TEST CASE FOR STRUT NOISE
$INPUT
TYPE=2,N=3.,C=1.,S=.5,DEXIT=1.5
L=0.01,U=.05,FL=100.,FU=1.E4
R=30.5,THL=45.,THU=135.,DELTH=45.
P=1.2,A=350.,V=130.,VEXIT=170.
$END
$INPUT
P=1.4,A=360.,V=200.,VEXIT=250.
$END
7FIN
```

PROGRAM LISTING

```
      COMMON/TITLE/ITITLE(13),SFL(45,50),PWR(45),FB(45),THARRY(50),IF,
     $ LF,
     $ OAPWL,OASPL(50)
        COMPLEX CA, E1, E2, E3, G1, XL
      REAL MI
      REAL FL,FU,C,S,L,CO,V,P,U,M,N,DEXIT,VEXIT,R,THL,THU,DELTH,MEXIT,
     $ KA,RSQ,ALPHA,SUM,OAPR,X,Y,Z
      INTEGER TYPE,PFLG
      NAMELIST /INPUT/ FL,FU,C,S,L,A,V,P,U,N,DEXIT,VEXIT,R,THL,THU,
     $                 DELTH,TYPE
      THL = 0.0
      THU = 180.0
      DELTH=10.
      FL = 50.0
      FU = 20000.0
      R = 0.0
      A=340.3
      P = 1.0
      FB(1) = 10.
      FB(2) = 12.5
      FB(3) = 16.
      FB(4) = 20.
      FB(5) = 25.
      FB(6) = 31.5
      FB(7) = 40.
      FB(8) = 50.
      FB(9) = 63.
      FB(10) = 80.
      DO 4 I = 1,10
      FB(I+10) = 10. * FB(I)
      FB(I+20) = 100. * FB(I)
4     FB(I+30) = 1000. * FB(I)
      READ(5,6) (ITITLE(I),I=1,13)
6     FORMAT(13A6)
5     READ (5,INPUT,ERR=100,END=100)
      CO = A
      M = V/CO
      MEXIT = VEXIT/CO
      IF (TYPE.EQ.1) N = 1.5708
      WRITE(6,70) FL,FU,C,S,L,CO,V,P
70    FORMAT(/,'0INPUT PARAMETERS --',/,
     $' FL=',F9.1,/,' FU=',F9.1,/,' C=',F9.4,/,' S=',F9.4,/,' L=',F9.4,
     $ /,' A=',F9.4,/,' V=',F9.4,/,' P=',F9.4)
      WRITE(6,71) U,DEXIT,VEXIT,R,THL,THU,DELTH,N
71    FORMAT(' U=',F9.4,/,' DEXIT=',F9.4,/,' VEXIT=',F9.4,/,' R=',F9.4,
     $ /,' THL=',F9.4,/,' THU=',F9.4,/,' DELTH=',F9.2,/,' N=',F9.4,///)
      IF = 1
      DO 10 I = 1,38
      IF (FL.LT.FB(I))GO TO 20
10    IF = I
20    LF = 38
      DO 21 I = 1, 38
      J = 39 - I
      IF (FU.GT.FB(J)) GO TO 41
21    LF = J
```

```
      44    IF ( IF.LT.LF) GO TO 5
            LF = IF
      5     CAPP = .
            DO 6 I = IF,LF


            KA = 3.1416*DEXIT*FR(I)/C
C***  REFLECTION COEFFICIENT FOR INCOMPRESSIBLE FLOW
            RSQ = 0.0
            IF (KA.GE.7) GO TO 51
            RSQ = (1.+(KA)**4.*(1.5833-LOG(1.4*KA))/6.)**2.*EXP(-(KA)**2.)
            IF (KA.LE.1.) GO TO 51
            RSQ = 3.1416*KA*(1.+.09375/(KA)**2.)**2.*EXP(-2.*KA)
C***  TRANSMISSION COEFFICIENT FOR SUBSONIC EXIT DUCT
 51         ALPHA = 1.-RSQ*((1.-MEXIT)/(1.+MEXIT))**2.
            SUM = 0.0
            DO 1 NX=1,45
            Z = .017453*(2.*NX-1)
            X = SIN(Z)
            Y = 1.0
            Z = COS (Z)
C***  INTEGRATE NOISE RADIATION OVER REAR QUADRANT USING INCIDENT
C***        TURBULENCE NOISE THEORY OF AMIET, NASA CR-2733
              CA = CMPLX(1.,1.)
              B = SQRT(1.-M**2)
              CC = S*(M**2*P*U*C)**2*M/C
              C2 = 3.14159*C/(M*CC)
              EK = .37342*C/L
              SG = SQRT(X**2 + B**2*(Y**2+Z**2))
              MI = M*SQRT(X**2+(B*Z)**2)/SG
              SQ1 = SQRT(1.+MI)
              SQP = SQRT(MI+M*X/SG)
              SQM = SQRT(MI-M*X/SG)
              SQ2 = SQRT(MI)
              C1 = CC*(Z/SG**2)**2
              XK = C2*FR(I)
              XKS = XK/R**2
              UMI = MI*XKS
              YK = M*XK*Y/SG
              XKE = XK/EK
              YKE = YK/EK
              XK2 = XKE**2 + YKE**2
              T = .1*XK2*XKE**2/(1.+XK2)**2.33333
              IF (UMI-.4) 30, 30, 40
 30           AL = 1./(SQRT(1./(1.+2.4*XKS)+6.28319*XKS)*B)
              GO TO 62
 40           SRT = SQRT(1.27324*XKS)
              CALL FRNL(SRT*SQM,E1)
              CALL FRNL(1.41421*SRT*SQ2,E2)
              CALL FRNL(SRT*SQP,E3)
              A1 = 2.*XKS*SQM**2
              G1 = CMPLX(COS(A1),SIN(-A1))
              XL = (1.41421*SQ2*CA*E3/SQP-1.)*G1+1.-CA*E2
              XL = (1.41421*E1/SQM + CMPLX(0.,1.)*XL
```

```
     1        /(2.*3.1416*SRT*SUM**2))*.31831*B/(XK*SQ1)
          AL = CABS(XL)
   62    SUM = SUM + T * AL**2. * 10.**10.546
   61    CONTINUE
C*** ONE- THIRD OCTAVE SOUND POWER SPECTRUM TRANSMITTED AT DUCT EXIT
         PRES = .232*FR(I)*ALPHA*3.0349*SUM
         OAPR = CAPR + PRES
   64    PWR(I) = 10.*ALOG10(62.832*N*PRES)
         PFLG = 2
         OAPWL = 10.*ALOG10(62.832*N*OAPR)
C*** SPL CALCULATION IS OMITTED IF R IS DELIBERATELY SET LESS THAN 0.1
         IF (R.LT.0.1) GO TO 95

         DEG2RD = .01745329
         THL = THL * DEG2RD
         THU = THU * DEG2RD
         DELTH = DELTH * DEG2RD
         DO 65 I = IF,LF
         THETA = THL - DELTH
         J = 0
   67    THETA = THETA + DELTH
         IF (THETA.LT.0) GO TO 67
         IF (THETA.GT.3.1415927) GO TO 65
         IF (THETA.GT.THU) GO TO 65
         J = J + 1
         THARAY(J) = THETA/DEG2RD
C*** ONE- THIRD OCTAVE SOUND PRESSURE LEVEL AT ANGLE THETA,DISTANCE R
         SPL(I,J)=PWR(I)+10.*ALOG10(.0079577/(1.-.5*COS(THETA))**3./(R*R))
         IF (THETA.GE.0.4416) SPL(I,J) = SPL(I,J)-20.*(1.-(3.1416-THETA)
        $    /.7)
         OASPL(J)=OAPWL+10.*ALOG10(.0079577/(1.-.5*COS(THETA))**2./(R*R))
         IF (THETA.GE.0.4416) OASPL(J)=OASPL(J)-20.*(1.-(3.1416-THETA)/.7)
         GO TO 67
   65    CONTINUE
         THL=THL/DEG2RD
         THU=THU/DEG2RD
         DELTH=DELTH/DEG2RD
C   PRINT TABLE
   300   IF (J.LT.14) GOTO 400
         CALL PRINT(TYPE,PFLG,1,13)
         IF (J.LT.27) GO TO 401
         CALL PRINT(TYPE,PFLG,14,26)
         CALL PRINT(TYPE,PFLG,27,J)
         GO TO 405
   400   CALL PRINT(TYPE,PFLG,1,J)
         GO TO 405
   401   CALL PRINT(TYPE,PFLG,14,J)
   405   GO TO 5
   95    PFLG = 1
         CALL PRINT(TYPE,PFLG,14,26)
         GOTO 5
   100   I = 1
         END
```

```
      SUBROUTINE P-INT(TYPE,PFLG,M,N)
      COMMON/TITLE/TITLE(13),SPL(45,50),PWR(45),FB(45),THARRY(50),IF,
     $ LF,
     $ OASPL(50)
      INTEGER TYPE,PFLG
      WRITE(6,1) (TITLE(K),K=1,13)
    1 FORMAT(1H1(/),'*** ',1A6,' ***',///)
      IF (TYPE.EQ.1) WRITE(6,2)
      IF (TYPE.EQ.2) WRITE(6,3)
    2 FORMAT(30X,'EXIT DUCT SPLITTER RING',/)
    3 FORMAT(30X,'EXIT DUCT STATORS',/)
      WRITE(6,4)
    4 FORMAT(' 1/3 OCTAVE     SOUND                    SOUND PRESSURE LEVEL FOR
     $DIRECTION ANGLE, DEG.')
      IF (PFLG.EQ.1) GOTO 100
      WRITE(6,5) (THARRY(K),K=M,N)
    5 FORMAT(' CTR FREQ,HZ  POWER,DB',13(1X,F5.1,2X))
      DO 11 I = IF,LF
      WRITE(6,6) FB(I),PWR(I),(SPL(I,K),K=M,N)
    6 FORMAT(1X,F8.1,2X,F8.1,13(1X,F7.1))
   11 CONTINUE
      GO TO 101
  100 WRITE(6,7)
    7 FORMAT(' CTR FREQ,HZ  POWER,DB')
      DO 12 I = IF,LF
      WRITE(6,8) FB(I),PWR(I)
    8 FORMAT(1X,F8.1,2X,F8.1)
   12 CONTINUE
  101 IF (PFLG.EQ.1) GOTO 102
      WRITE(6,15) OAPWL,(OASPL(J),J=M,N)
   15 FORMAT(/,' OVERALL',7X,F6.1,13(1X,F7.1))
      GOTO 103
  102 WRITE(6,16) OAPWL
   16 FORMAT( /,' OVERALL',7X,F6.1)
  103 RETURN
      END
```

```
      SUBROUTINE FRNL(X,E)
      COMPLEX E, G, H
      G = CMPLX((1.+.92*X)/(2.+ 1.97*X + 3.104*X**2),
     1      1./(2.+ 4.142*X + 3.492*X**2 + 6.67*X**3))
      D90 = 1.5707963
      H = CMPLX(SIN(D90*X**2),COS(D90*X**2))
      E = G*H + CMPLX(.5,(-.5))
      RETURN
      END
```

INPUT PARAMETERS --
FL= 100.0
FU= 10000.0
C= 1.0000
S= .5000
L= .0100
A= 350.0000
V= 130.0000
P= 1.2000
U= .0500
DEXIT= 1.5000
VEXIT= 170.0000
R= 30.5000
THL= 45.0000
THU= 135.0000
DELTH= 45.00
N= 5.0000

** TEST CASE FOR STRUT NOISE

EXIT DUCT STATORS

1/3 OCTAVE CTR FREQ,HZ	SOUND POWER,DB	SOUND PRESSURE LEVEL FOR DIRECTION ANGLE, DEG. 45.0	90.0	135.0
100.0	98.7	42.5	48.1	52.1
125.0	102.1	45.9	51.6	55.5
160.0	105.4	49.2	54.9	58.8
200.0	108.3	52.1	57.8	61.8
250.0	111.3	55.1	60.8	64.7
315.0	113.8	57.6	63.3	67.2
400.0	116.9	60.7	66.4	70.3
500.0	119.5	63.3	69.0	72.9
630.0	121.9	65.7	71.4	75.3
800.0	124.3	68.0	73.7	77.7
1000.0	126.1	69.8	75.5	79.5
1250.0	127.4	71.1	76.8	80.8
1600.0	128.4	72.1	77.8	81.8
2000.0	128.7	72.5	78.1	82.1
2500.0	128.6	72.3	78.0	81.9
3150.0	128.0	71.8	77.4	81.4
4000.0	127.0	70.8	76.5	80.4
5000.0	125.9	69.7	75.4	79.3
6300.0	124.6	68.3	74.0	78.0
8000.0	123.0	66.8	72.5	76.5
10000.0	121.6	65.4	71.1	75.0
OVERALL	137.7	81.4	87.1	91.1

INPUT PARAMETERS --
FL= 100.0
FU= 10000.0
C= 1.0000
S= .5000
L= .0100
A= 350.0000
V= 200.0000
P= 1.4000
U= .0500
DEXIT= 1.5000
VEXIT= 250.0000
R= 30.5000
THL= 45.0000
THU= 135.0000
DELTH= 45.00
N= 3.0000

** TEST CASE FOR STRUT NOISE

EXIT DUCT STATORS

1/3 OCTAVE CTR FREQ,HZ	SOUND POWER,DB	SOUND PRESSURE LEVEL FOR DIRECTION ANGLE, DEG. 45.0	90.0	135.0
100.0	103.6	47.4	53.1	57.1
125.0	106.7	50.5	56.2	60.1
160.0	109.9	53.7	59.4	63.4
200.0	113.0	56.8	62.4	66.4
250.0	116.6	59.4	65.8	69.0
315.0	118.6	62.4	68.1	72.0
400.0	121.7	65.5	71.2	75.1
500.0	124.4	68.2	73.9	77.8
630.0	127.3	71.1	76.7	80.7
800.0	129.9	73.7	79.4	83.4
1000.0	132.3	76.1	81.8	85.7
1250.0	134.4	78.2	83.9	87.8
1600.0	136.4	80.2	85.8	89.8
2000.0	137.6	81.4	87.1	91.0
2500.0	138.4	82.2	87.9	91.8
3150.0	138.7	82.5	88.2	92.1
4000.0	138.5	82.3	87.9	91.9
5000.0	137.9	81.6	87.3	91.3
6300.0	136.9	80.7	86.4	90.3
8000.0	135.6	79.5	85.2	89.2
10000.0	134.4	78.2	83.9	87.8
OVERALL	147.5	91.2	96.9	100.9

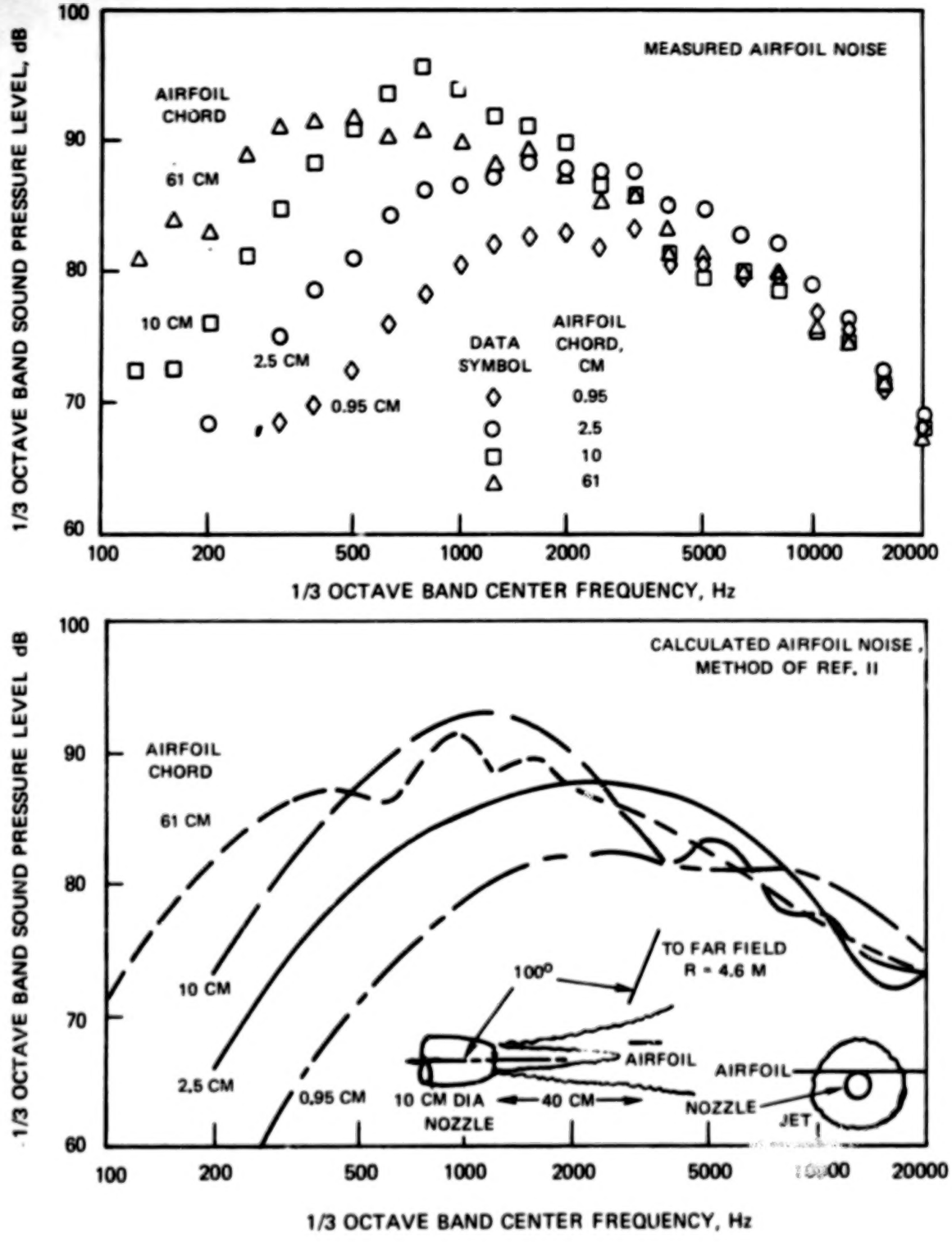

FIGURE 1 – MEASURED AND CALCULATED NOISE SPECTRA ABOVE AIRFOILS OF DIFFERENT CHORD AND 0.32 CM THICKNESS, EXTENDING ACROSS A JET REGION, 94 M/SEC PEAK IMPINGEMENT VELOCITY.

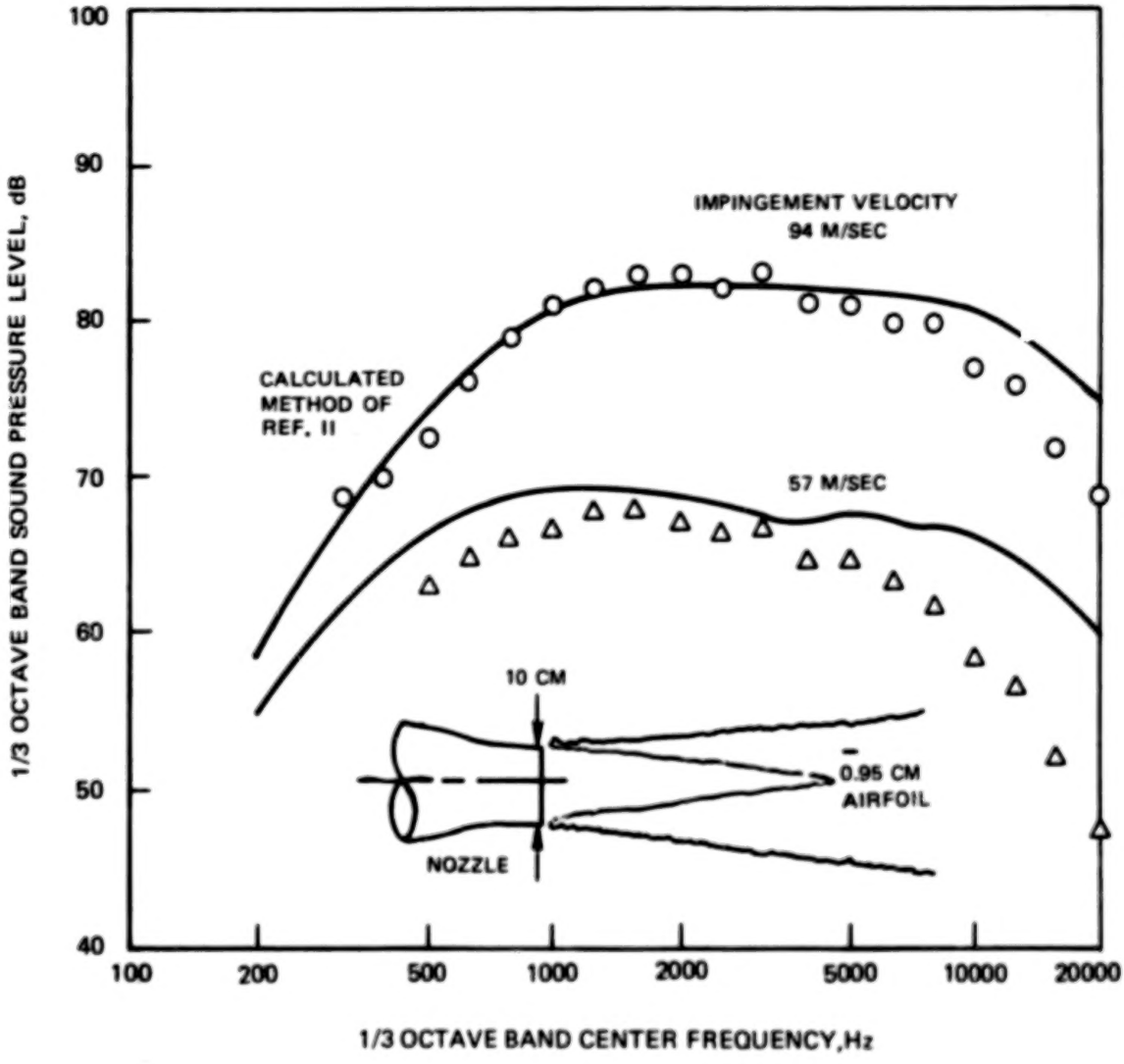

FIGURE 2 – COMPARISON OF CALCULATED AND MEASURED SPECTRA AT 90° GENERATED BY AIRFOIL EXTENDING ACROSS A JET MIXING REGION. (a) 0.95 CM (3/8 IN.) CHORD AIRFOIL

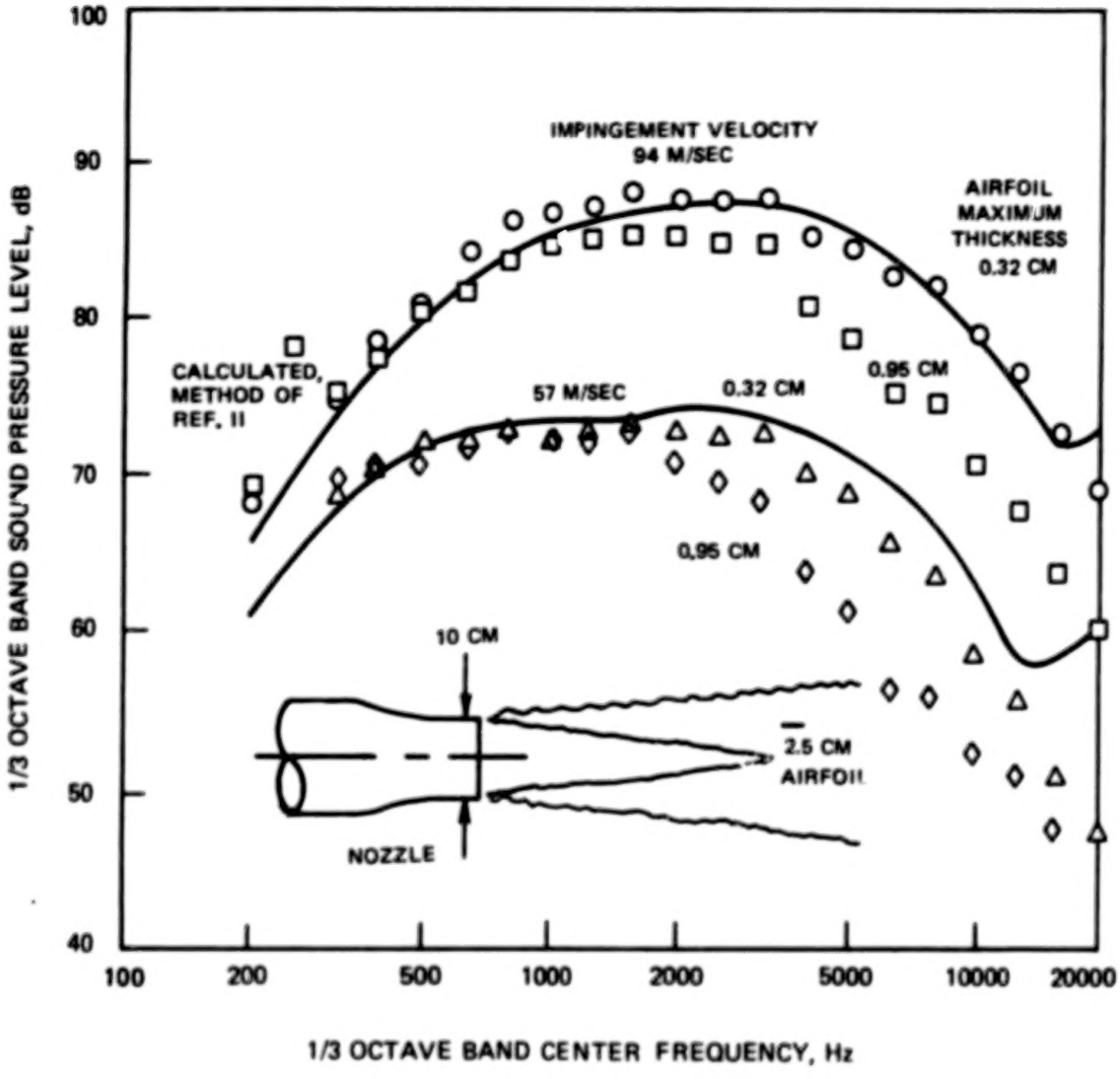

FIGURE 2 – CONTINUED (b) 2.5 CM (1 IN.) CHORD AIRFOIL, TWO THICKNESSES

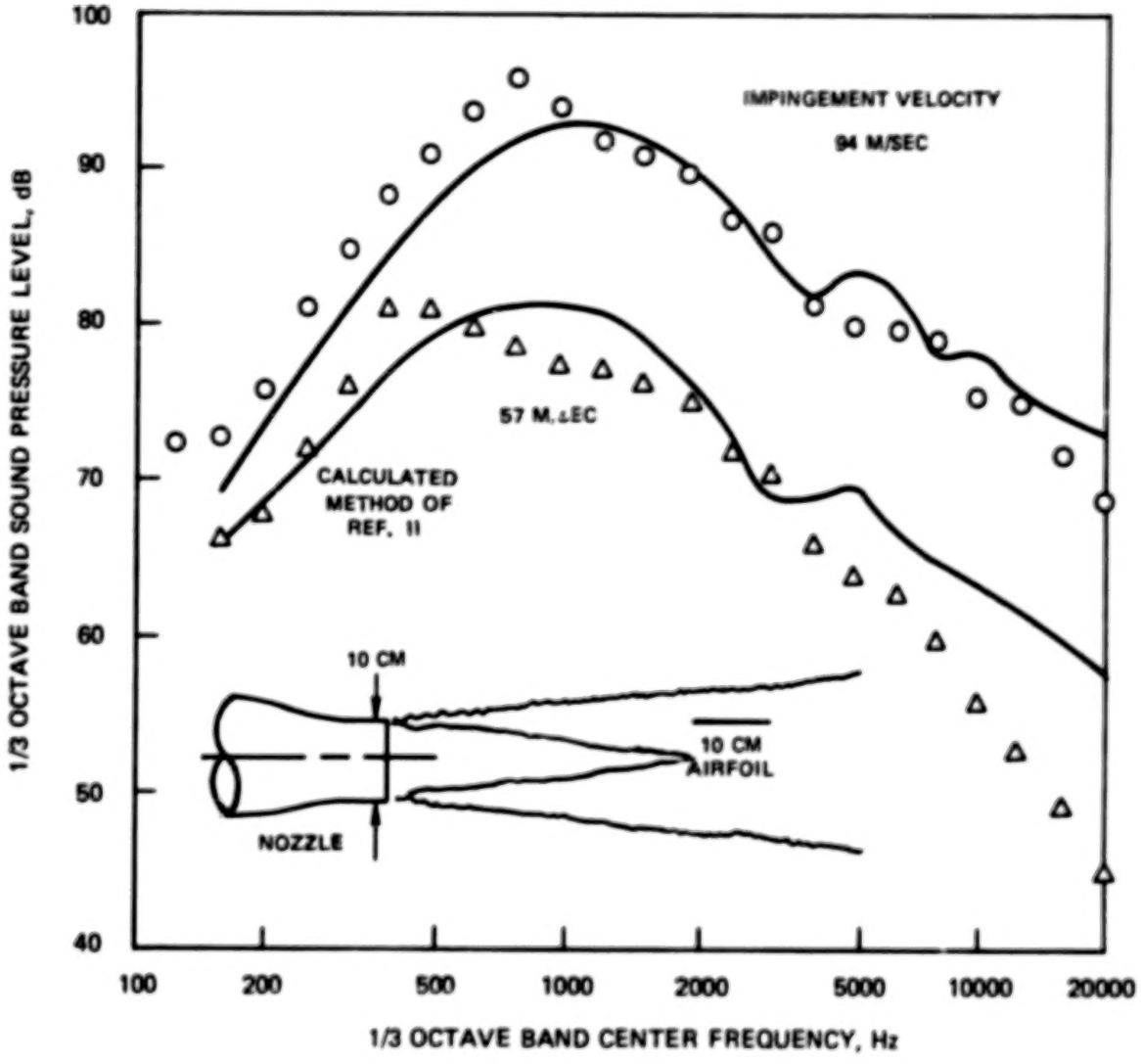

FIGURE 2 – CONTINUED (c) 10 CM (4 IN.) CHORD AIRFOIL

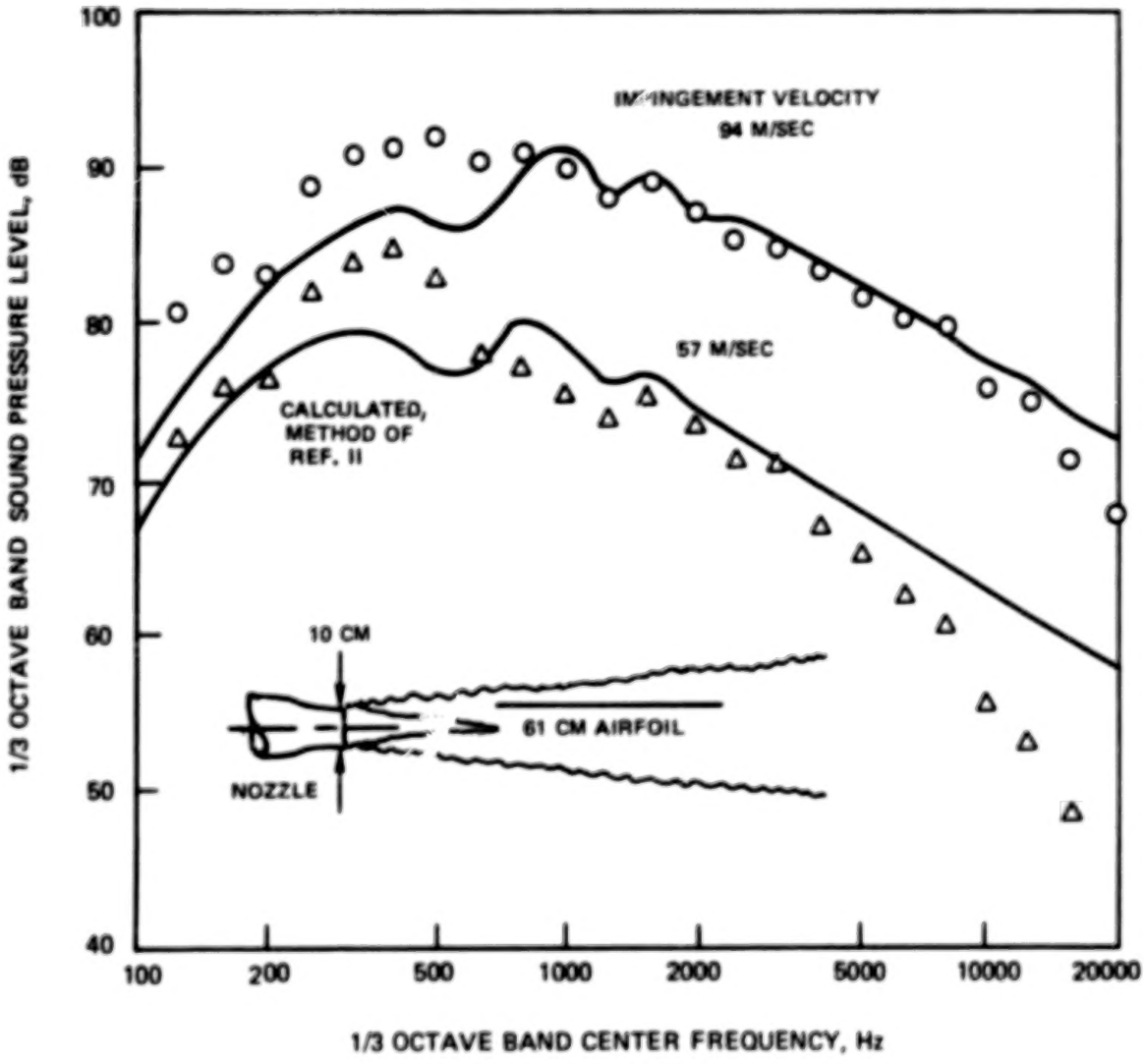

FIGURE 2 – CONCLUDED (d) 61 CM (24 IN.) CHORD AIRFOIL

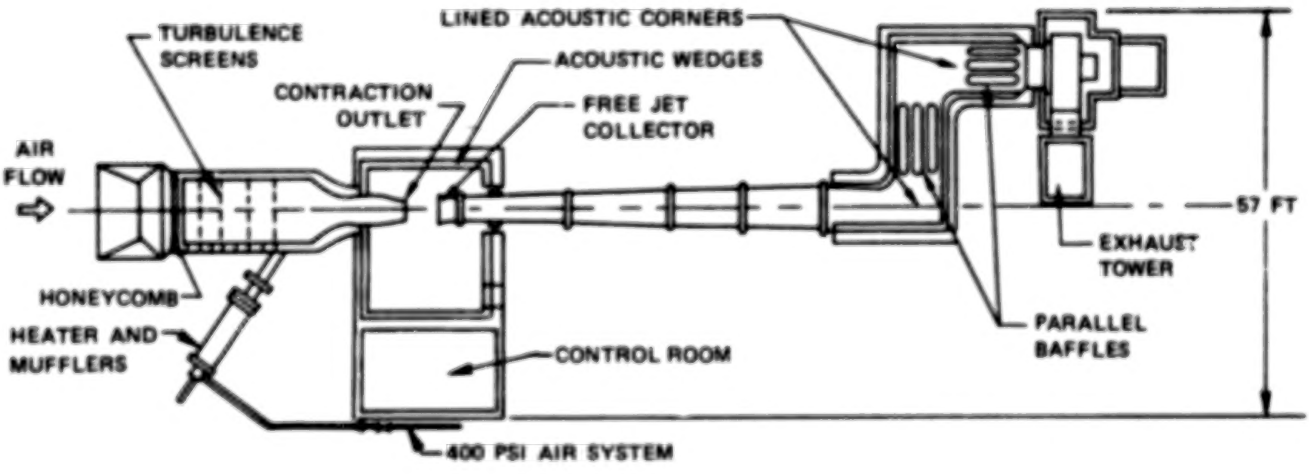

TOP VIEW

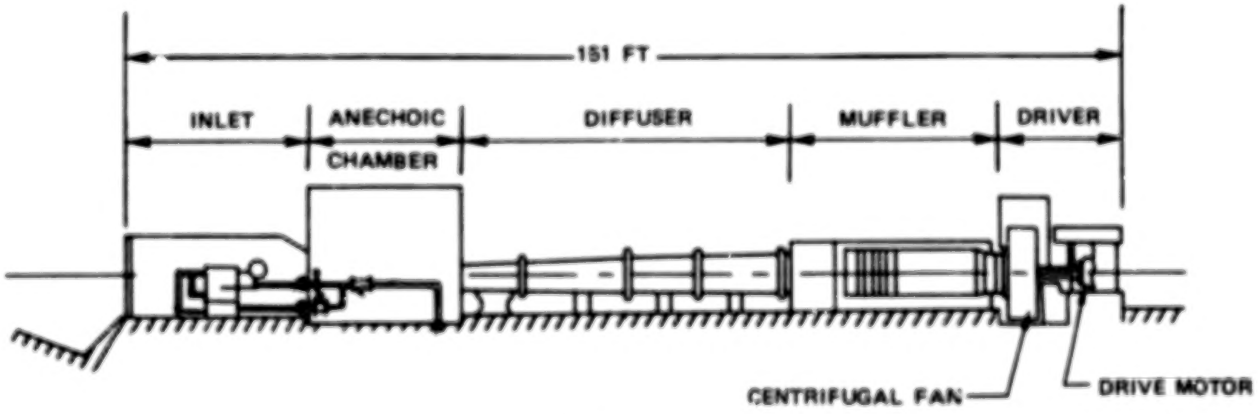

SIDE VIEW

FIGURE 3 – UTRC ACOUSTIC RESEARCH TUNNEL

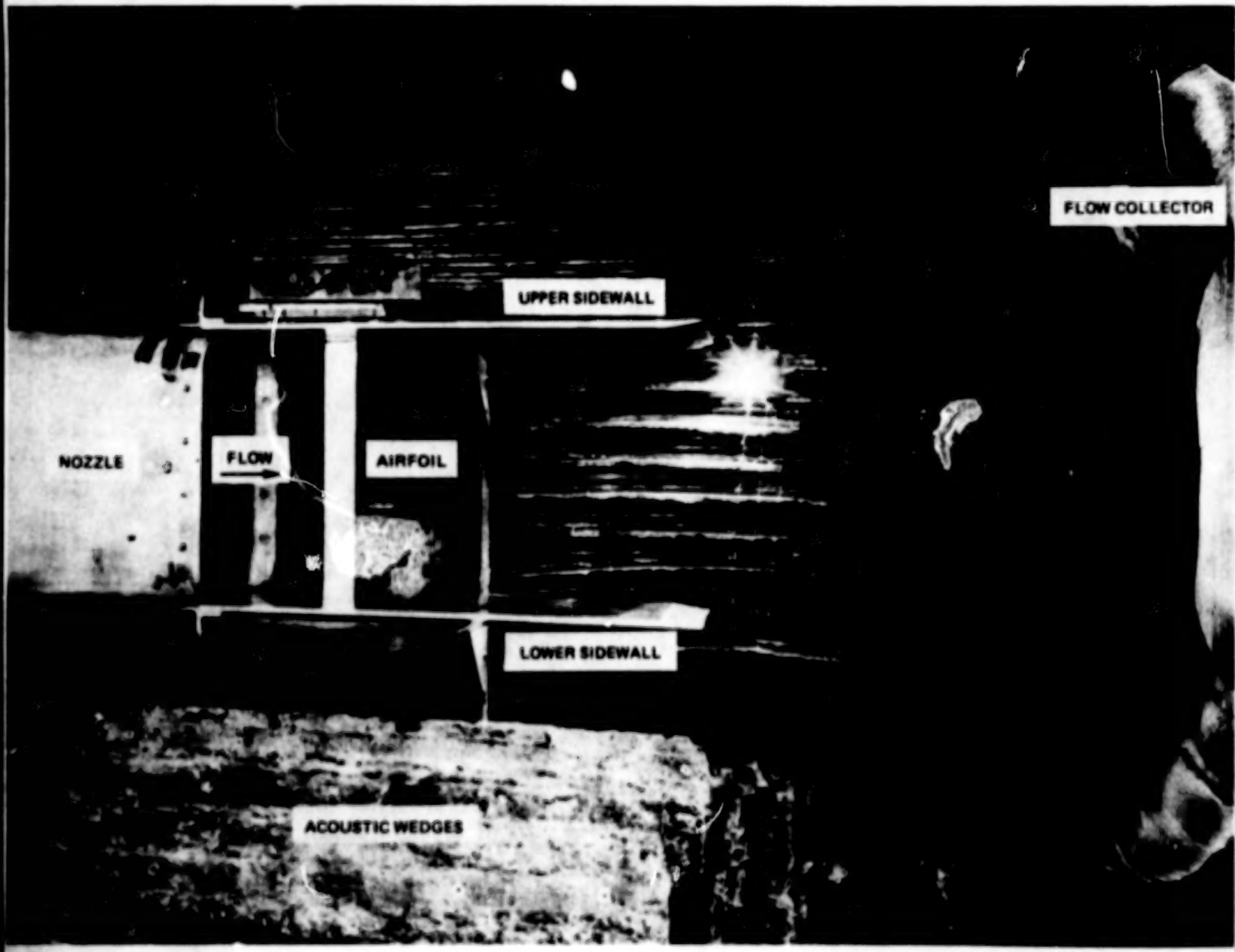

FIGURE 4 – ACOUSTIC TUNNEL TEST SECTION WITH 11.4 CM (4.5 IN.) CHORD AIRFOIL

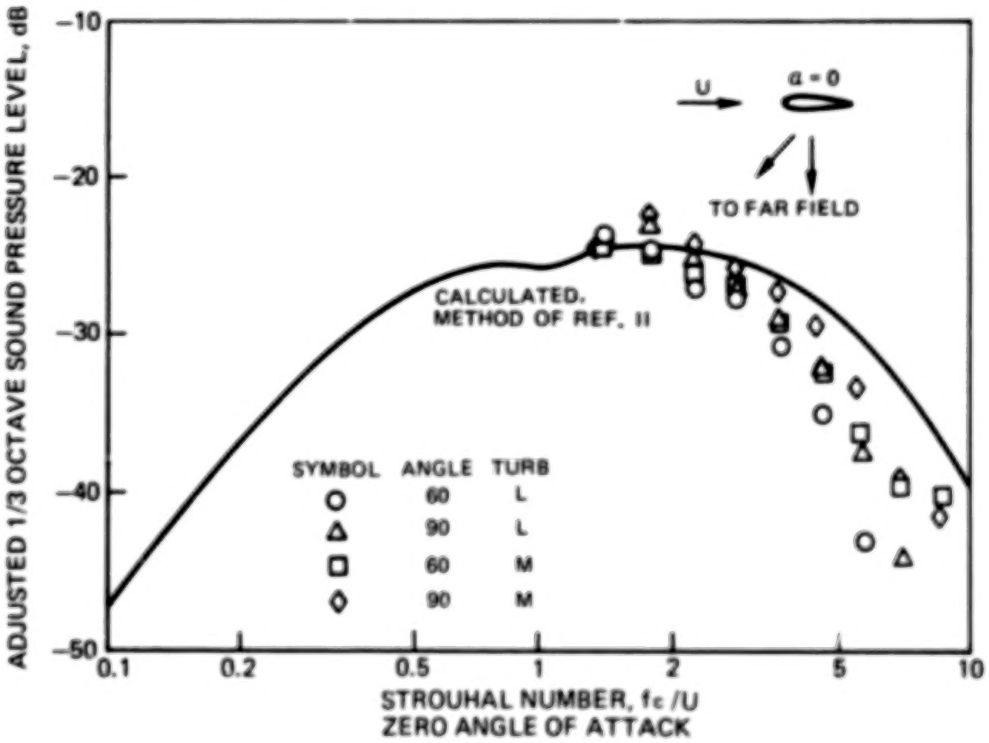

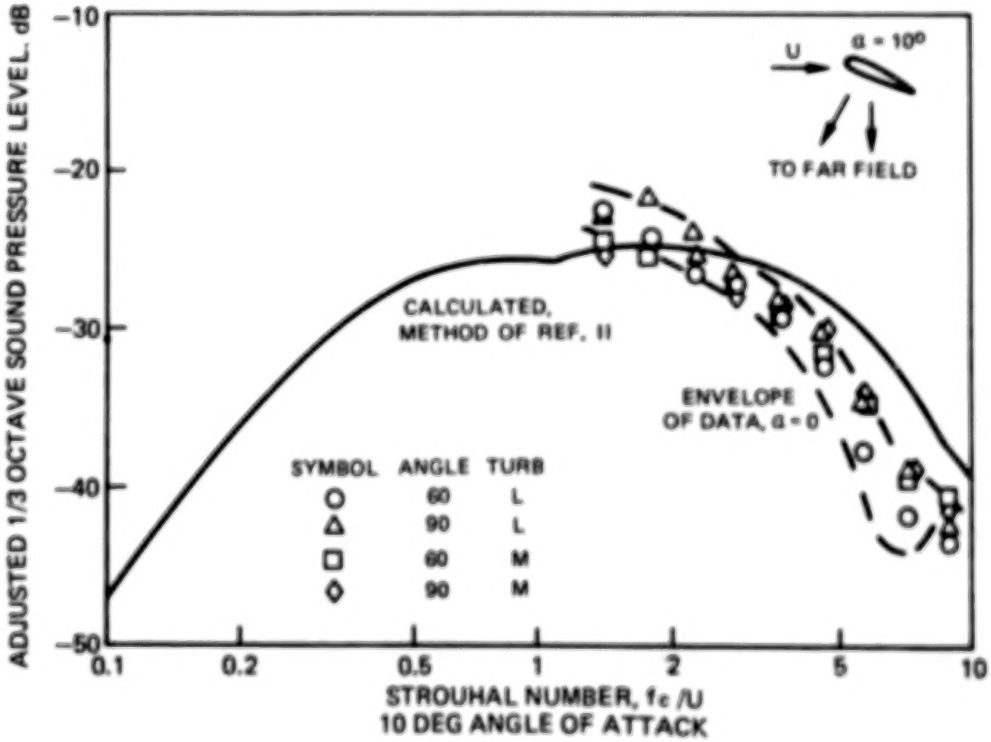

FIGURE 5 –MEASURED AND CALCULATED ADJUSTED SPECTRA FOR SMALL THIN AIRFOIL IN TURBULENT FLOW, (a) 31.5 M/SEC VELOCITY

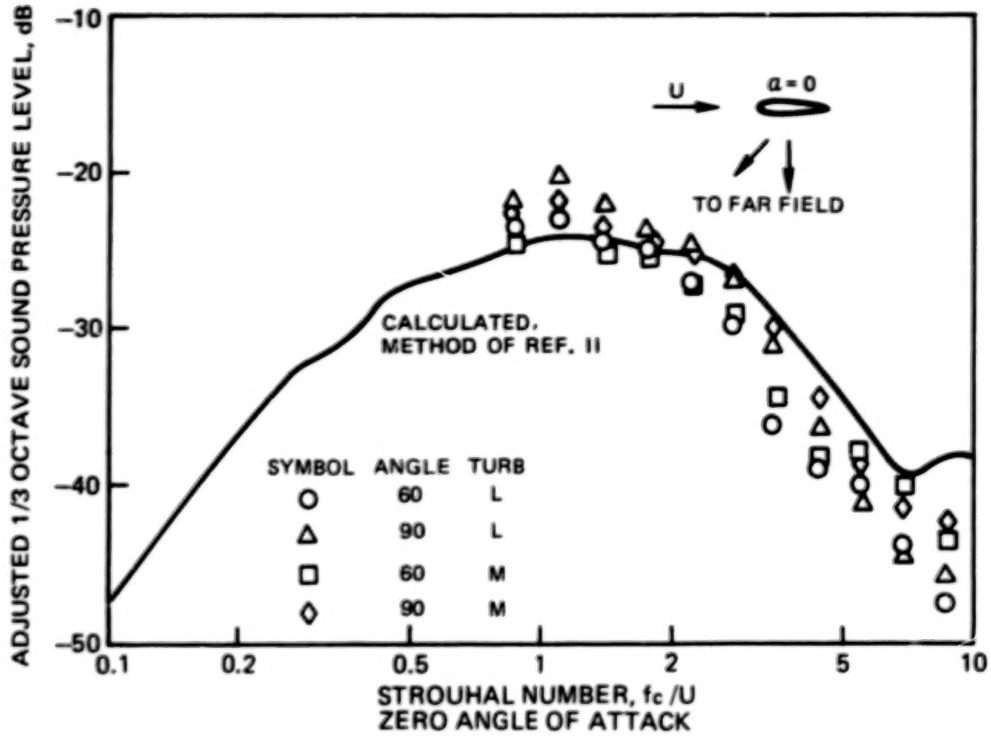

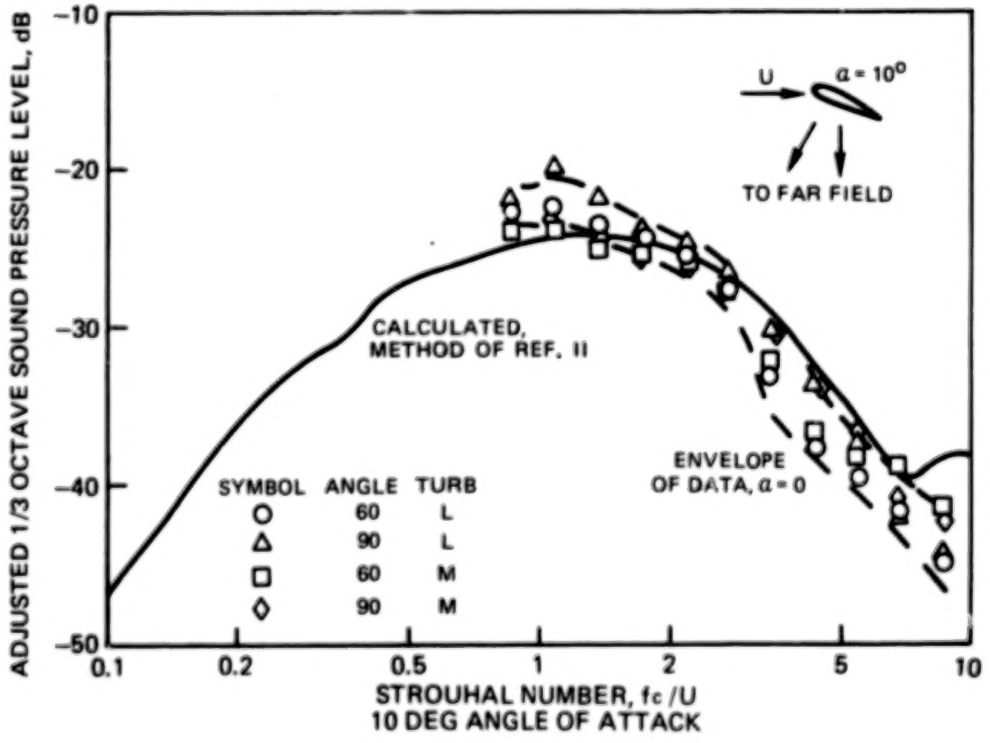

FIGURE 5 –CONTINUED. (b) 50 M/SEC VELOCITY

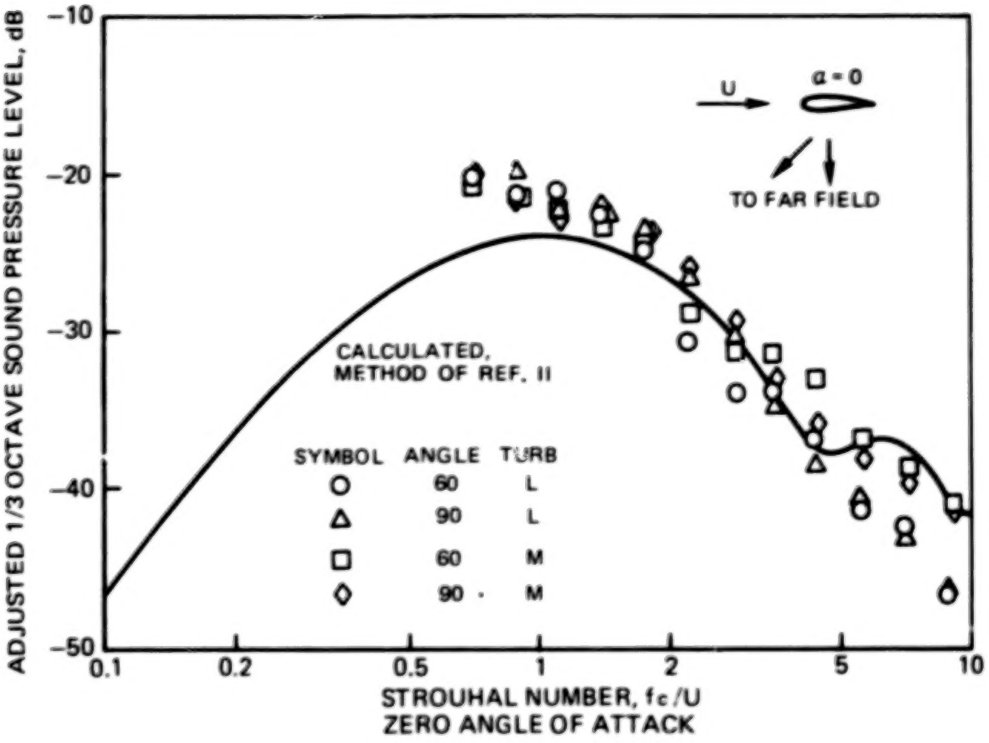

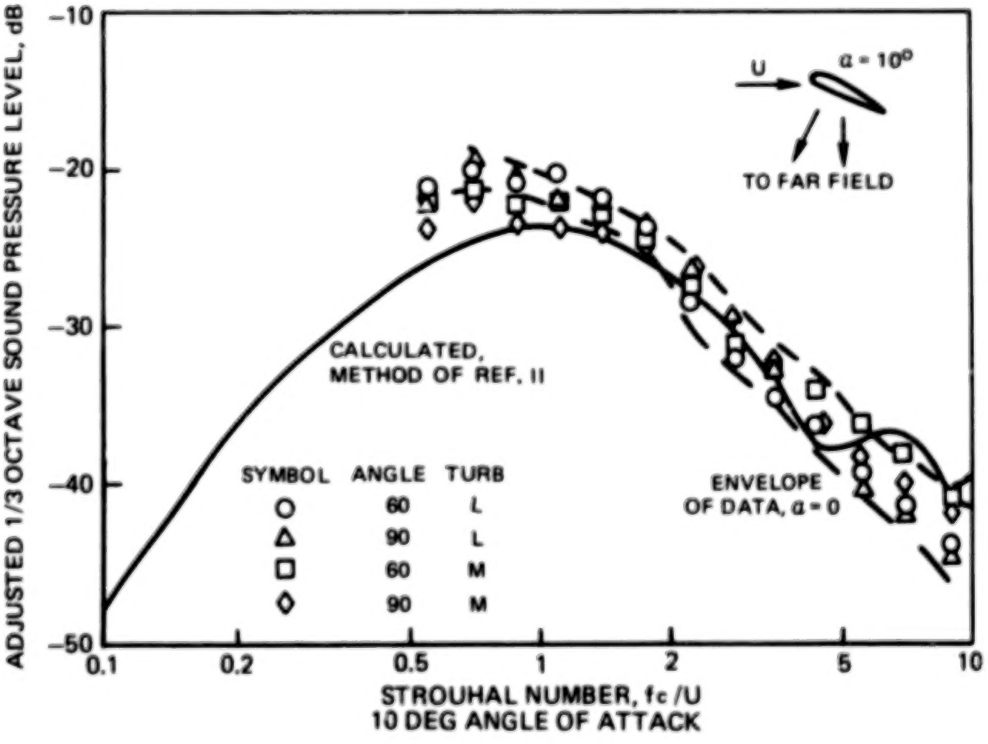

FIGURE 5 –CONTINUED. (c) 80 M/SEC VELOCITY

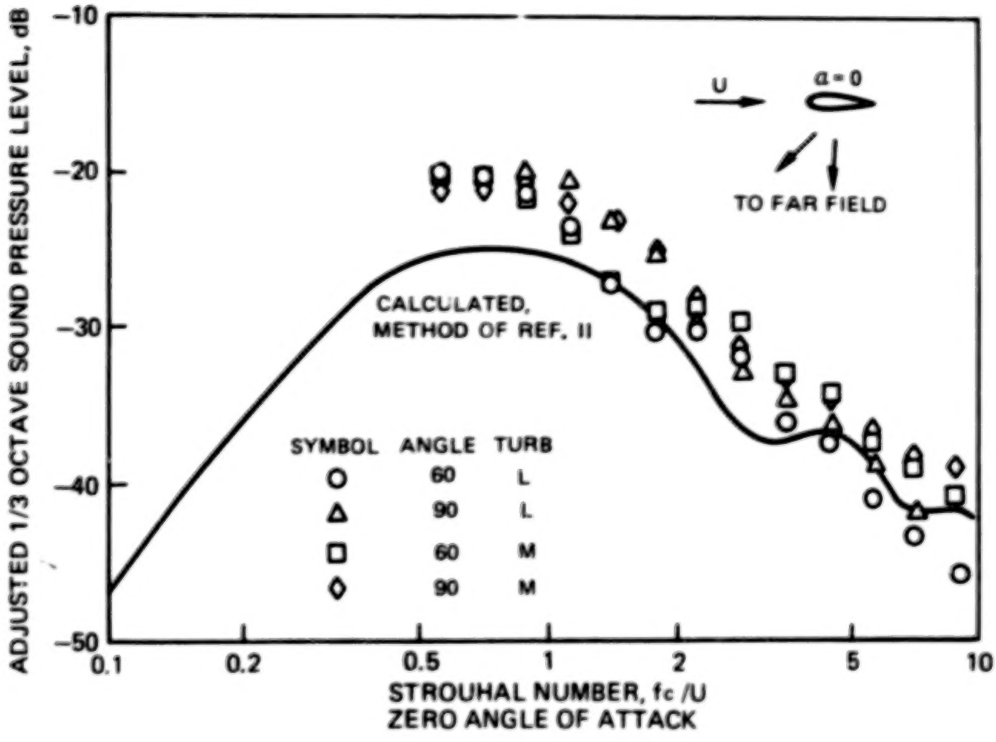

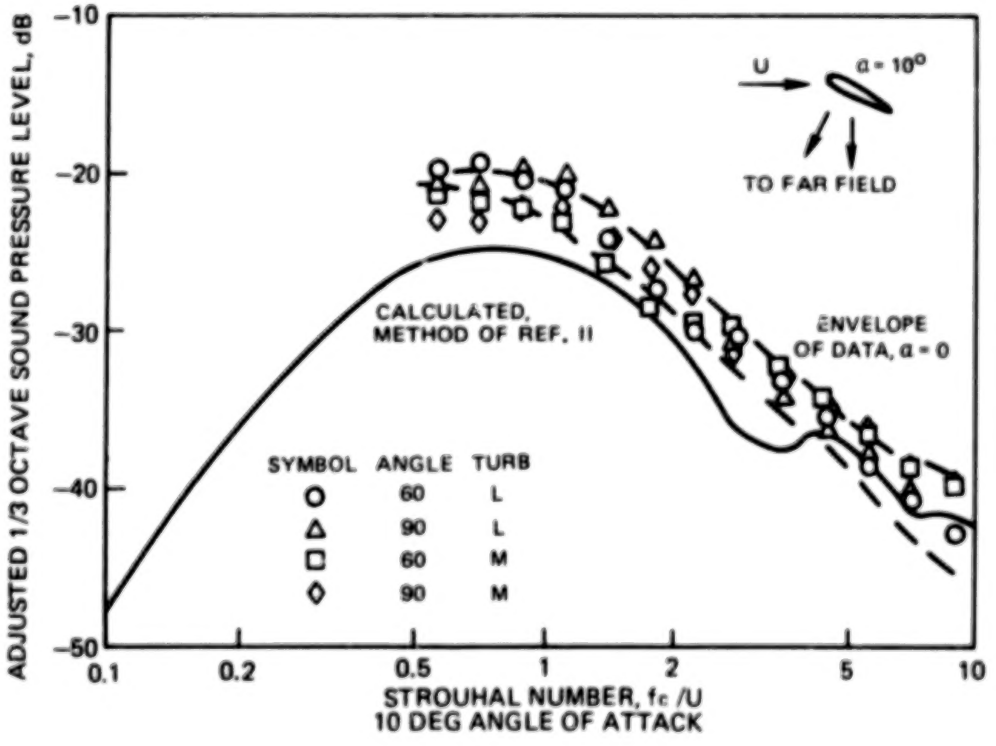

FIGURE 5 –CONTINUED. (d) 125 M/SEC VELOCITY

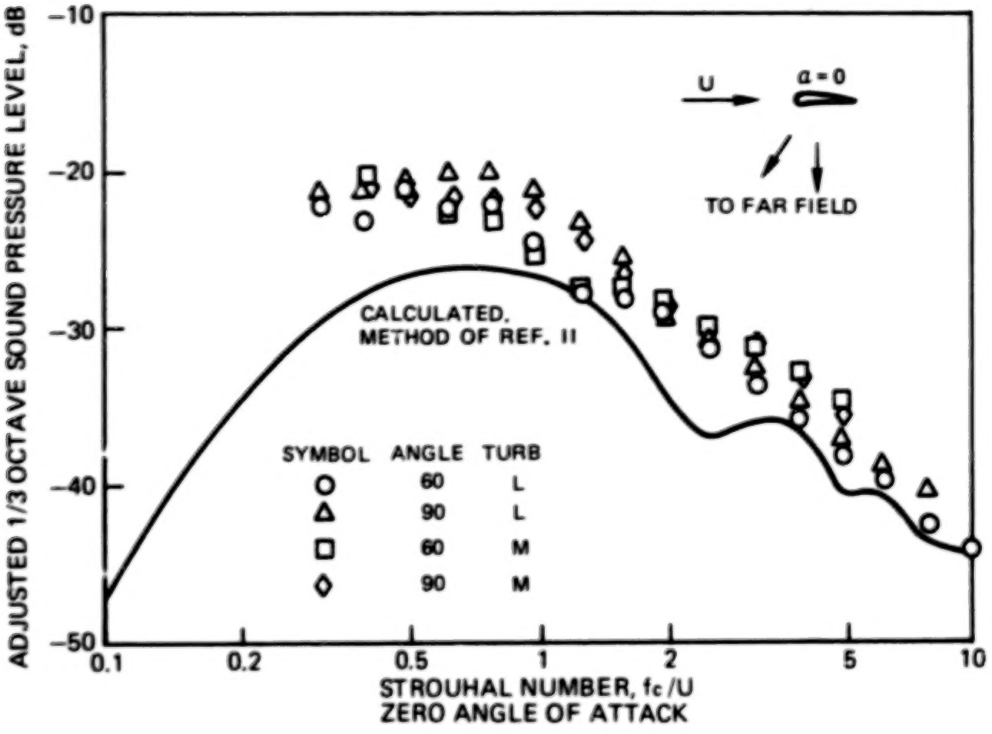

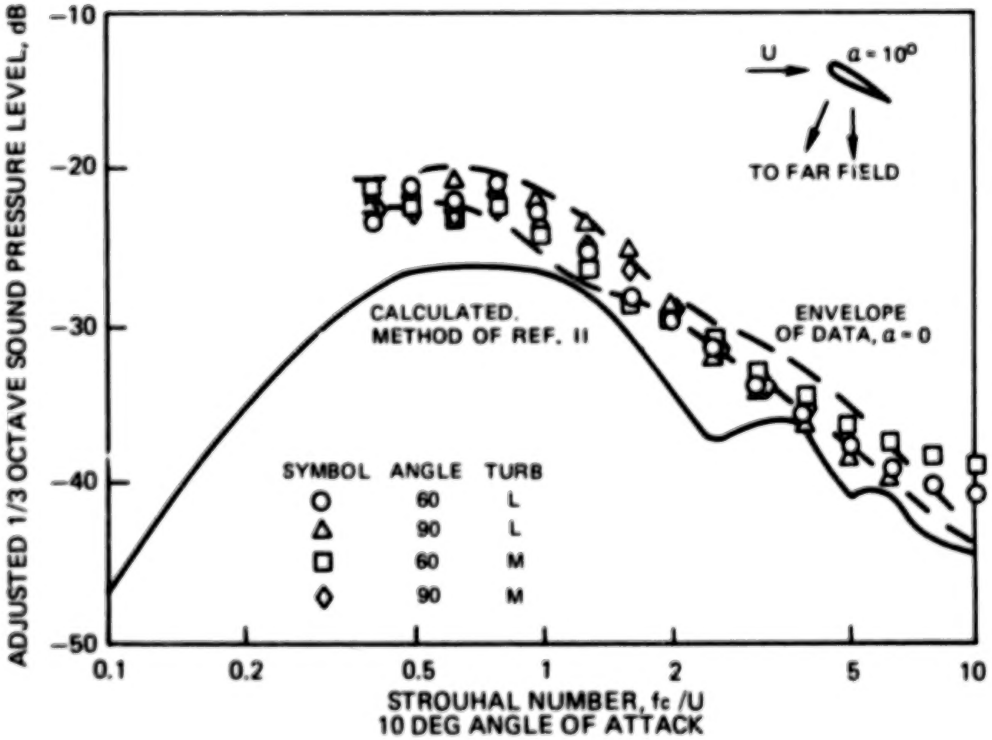

FIGURE 5 –CONCLUDED. (e) 177 M/SEC VELOCITY

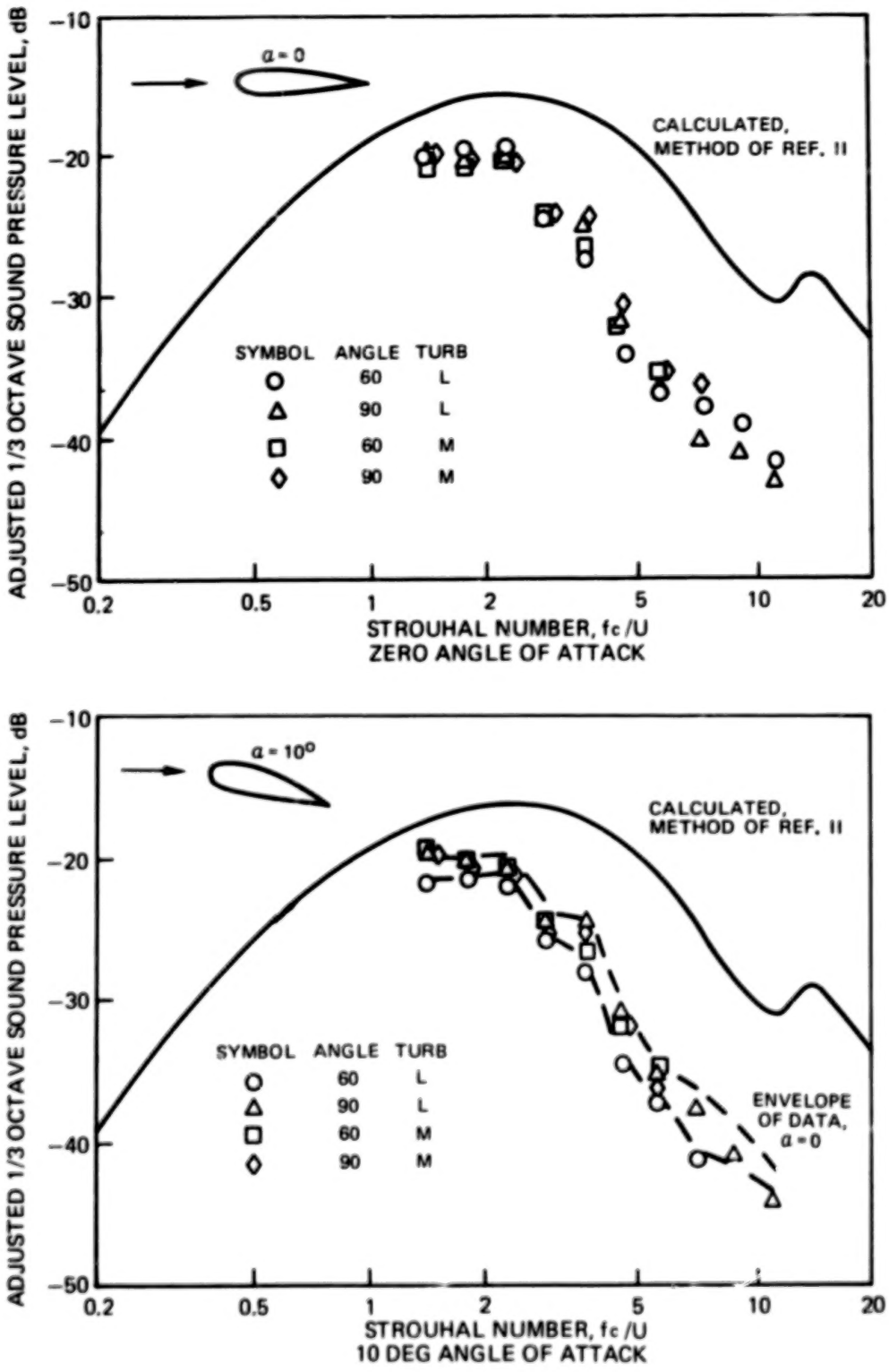

FIGURE 6 –MEASURED AND CALCULATED ADJUSTED SPECTRA FOR THICK AIRFOIL IN TURBULENT FLOW. (a) 31.5 M/SEC VELOCITY

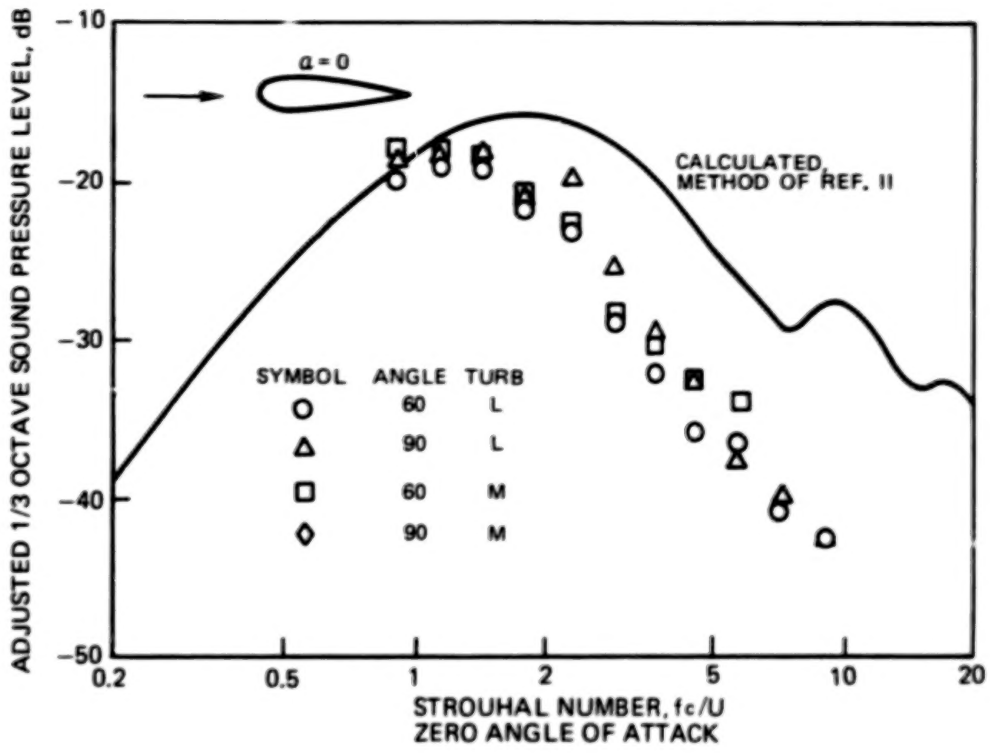

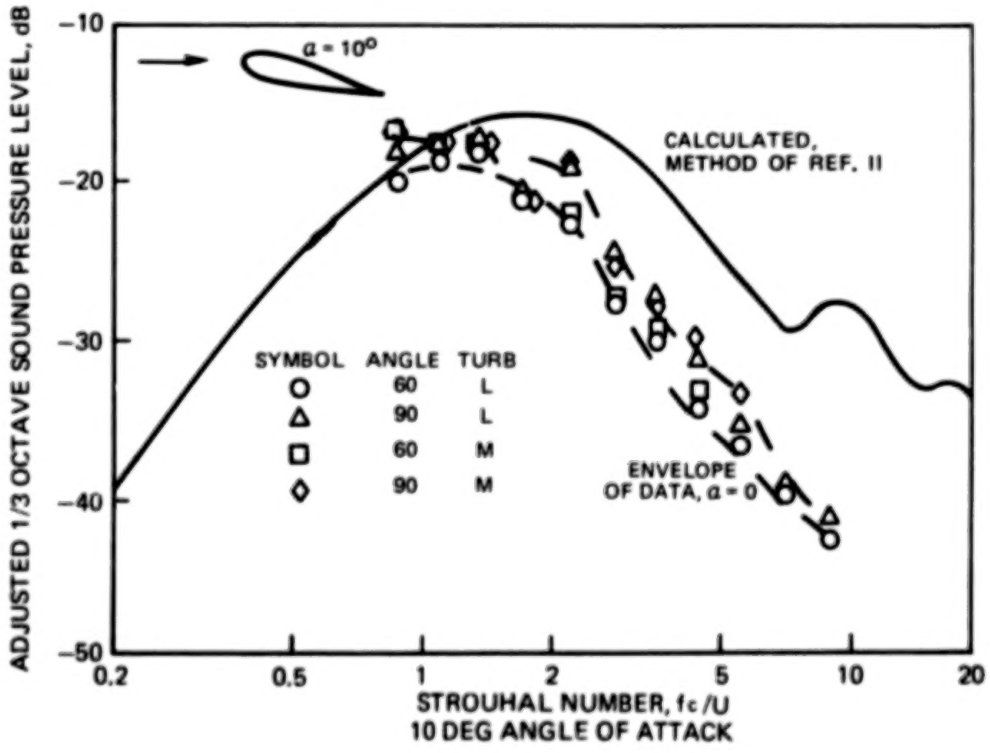

FIGURE 6 –CONTINUED. (b) 50 M/SEC VELOCITY

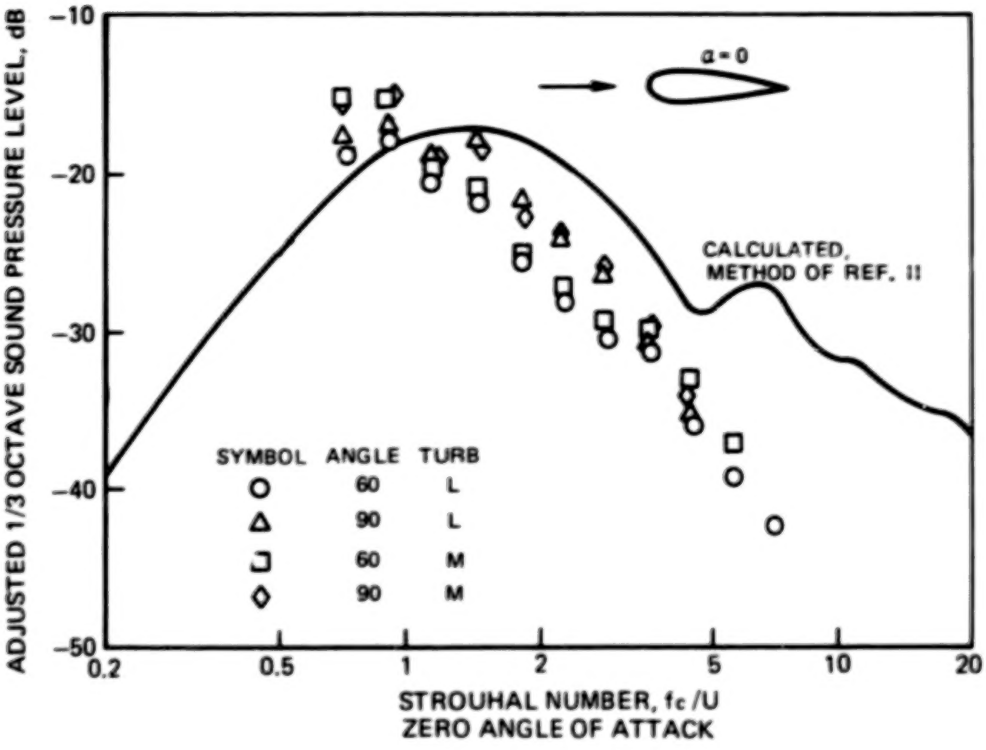

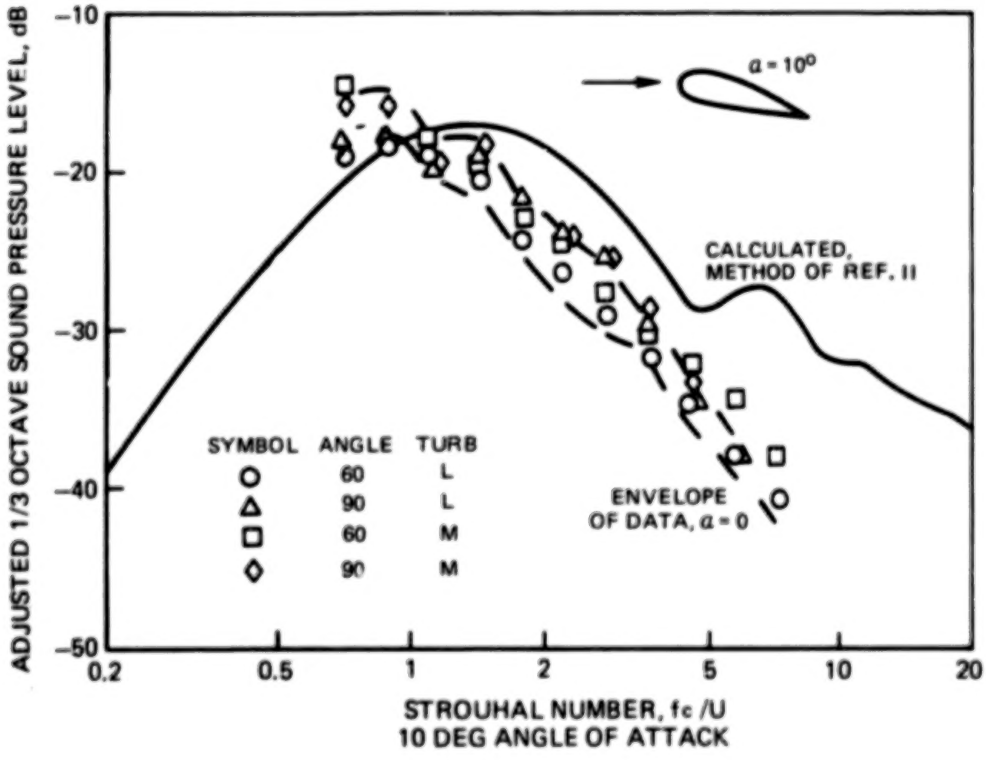

FIGURE 6 –CONTINUED, (c) 80 M/SEC VELOCITY

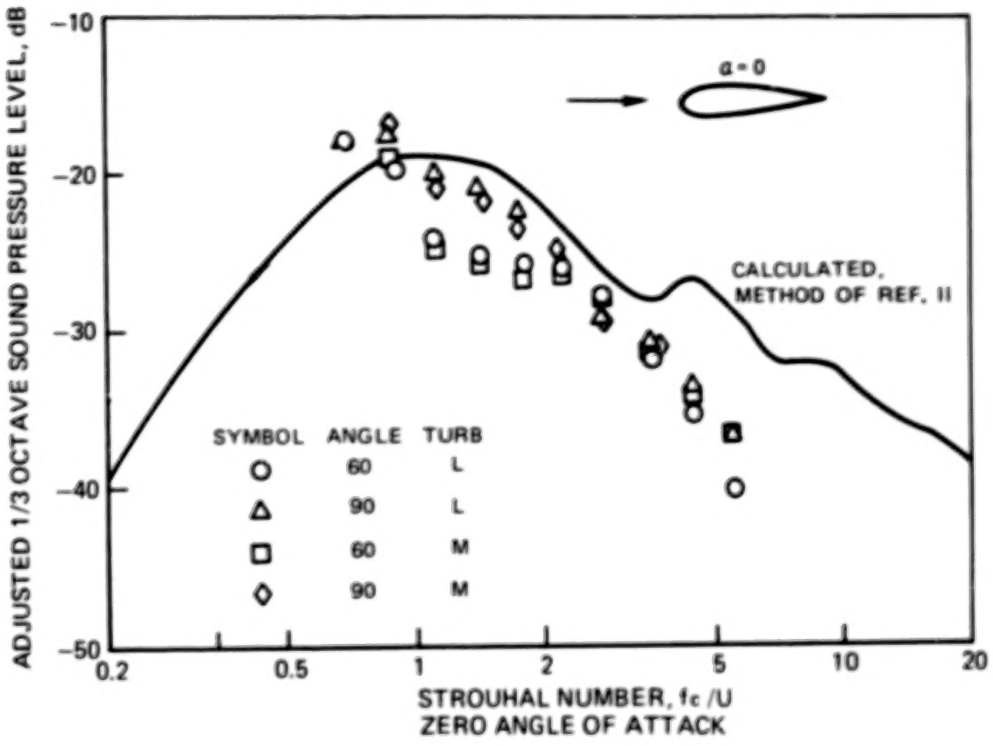

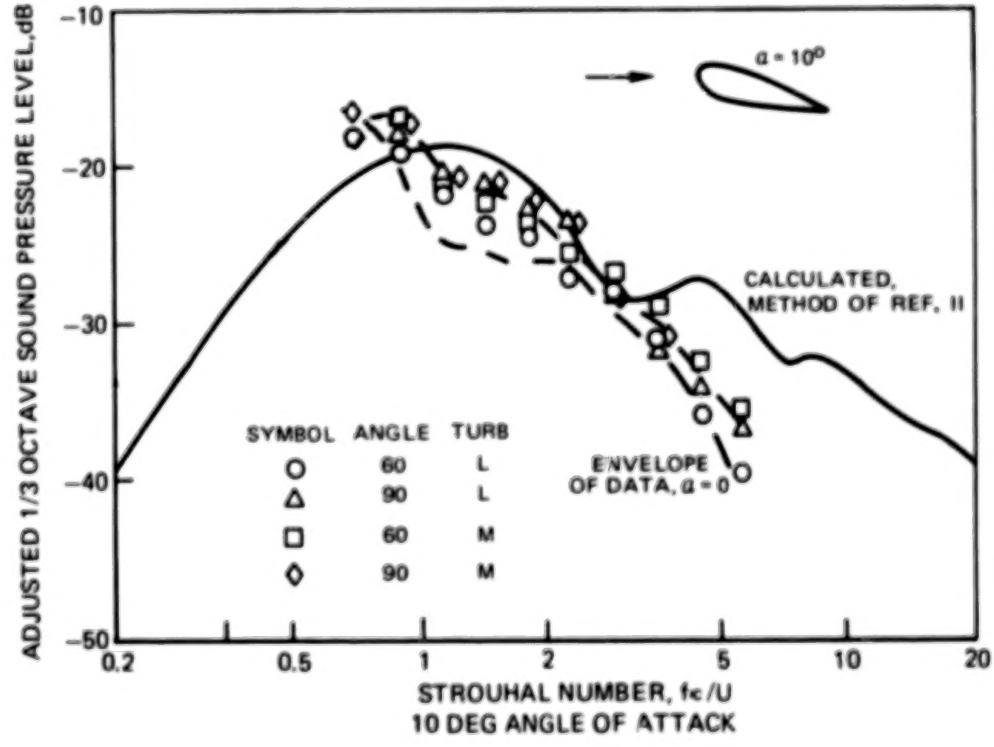

FIGURE 6 –CONTINUED. (d) 125 M/SEC VELOCITY

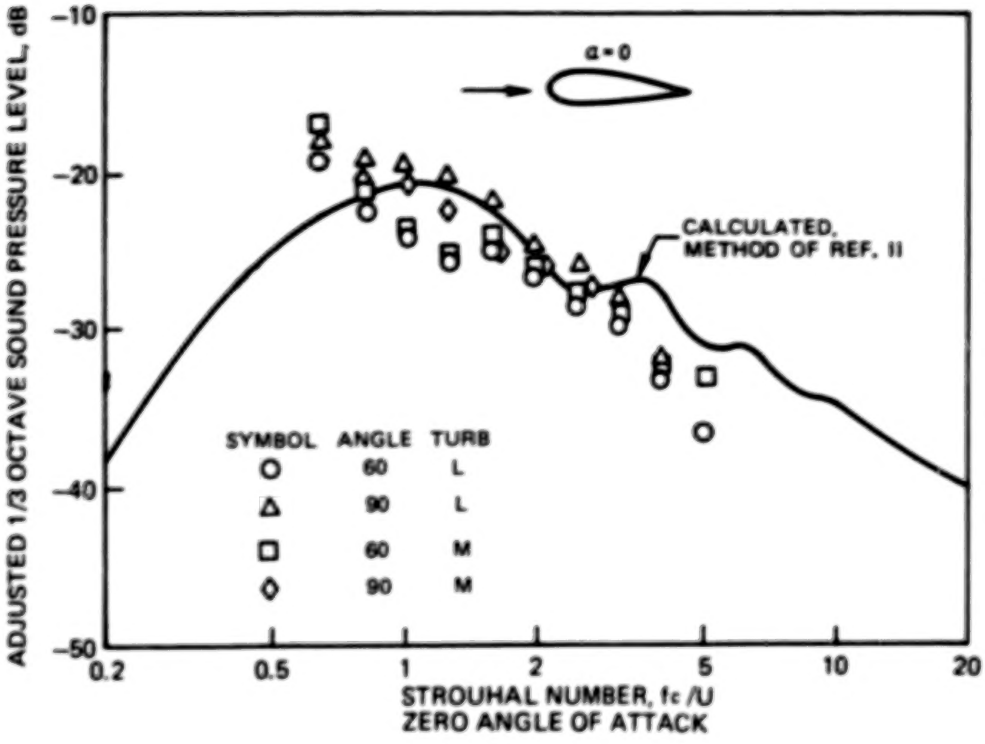

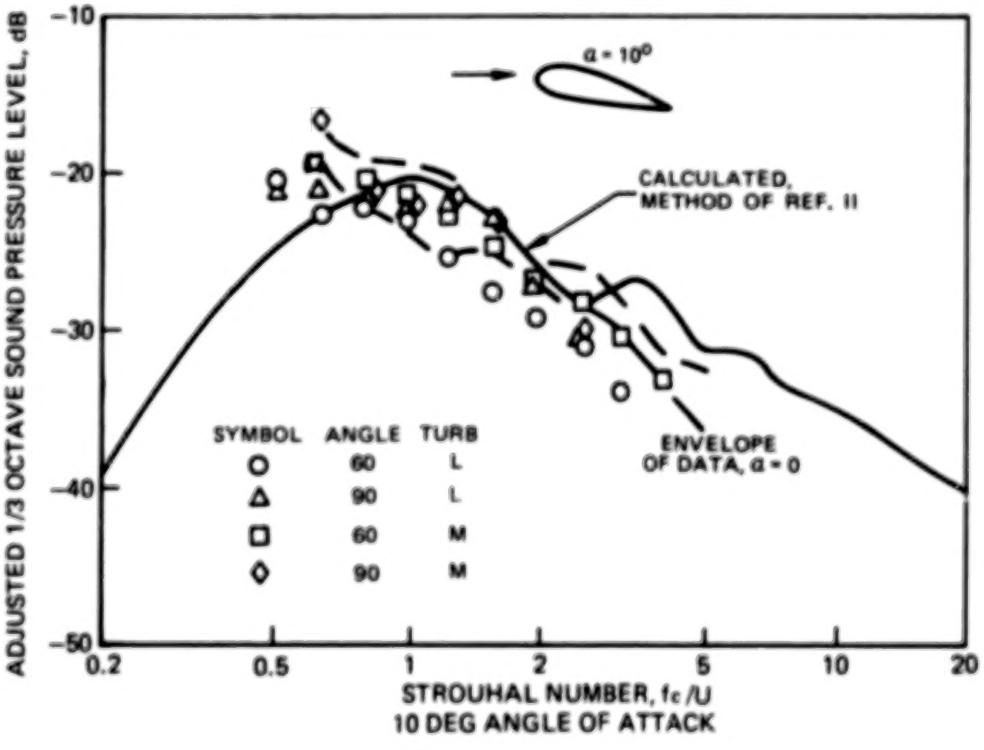

FIGURE 6 –CONCLUDED. (e) 177 M/SEC VELOCITY

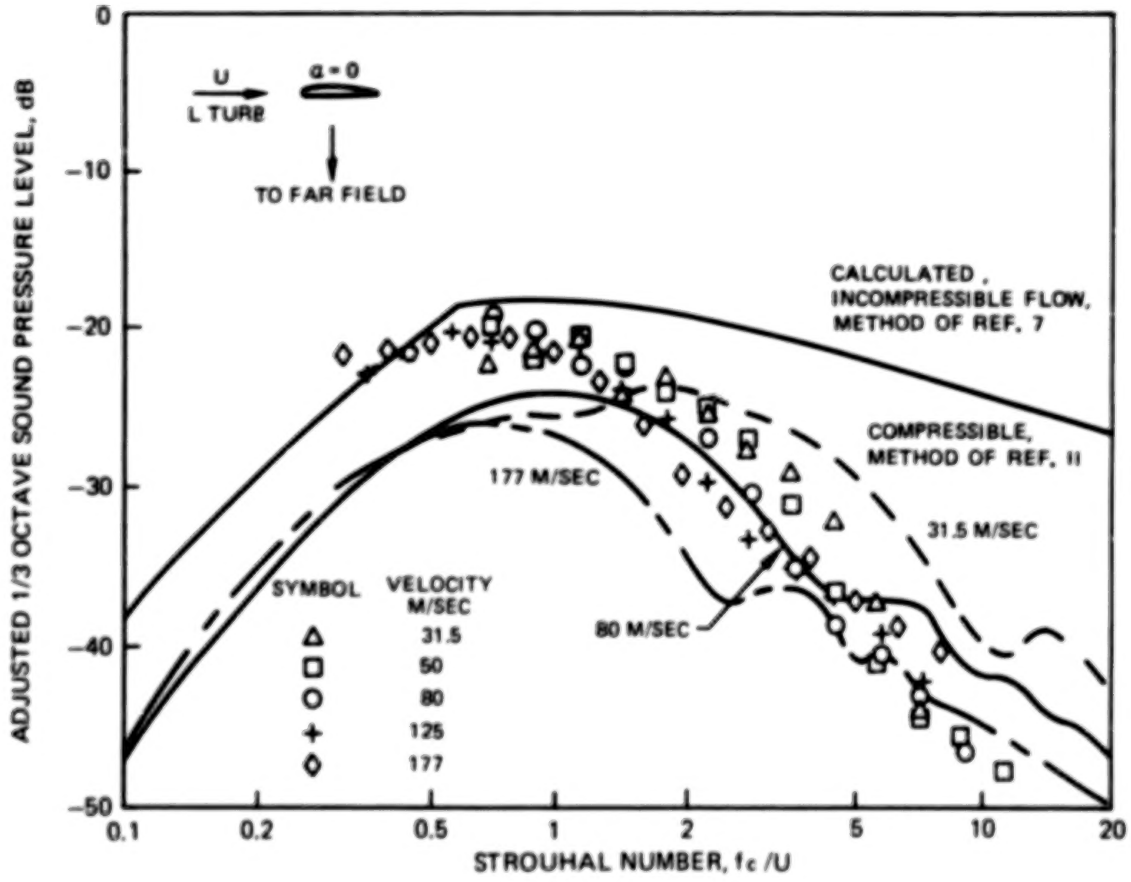

FIGURE 7 –MEASURED AND CALCULATED EFFECTS OF VELOCITY ON ADJUSTED SPECTRA FOR THIN SMALL AIRFOIL IN LARGE TURBULENCE

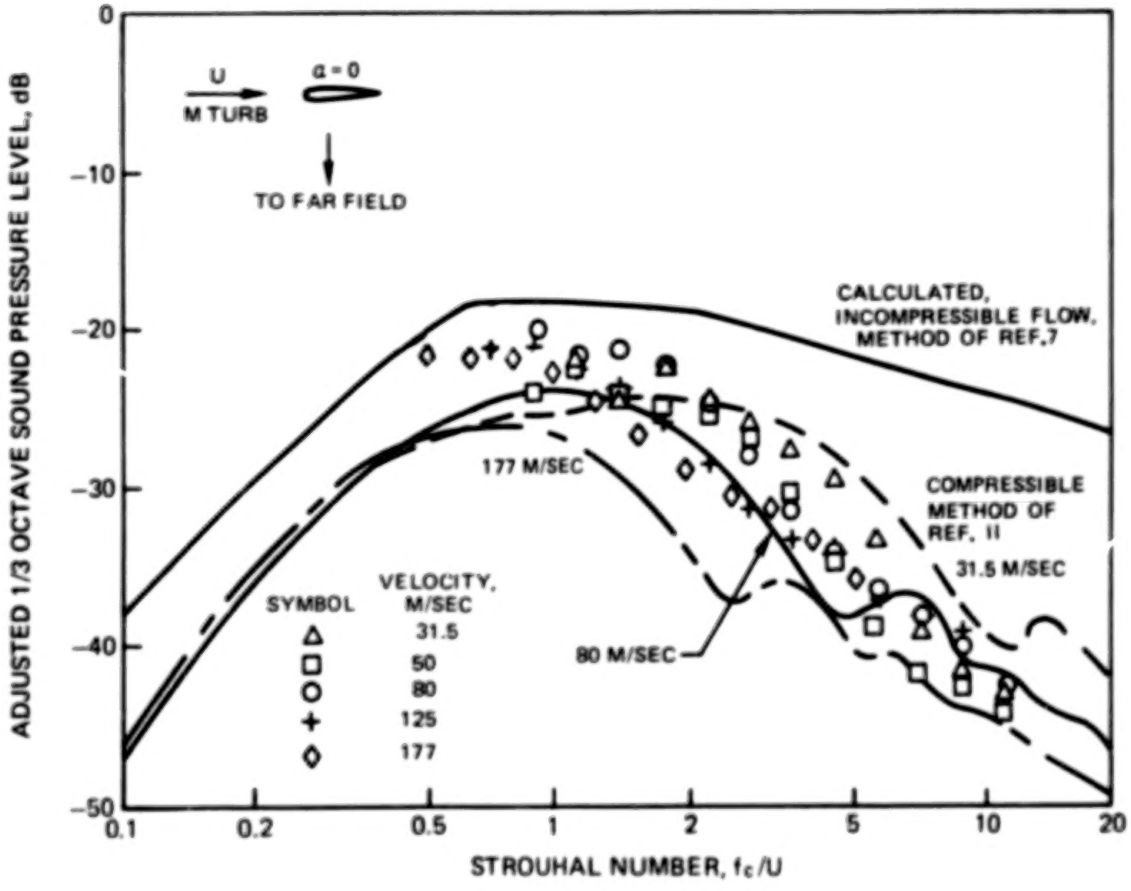

FIGURE 8 –MEASURED AND CALCULATED EFFECTS OF VELOCITY ON ADJUSTED SPECTRA FOR THIN SMALL AIRFOIL IN MEDIUM TURBULENCE

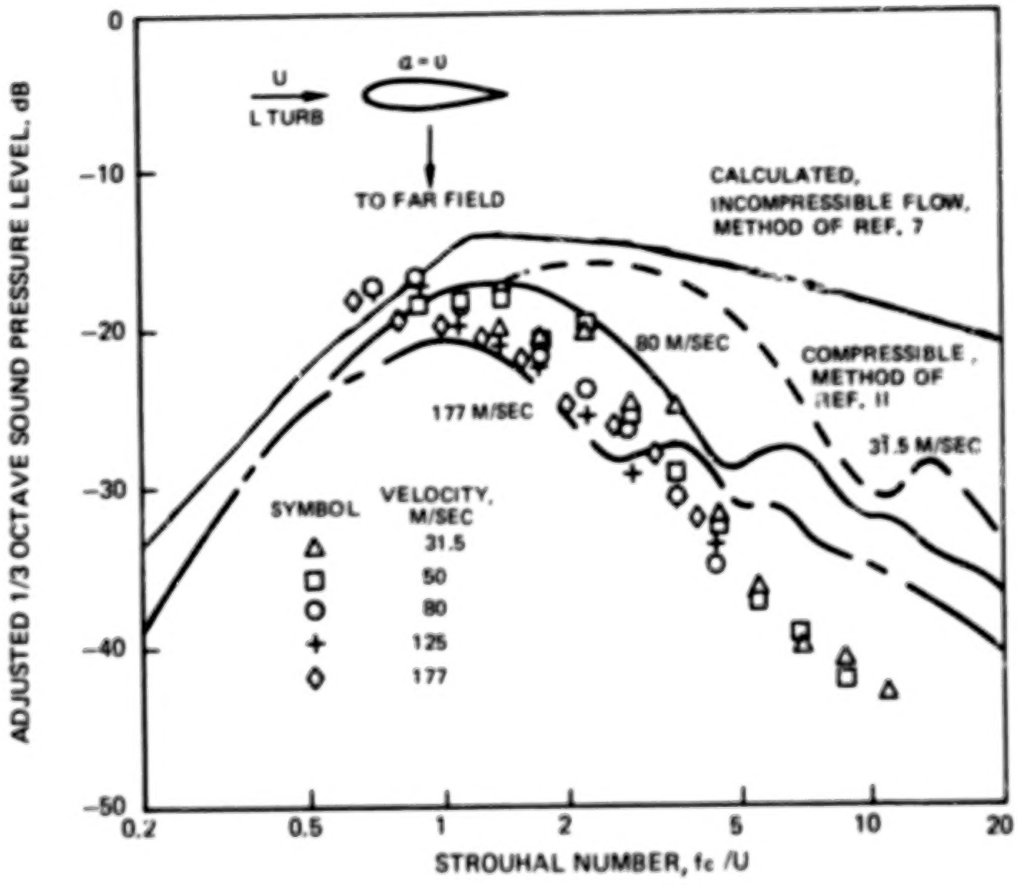

FIGURE 9 –MEASURED AND CALCULATED EFFECTS OF VELOCITY ON ADJUSTED SPECTRA FOR THICK AIRFOIL IN LARGE TURBULENCE

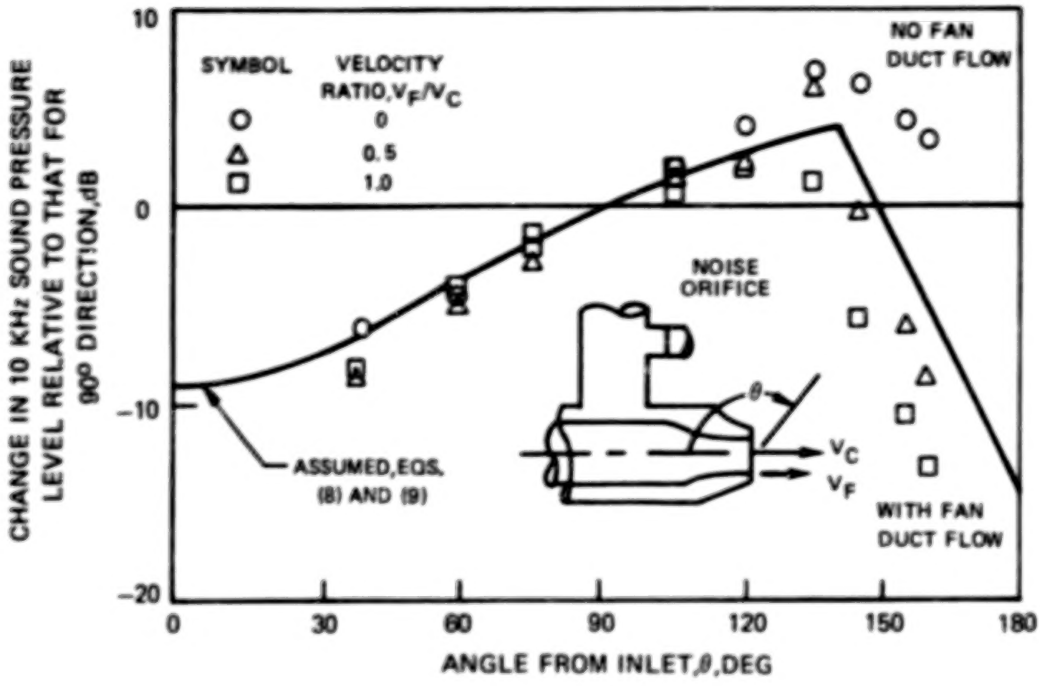

(a.) DIRECTIVITY OF NOISE INTRODUCED INTO FAN DUCT

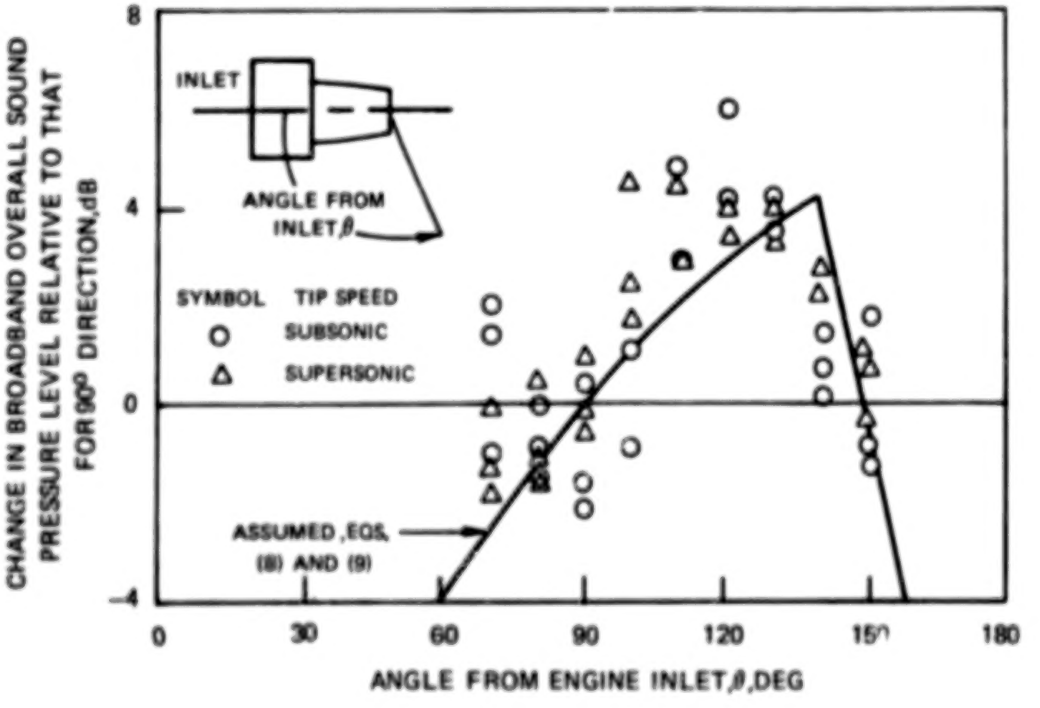

(b.) DIRECTIVITY OF FAN AFT-RADIATED BROADBAND NOISE

FIGURE 10–COMPARISION OF ASSUMED AND MEASURED DIRECTIVITY PATTERNS FOR AFT-RADIATED FAN DUCT NOISE

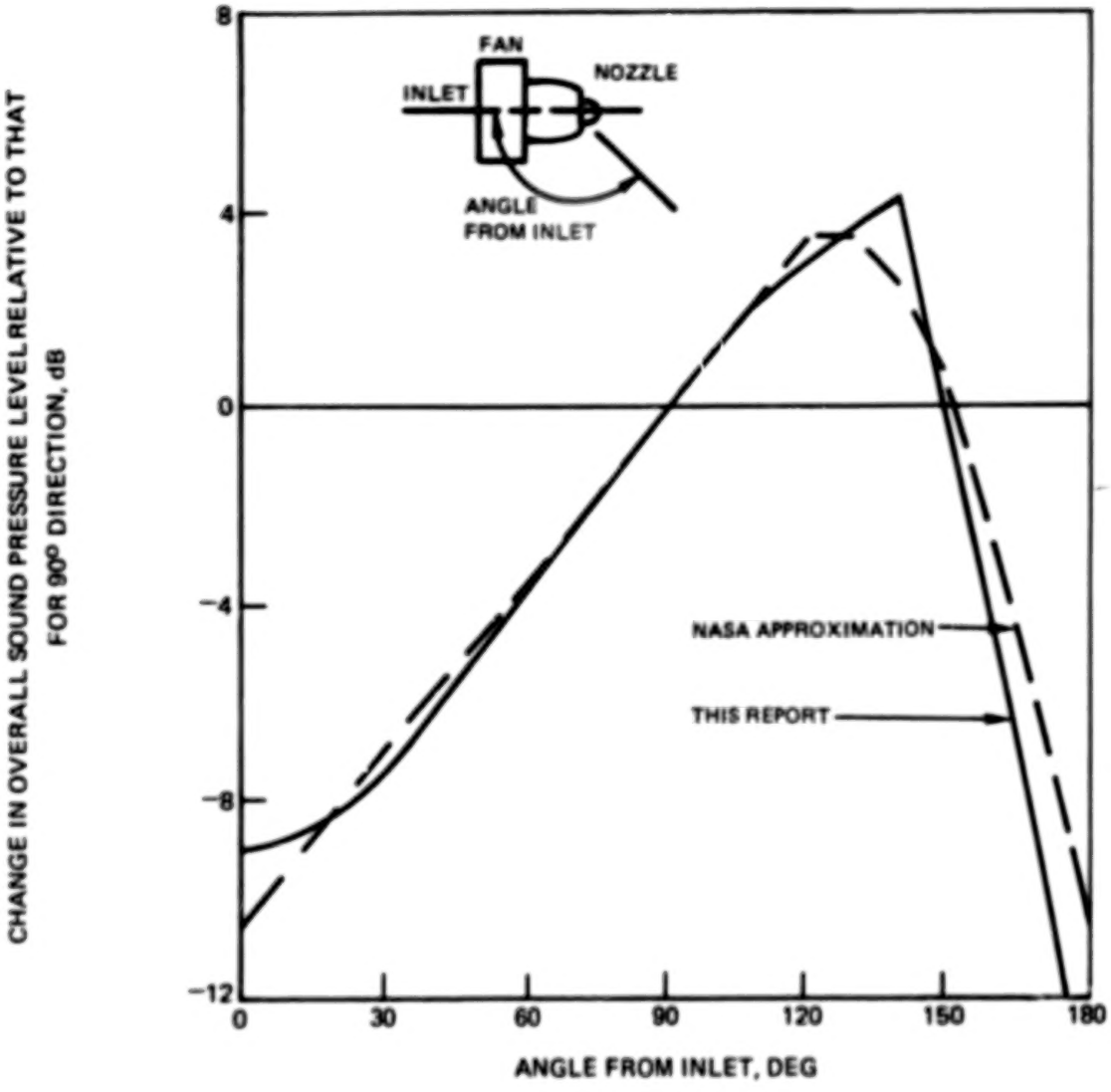

FIGURE 11 – COMPARISON OF ASSUMED DIRECTIVITY SHAPES FOR AFT–RADIATED INTERNALLY GENERATED NOISE

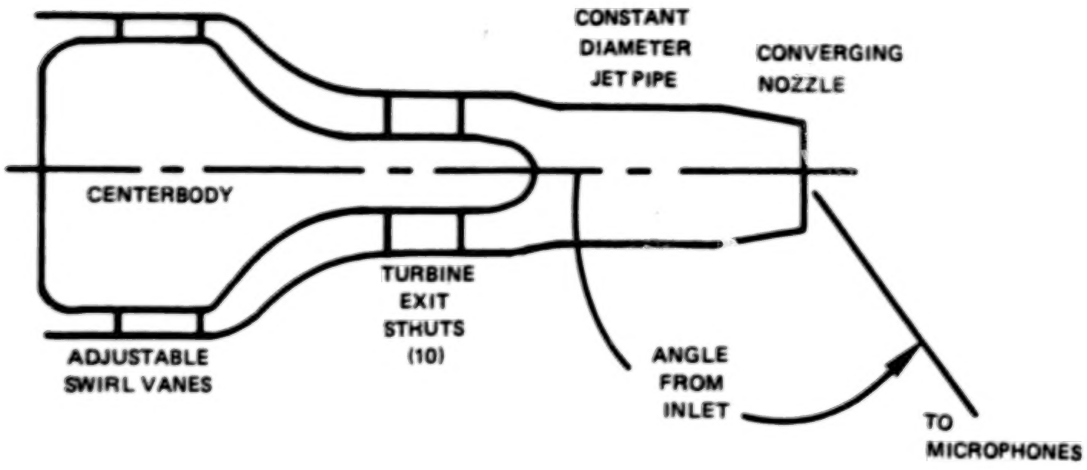

(a) SKETCH OF ENGINE EXHAUST SYSTEM MODEL

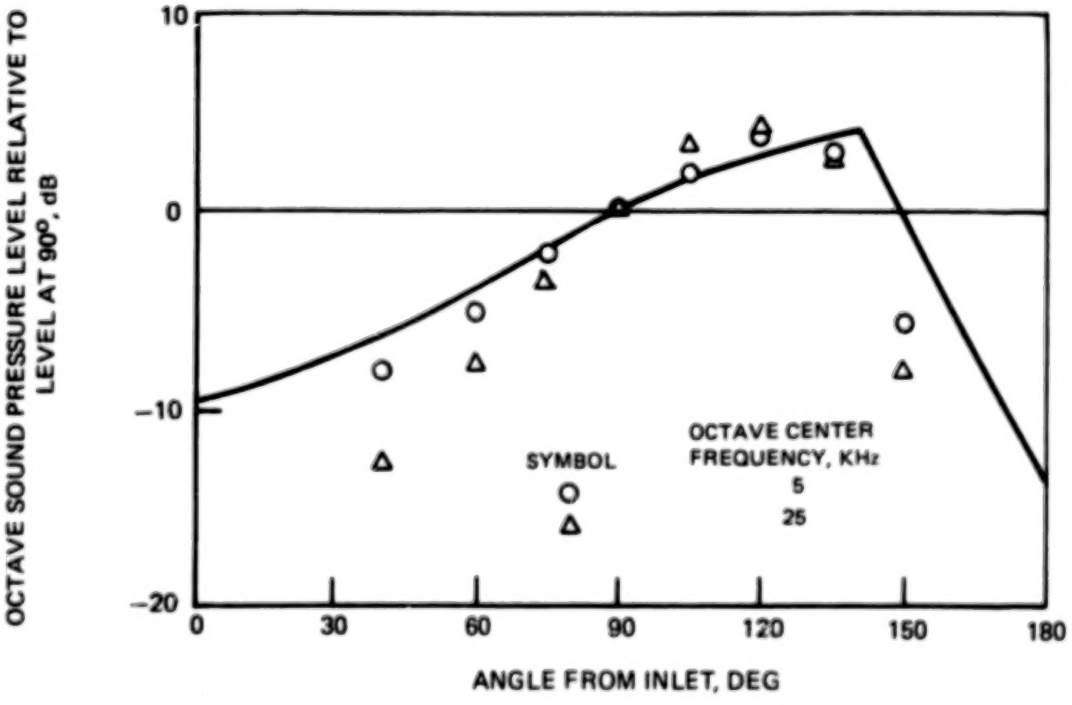

(b) NORMALIZED DIRECTIVITIES AT 146 M/SEC EXHAUST VELOCITY

FIGURE 12 – COMPARISON OF CALCULATED AND MEASURED DIRECTIVITY PATTERNS FOR TURBINE EXIT STRUT NOISE

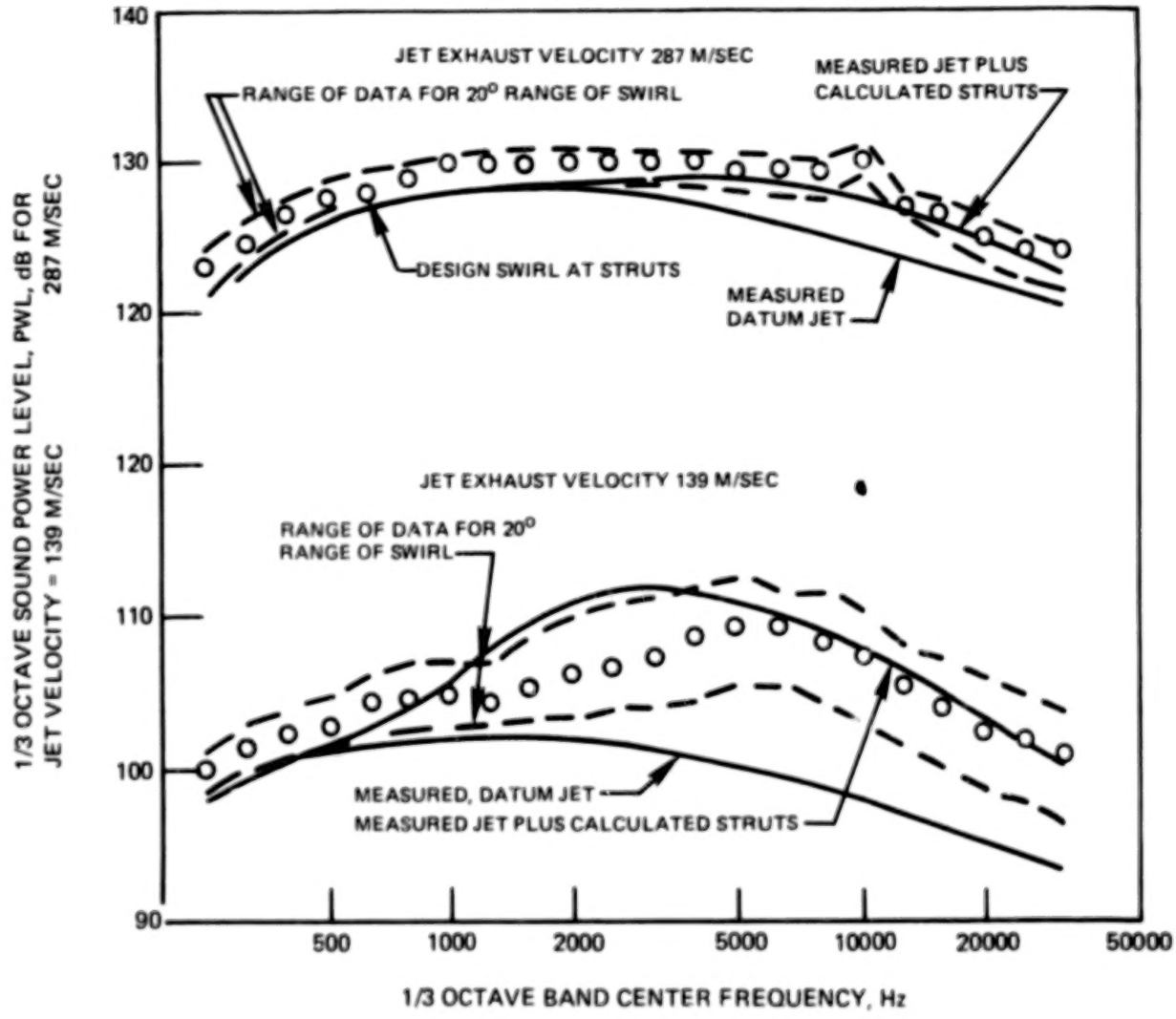

FIGURE 13– CALCULATED AND MEASURED NOISE OF TURBINE EXIT STRUTS IN 1/8 SCALE MODEL TURBOJET ENGINE

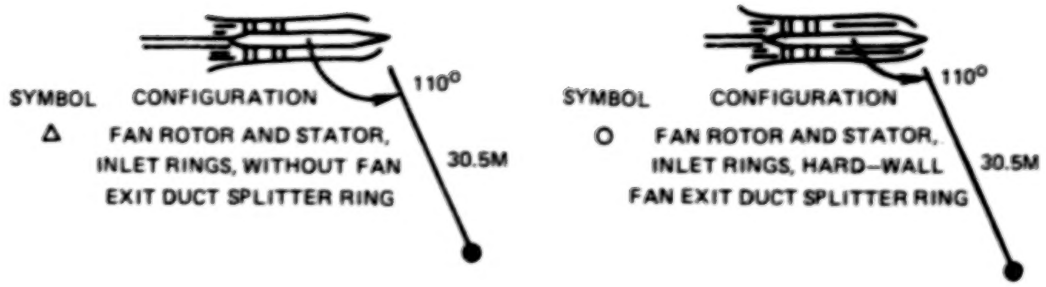

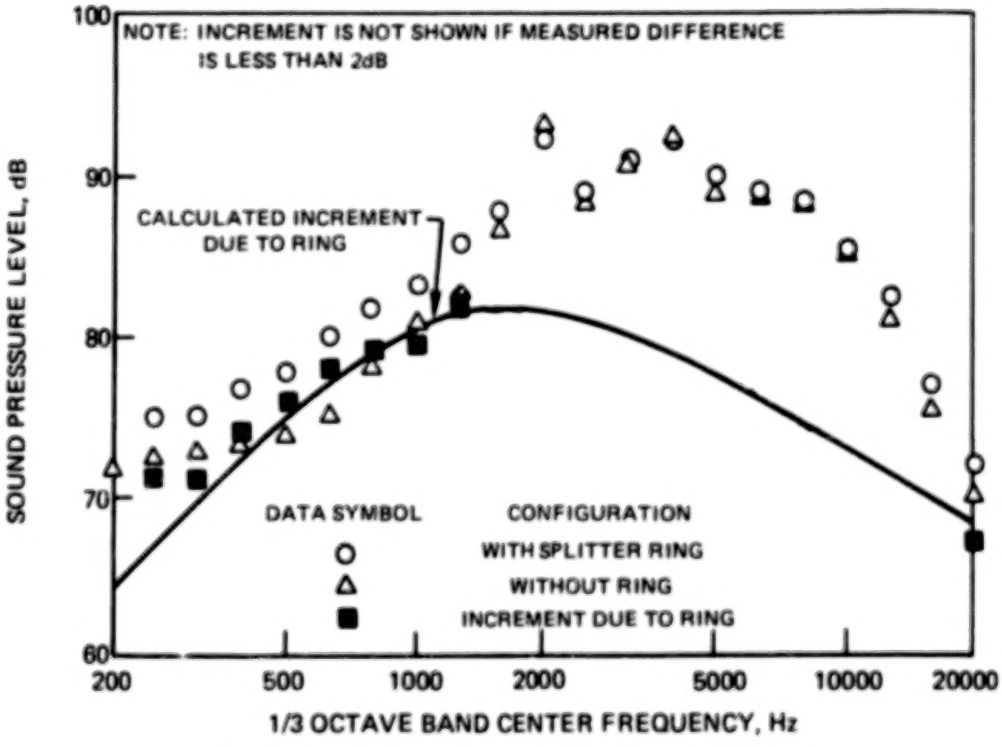

(a) 60 PERCENT SPEED

FIGURE 14- MEASURED AND CALCULATED NOISE SPECTRUM AT 110° POLAR ANGLE GENERATED BY HARD–WALL FAN EXIT DUCT SPLITTER RING

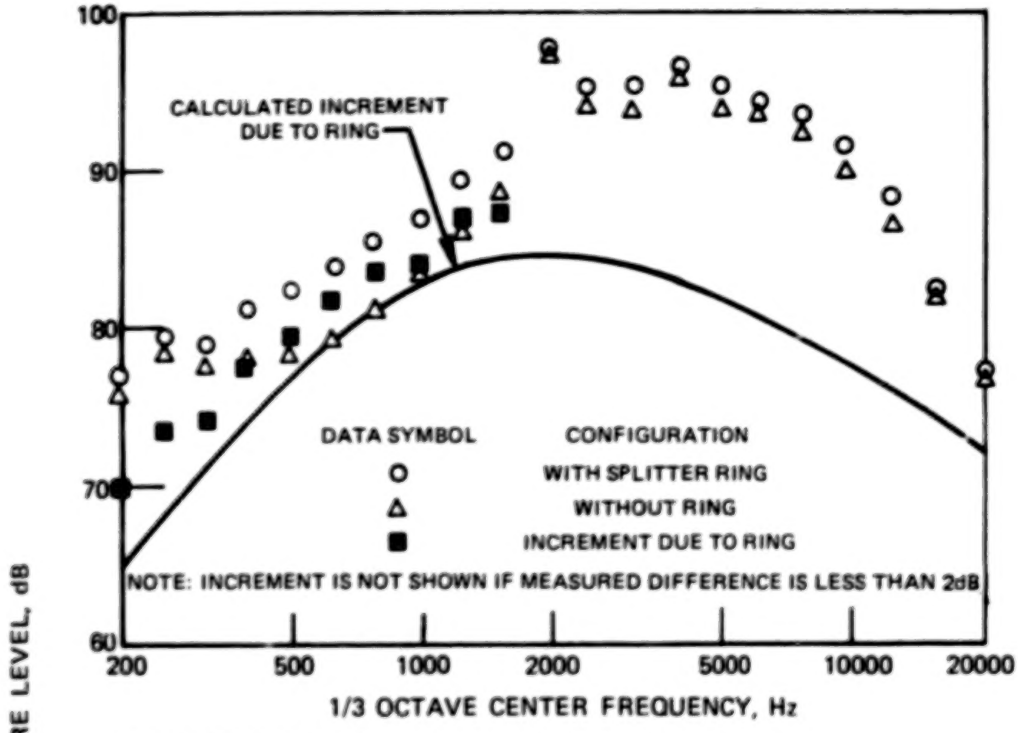

(b) 70 PERCENT SPEED

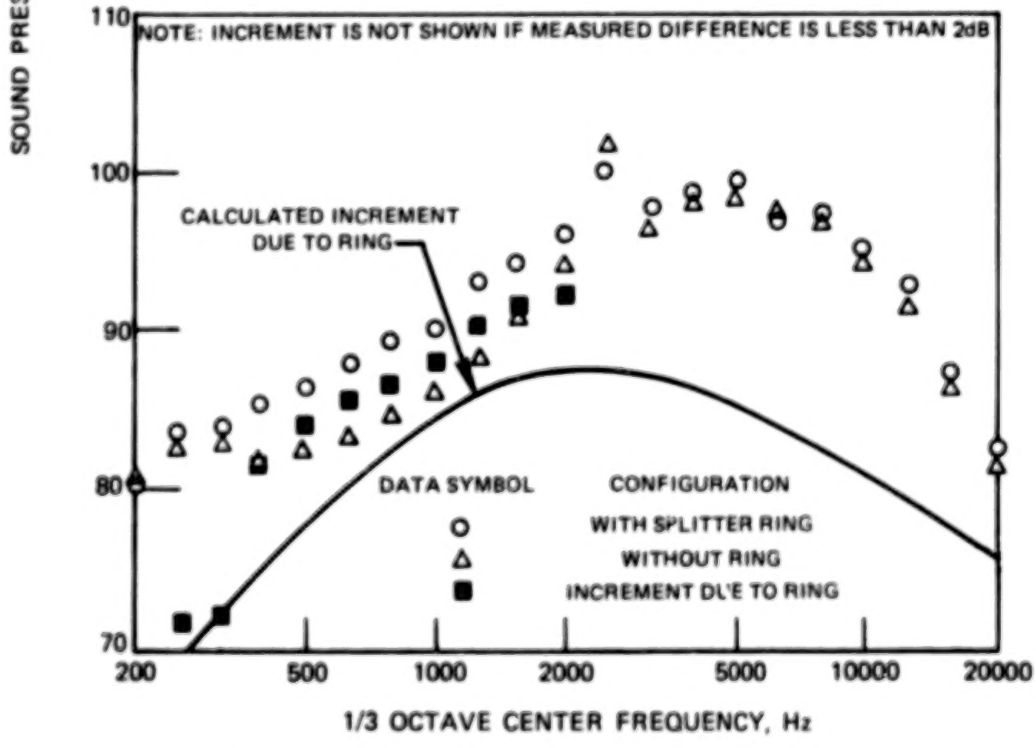

(c) 80 PERCENT SPEED

FIGURE 14 –CONCLUDED

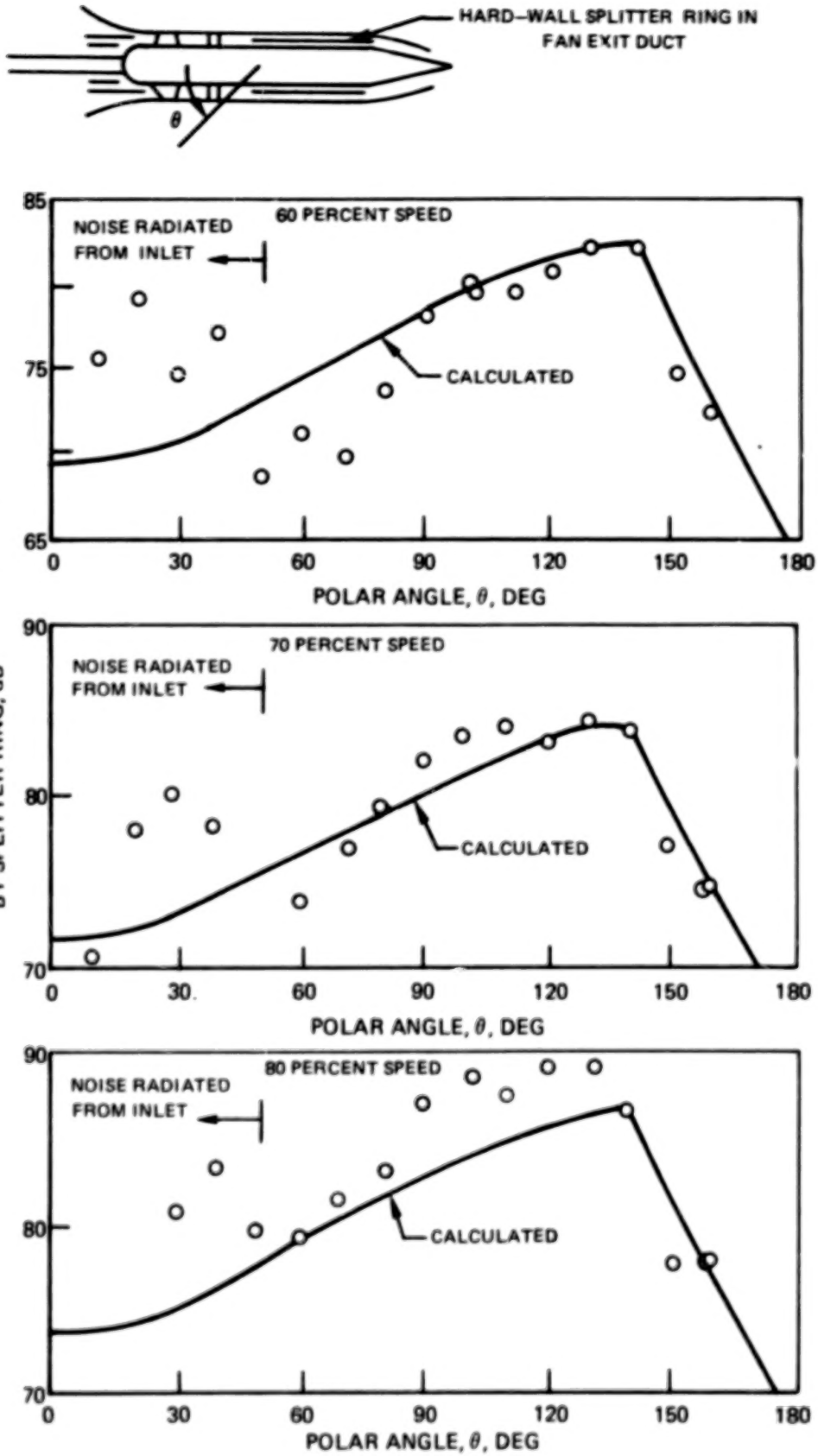

FIGURE 15 – MEASURED AND CALCULATED DIRECTIVITY OF NOISE GENERATED BY HARD–WALL FAN EXIT DUCT SPLITTER RING

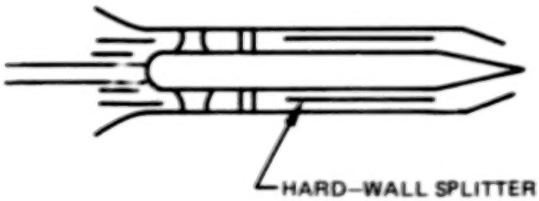

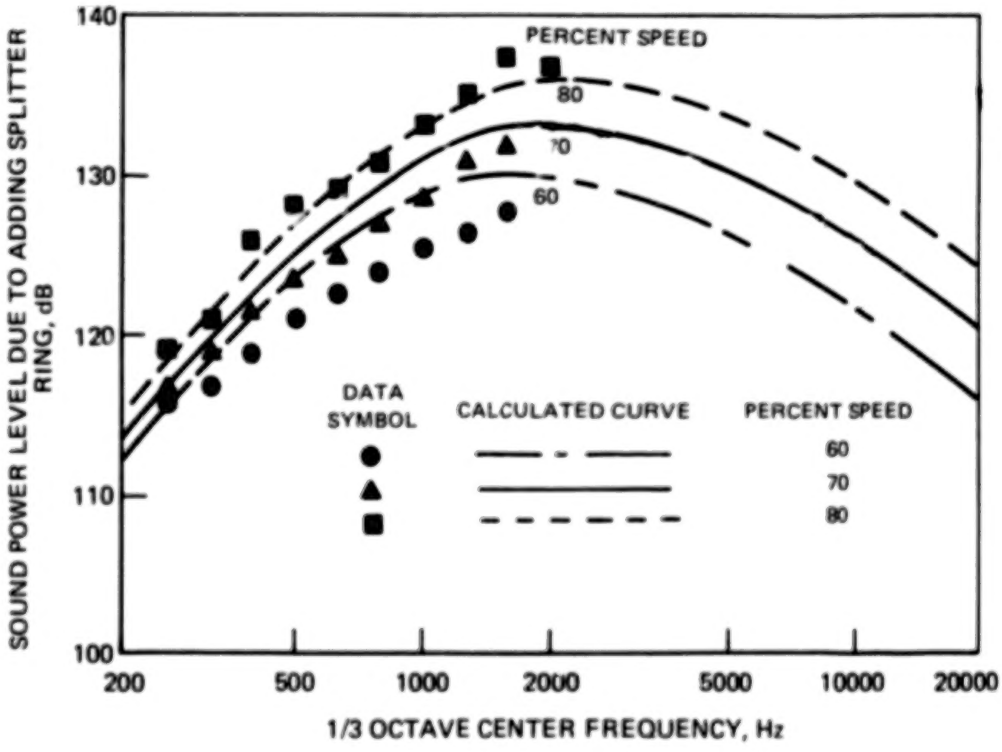

FIGURE 16– MEASURED AND CALCULATED SOUND POWER LEVEL DUE TO ADDITION OF HARD–WALL AFT SPLITTER RING

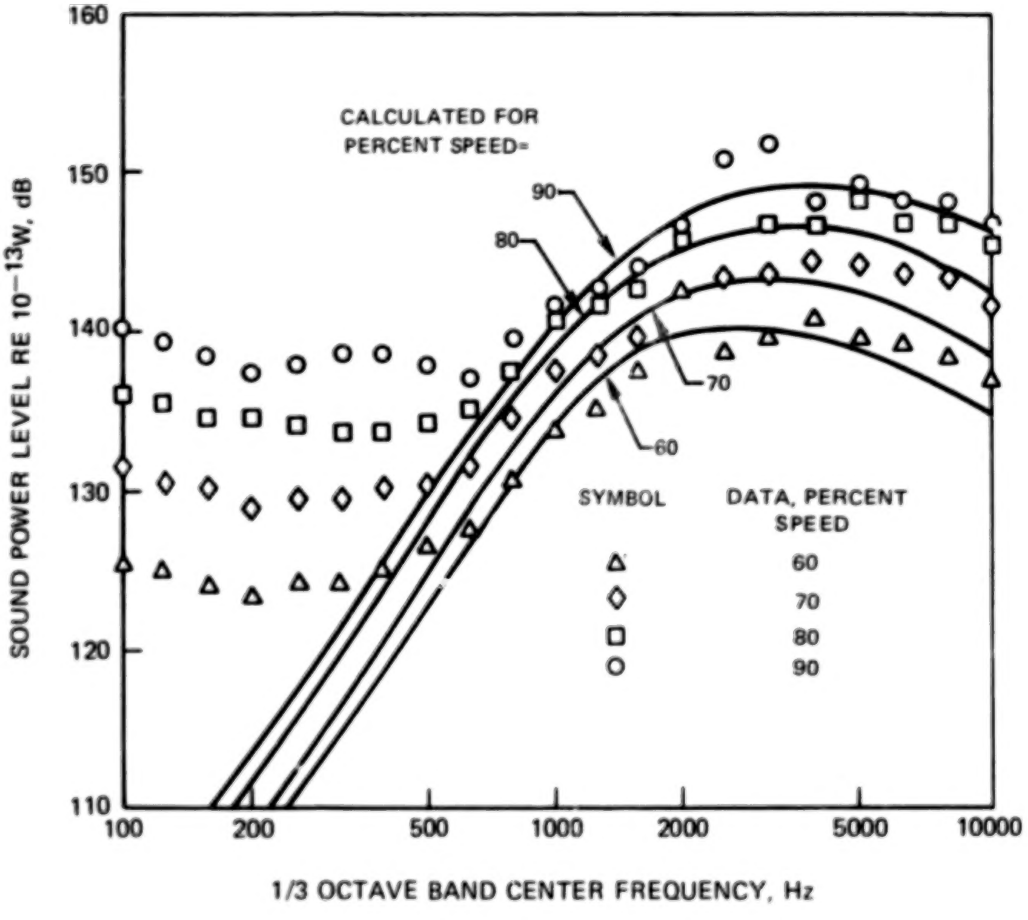

FIGURE 17– CALCULATED AND MEASURED 1/3 OCTAVE SOUND POWER SPECTRA OF FULL SCALE FAN NOISE FOR ORIGINAL STATOR VANES. ASSUMED TURBULENCE PROPERTIES VARIED TO ACHIEVE GOOD MATCH WITH DATA

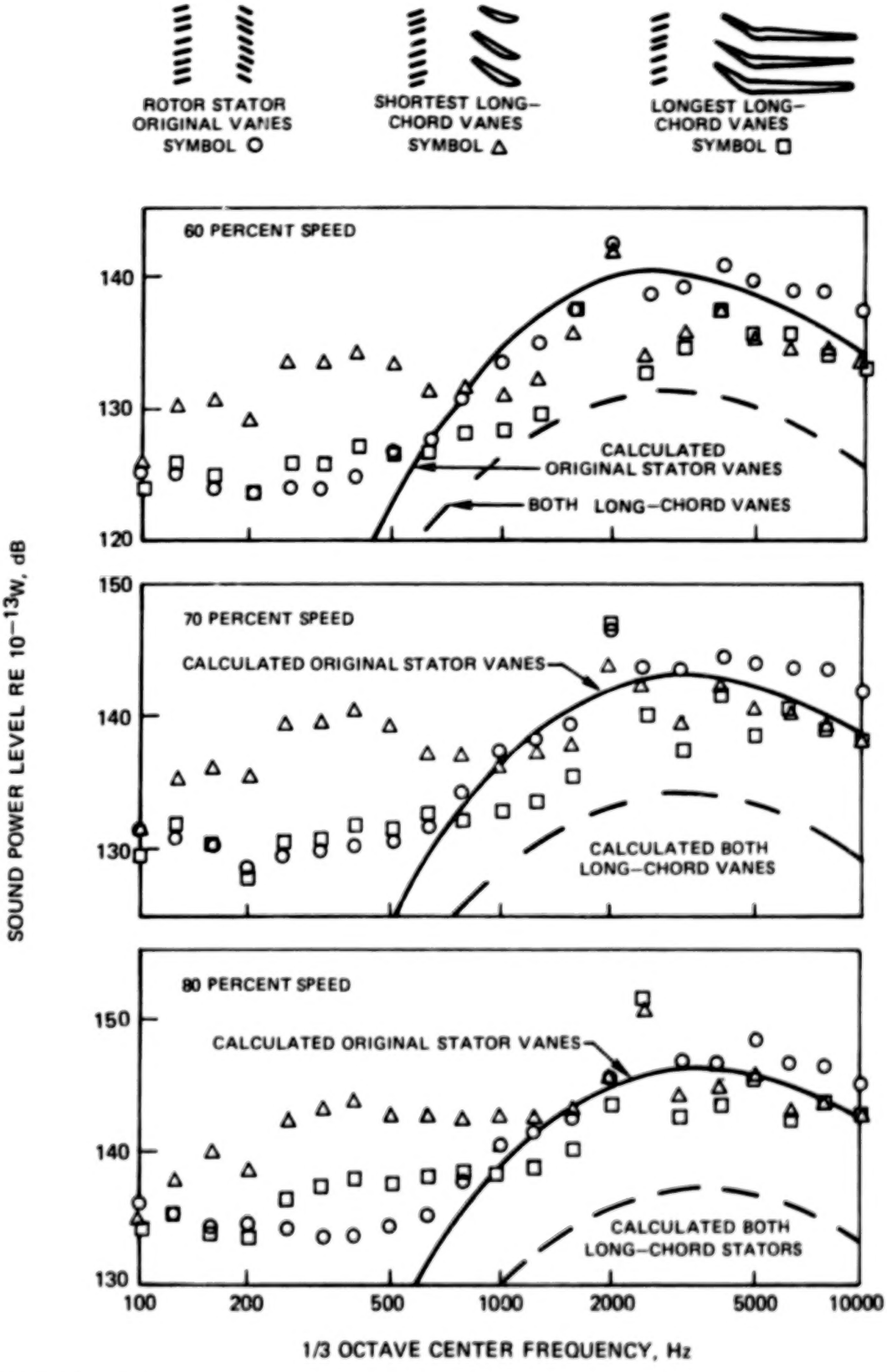

FIGURE 18 – COMPARISON OF CALCULATED AND MEASURED 1/3 OCTAVE SOUND POWER SPECTRA OF FULL SCALE FAN WITH ORIGINAL AND LONG–CHORD STATOR VANES AT 60, 70, AND 80 PERCENT SPEED

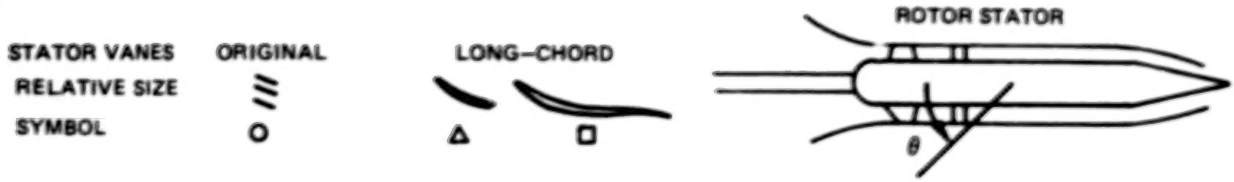

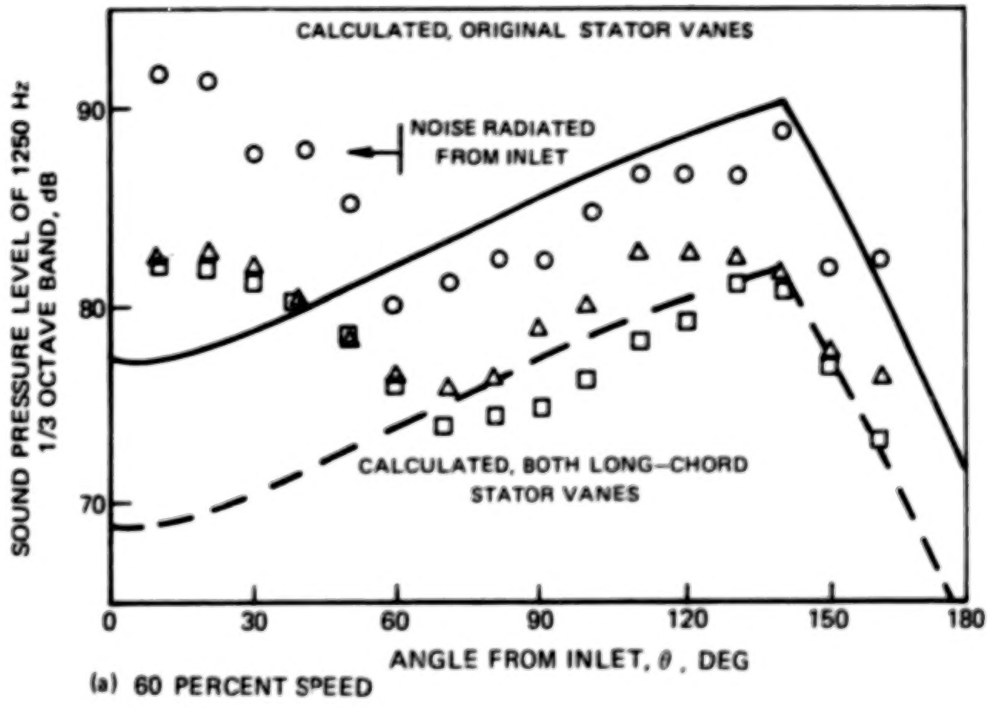

(a) 60 PERCENT SPEED

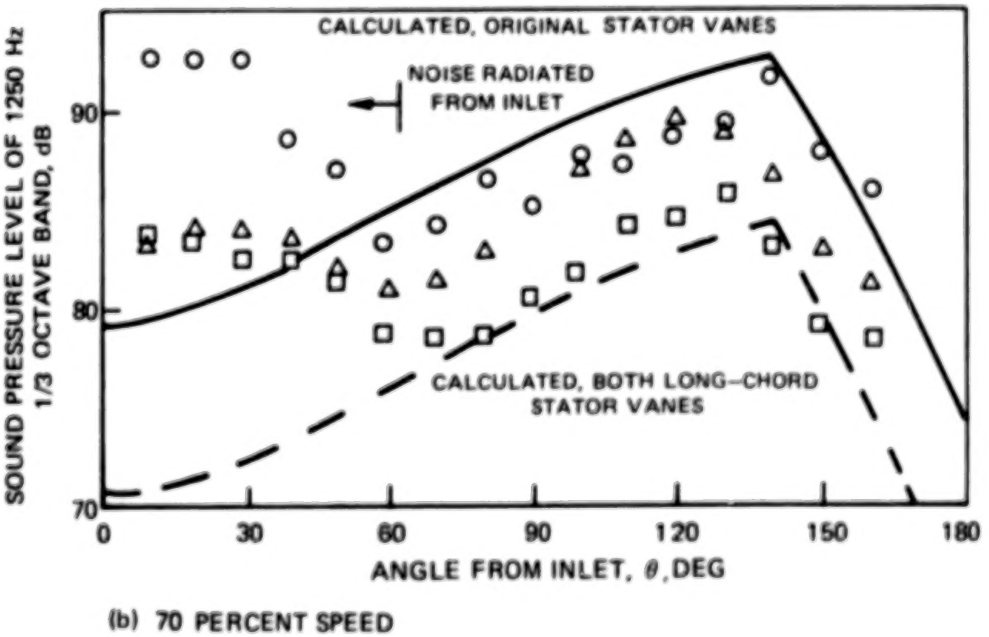

(b) 70 PERCENT SPEED

FIGURE 19 –EFFECT OF LONG–CHORD STATOR VANES ON FULL–SCALE FAN NOISE DIRECTIVITY IN 1250 Hz 1/3 OCTAVE BAND

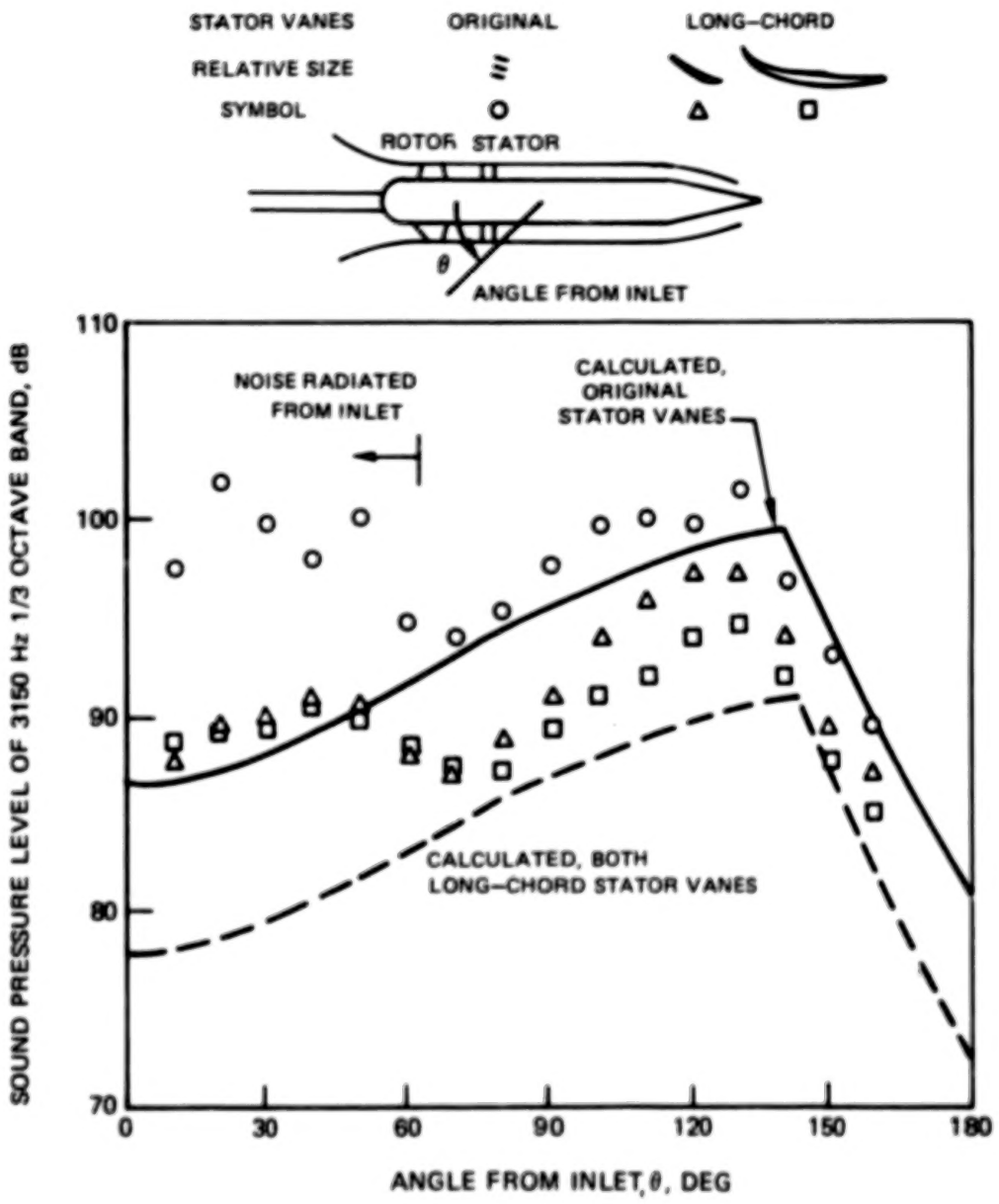

FIGURE 20– EFFECT OF LONG–CHORD STATOR VANES ON FULL–SCALE FAN NOISE DIRECTIVITY IN 3150 Hz 1/3 OCTAVE BAND AT 80 PERCENT SPEED

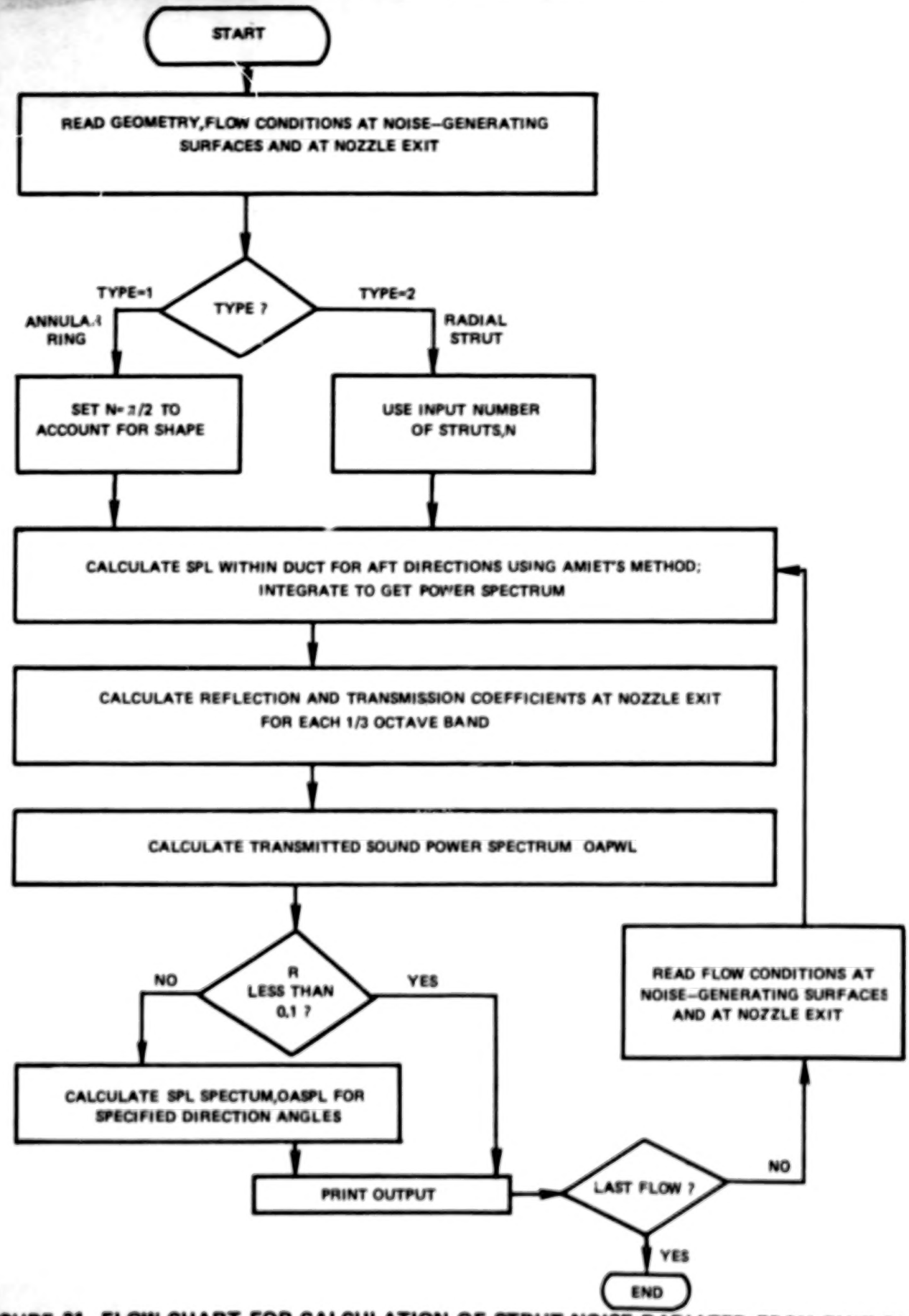

FIGURE 21–FLOW CHART FOR CALCULATION OF STRUT NOISE RADIATED FROM EXIT DUCT

77–11–75–1

1. Report No.	2. Government Accession No.	3. Recipient's Catalog No.
NASA CR-2955		

4. Title and Subtitle	5. Report Date
A METHOD FOR CALCULATING STRUT AND SPLITTER PLATE NOISE IN EXIT DUCTS - THEORY AND VERIFICATION	March 1978
	6. Performing Organization Code

7. Author(s)	8. Performing Organization Report No.
Martin R. Fink	R77-911739-18
	10. Work Unit No.

9. Performing Organization Name and Address	11. Contract or Grant No.
United Technologies Research Center Silver Lane East Hartford, Connecticut 06108	NAS3-17863
	13. Type of Report and Period Covered
12. Sponsoring Agency Name and Address	Contractor Report
National Aeronautics and Space Administration Washington, D.C. 20546	14. Sponsoring Agency Code

15. Supplementary Notes

Final report. Project Manager, William A. Olsen, V/STOL and Noise Division, NASA Lewis Research Center, Cleveland, Ohio 44135.

16. Abstract

Portions of a four-year analytical and experimental investigation relative to noise radiation from engine internal components in turbulent flow are summarized. Spectra measured for such airfoils over a range of chord, thickness ratio, flow velocity, and turbulence level are compared with predictions made by an available rigorous thin-airfoil analytical method. This analysis includes the effects of flow compressibility and source noncompactness. Generally good agreement is obtained. This noise calculation method for isolated airfoils in turbulent flow is combined with a method for calculating transmission of sound through a subsonic exit duct and with an empirical far-field directivity shape. These three elements were checked separately and were individually shown to give close agreement with data. This combination provides a method for predicting engine internally generated aft-radiated noise from radial struts and stators, and annular splitter rings. A FORTRAN program listing and users guide is included for the resulting digital computer program. Calculated sound power spectra, directivity, and acoustic pressure spectra are compared with the best available data. These data were for noise caused by a fan exit duct annular splitter ring, large-chord stator blades, and turbine exit struts. However, the lack of turbulence intensity and scale length measurements for these flow ducts prevented an absolute validation of the prediction method.

17. Key Words (Suggested by Author(s))	18. Distribution Statement
Noise, Aerodynamic noise, Engine noise, Strut noise, Splitter plate noise, Duct noise	Unclassified - unlimited STAR Category 71

19. Security Classif. (of this report)	20. Security Classif. (of this page)	21. No. of Pages	22. Price*
Unclassified	Unclassified	79	A05

* For sale by the National Technical Information Service, Springfield, Virginia 22161

NASA-Langley, 1978

END

8-30-78